UiT The Arctic University of Norway

Faculty of Health Sciences – Department of Medical Biology

Assessment of tertiary lymphoid structures in salivary glands, pancreas, and lungs of NZB/W lupus prone mice

Diana Roza Kibancha Miancho

Master's thesis in Biomedicine (MBI-3911) November 2020

Table of contents

Abstract

Autoimmune diseases are complex genetic traits. Factors that trigger autoimmune diseases have yet to be deciphered. It is however suspected that a combination of copious risk factors is implicated in the development of autoimmunity. Genetics, environmental and stochastic factors each contribute to a small degree to the risk of autoimmune disease advancement. SLE is a chronic multisystemic autoimmune disease with various range of clinical manifestations. Autoantibodies are believed to be the primary culprit' effectors in the development of systemic lupus erythematosus (SLE). SLE is typified by loss of tolerance against nuclear autoantigens, the formation of immune complexes, as well as a multiorgan tissue inflammation. Formation of tertiary lymphoid structure (TLS) emanates in tissue assaulted by chronic inflammatory processes such as infection and autoimmunity. TLS has been observed in almost all organs of the body, these are aggregates of lymphoid and stromal cells that develop at ectopic sites in response to chronic inflammation in autoimmune disease. TLS formation is consociated with tissue damage, indicating that TLSs are paramount regions for self-reactive T- and B-lymphocytes including autoantibody secreting plasma cells that are conducive to the disease state. However, the inaugurating events and signals involved in TLS development and maturation are predominantly unascertained. This study sought to disclose TLS in various tissues of lupus prone NZB/W mice. Immunohistochemistry was used for the detection of TLS in tissues. Immunostaining of formalin-fixed and paraffin-embedded tissues was performed to examine protein expression of CD3 and B220 in the lung, salivary gland, and pancreatic tissue. RNA isolation, reverse transcription, and qPCR was employed to study and evaluate mRNA expression of *IL-1β, IL-18, TNFα, Pigr, Gpr132, Emr4, CD62L(Sell), Gdf3, and Relt in the* spleen, lung, and pancreatic tissue. Results illustrated (TLS) occurred predominantly around or adjacent large and small arteries, veins including ducts in the various tissue sample, additionally TLS in pancreatic tissues were detected in Islets of Langerhans. The upregulated genes within the various tissues of lupus prone NZB/W mice established a correspondence between TLS formation and SLE.

Preface

Due to unforeseen circumstances, and the corona pandemic less laboratory work was performed. Much attention was therefore devoted to the introduction part of the thesis compared to laboratory work.

Acknowledgment

The work of this thesis in biomedicine was performed at RNA and Molecular Pathology (RAMP) research group, department of Medical Biology, Faculty of Health and Science at The Arctic University of Tromsø, Norway.

My gratitude goes to Professor Kristin A. Fenton, my main supervisor, for accepting me as a student into the RAMP group and all the members of the research group for the cordial and warm welcome they gave and their various contributions made for this work to be a success. I shall forever appreciate all of this research group members.

I would also like to extend my gratitude to Hege Lynum Pedersen, Premasany Kanapathippilla, Anita Ursvik for all their scientific help, guidance, and aid offered during this study.

A special thanks go to Aud-Malin, thank you for helping me through the various tasks, and for your patient advice and guidance throughout the research process.

Lastly, my appreciations go to my father Evariste Miancho, my mother Mawazo Myatsi, and all my siblings for their moral support, love, and encouragement.

Abbreviations

ANA	Antinuclear antibody
APC:	Antigen-presenting cell
BAFF:	B-lymphocyte activating factor
BCR:	B-cell receptor
BILAG:	British Isles lupus activity group
C1q:	Complement component 1q
CCL:	C-C chemokine ligand
CD:	Cluster of differentiation
cDNA:	Complementary DNA
CFU-L:	Colony-forming unit-lymphocyte
CXCR:	C-X-C motif chemokine receptor
DC:	Dendritic cell
DCU:	Deep cortical unit
dsDNA:	Double-stranded deoxyribonucleic acid
ECM:	Extracellular matrix
FDC:	Follicular dendritic cell
FRC:	Fibroblastic reticular cell
GEM:	Genetically engineered mice
GWAS:	Genome-wide association study
HEV:	High endothelial venule
HLA:	Human leukocyte antigen
HSC:	Hematopoietic stem cell
IFN:	Interferon
Ig:	Immunoglobulin
IHC:	Immunohistochemistry
LEC:	Lymphatic endothelial cell
LT:	Lymphotoxin
MHC:	Major histocompatibility complex
MSC:	Mesenchymal stem cell
NF-kB:	Nuclear factor-kappa B
NZB/W:	New Zealand black x New Zealand white
PALS:	Periarteriolar lymphoid sheaths
qPCR:	quantitative Polymerase chain reaction
ER:	Round endoplasmic reticulum
SLAM:	Systemic lupus activity measure
SLE:	Systemic lupus erythematosus
SLEDAI:	SLE disease activity index
SLO:	Secondary lymphoid organ
SS:	Sjogren’s syndrome

TLO:	Tertiary lymphoid organs
TLR:	Toll-like receptor
TLS:	Tertiary lymphoid structure
TNF:	Tumor necrosis factor

1. Introduction

In order to fully understand the physiology, function, and how disorders arise within an organ, one must first comprehend the basic development, the anatomy of the organ in question (1).

Mice are a pivotal partner in concurrent translational science and are one of the most invaluable expedient species for genetic modeling of mammalian maladies attributable to the genetic characterization of myriad inbred and recombinant inbred mice and expanding quantity of genetically engineered mice (GEM) (2). Murine models of maladies are utilized widely in biomedical research with many hundreds of new models being manufactured each year (2). Nevertheless, even though most tissue at the level of the light microscope is similar amidst *Mus musculus* and *Homo sapiens*, there still are vital differences (3).

Investigating the anatomy, function, and morphology of organs prior and post maladies will give a wholesome picture of how an autoimmune disease such as systemic lupus erythematosus (SLE) affects, not only the morphology of the organs but also their function. This section focuses on providing background information on organs that are of significance in this thesis (**Figure 1**).

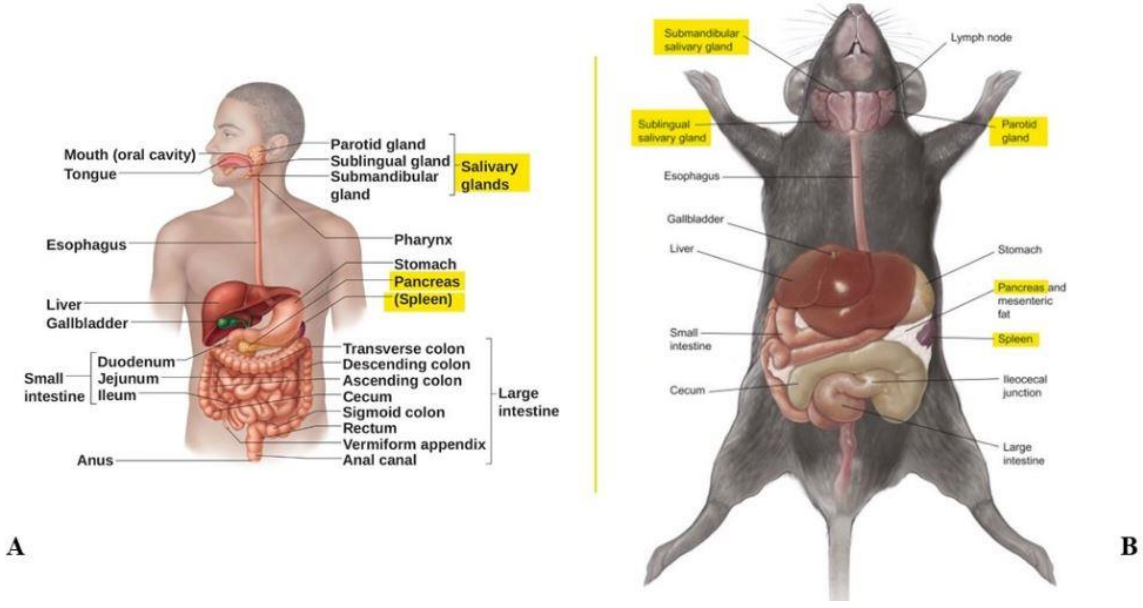

Figure 1: Overview image of the human regional adnominal (A) and mouse regional abdominal architectural anatomy (B). *Image delineates organs of significance for this thesis which includes the salivary glands with its various components such as the submandibular, sublingual, and parotid salivary glands, the pancreas, and the spleen. Respiratory(lungs), lymphatic and cardiovascular system not shown. Figure 1A is taken from Figure 23.1 by Marieb & Hoehn (4). Figure 1B is taken from Figure 1 by Treuting et al. (5).*

1.1 Architectural anatomy and function of the cardiovascular system

The cardiovascular system (circulatory system) consists of the heart, blood vessels, and blood(6). The cardiovascular apparatus is a transport circuit (7), it carries oxygen and other nutrients to practically all body cells (6). Not only that, but the cardiovascular system also removes carbon dioxide and other waste materials from cells of the body (6) by conveying wastes formed by working cells to their final destinations such as lungs, liver, and kidneys (7). Furthermore, the cardiovascular system is made up of the cardiac pump and vasculature which comprise two circulatory networks: systemic and pulmonary circulation (7).

The blood circulation's objective is perfusing and draining the body's organs and their corresponding tissues (7). The blood circulation complex constitutes serial compartments in accordance with blood vessel size and blood flow dynamics (7). Three kinds of blood circulatory networks exist, the systemic circulation, the pulmonary circulation, and the portal system (8). Two of the blood circulatory systems, the systemic and the pulmonary, depends on the heart, a central pump, that propels blood around (8). The systemic circulatory network transports oxygenated blood from the heart to all of the body tissues and carries back deoxygenated blood from the tissues to the heart (8). The deoxygenated blood has a high carbon dioxide content(8). The pulmonary circulatory network, on the other hand, convey deoxygenated blood from the heart to the lungs, with the addition of transporting reoxygenated blood from the lungs back to the heart(8). Finally, the portal system, which consists of specialized vasculature channels, transfers substances from one site to another (8). This blood circulatory system does not, however, depend on the central pump (8).

The systemic circulation, as previously established, supplies blood to all tissues of the body apart from the lungs (9). The systemic circulation comprises a "pump"- the left ventricle which propels blood through the systemic vessels (10). The arterial system, which is composed of arteries and arterioles (10). Other constituent units of the systemic circulation include the capillaries and the venous system which comprise the venules and veins (10). The systemic arterial circulation is segmented from the aorta into larger arteries, smaller arteries, and eventually into arterioles before coalescing with the capillary networks (10).

The heart frequent contractions transfer blood into arteries, which carries oxygen-rich blood through the body (6). All arteries, with the exclusion of the pulmonary arteries, carry oxygenated

blood from the heart towards the organs and tissues (6). The arteries are found in virtually every part of the body, with the omission of the hairs, nails, epidermis, cartilages, and the cornea (11). The systemic arterial circulation is a rather extensive high-pressure system, by which the vessels of the system reflects the high pressure they are exposed to (8).

The walls of the blood vessels of the cardiovascular network normally comprise three layers, tunica externa also known as adventitia, tunica intima, and tunica intima (12). Tunica externa is the outer connective tissue layer, tunica media represents the middle smooth muscle layer and the tunica intima which is the inner endothelial lining of the blood vessels (12). Structurally the arteries are dense and highly elastic (11). These vessels, due to their thick walls, muscular and elastic layers can endure the high pressure that occurs when the heart contracts (6). There is a variation in the way in which arteries divide, periodically a short trunk splits into several branches (11). Other times a trunk subdivides into several divisions in succession, at the same time as it continues as the main trunk. Nevertheless, the frequent division is dichotomous (11). Arteries are furthermore subdivided into three categories; the division is purely based on the variable amount of smooth muscle and elastic fibers (12). The size of the smooth muscle and the elastic fibers are factors that contribute to the thickness of the arterial tunica media, the overall size of the vessel, and the arteries function (12). The three classes of the arterial subdivisions include the large elastic arteries, medium muscular arteries, and small arteries and arterioles (12). The large elastic arteries are composed of a considerable amount of elastic fiber in the tunica media (12). Consequently, the sizable amount of elastic fibers give room for expansion and recoiling of the large elastic arteries during the normal cardiac cycle (12). The expansion and recoiling ability of the large elastic arteries aids in upholding a constant flow of blood in the course of diastole (12). Medium muscularis arteries are smaller vessels, the arterial walls within these vessels are more muscular (8). The tunica media of medium muscularis arteries are mostly composed of smooth muscle fibers (12). For this reason, the medium muscularis arteries are able to regulate their diameter, allowing the vessels to control the flow of blood to different parts of the body (12). As the arteries continue to divaricate within tissues, the muscular arteries progressively decrease in size until they form arterioles (8). The arterioles are the vessels possessing the smallest radii of the arterial tree. Thusly, the arterioles are the chief source of resistance to blood flow (10). The tunica media of the arterioles is composed of one or two sheets of circumferential smooth muscle (10). In opposition to arteries, the arterioles do not have elastin in their tunica media (10). Small arteries and arterioles manage

the filling of the capillaries (12), by conduction of blood from small arteries to the capillaries (10). Arterioles have additional roles, they control the distribution of blood flow to various organs, arterioles accomplish this feat by altering vascular resistance of the different organs(10). Supplementary, arterioles other role is to control the total systemic vascular resistance as well as altering the capillary hydrostatic pressure (10). Arterioles can effectively control bulk flow of water between intravascular and interstitial body fluid compartments and thus they are able to alter capillary hydrostatic pressure (10).

The arterioles ultimately branch into a system of very fine small vessels termed capillaries (8). The capillaries are tiny slender walls that allow passage of fluid, small and large molecules, gas exchange across the walls of the vessel, and into the interstitial respectively (8). Capillaries are the smallest vessels of the blood circulatory system (8), they convey blood between arteries and veins (6). Capillaries are organized in an intertwining plexus known as the capillary bed (10). Furthermore, the capillaries' role is to transport nutrients to the tissues but also remove metabolites from the tissues (10). Another role the capillaries have is that they distribute body water between intravascular and interstitial fluid compartments (10). Differently from arteries and veins, the capillary walls are constructed fully of endothelial cells that are supported by a basement membrane (8). The capillaries seldom contain scattered contractile cells termed pericytes (8). Essentially, there are three different capillary classes, each with its distinguishing characteristics (**Figure 2**)(13). There are for instance continuous capillaries, this type is the most common class of capillary (13). Continuous capillaries are commonly found in muscle, brain, and connective tissue (13). Characteristic features of continuous capillaries include a continuous basement membrane, with neighboring cells connected by tight junctions where endothelial cells are closely linked (13). The endothelial cells of continuous capillaries create an unbroken internal lining to the capillary without any intercellular or intracytoplasmic deformity (8). An example of this is the blood-brain barrier, where endothelial cells are tightly held together by tight junctions whereby only the smallest molecules such as water, oxygen, and carbon dioxide can facilely diffuse from one side of the cell to the next (13). Meanwhile, larger molecules such as nutrients, metabolites, and drugs, situated crossway the capillary rely on carrier-mediated transport mechanisms (13). Fenestrated capillaries, on the other hand, occur in the renal glomeruli, intestinal mucosa as well as in choroid plexus (13). Different from continuous capillaries, the distinguishing feature of fenestrated capillaries is that they possess large pores in the interior of the endothelial cells termed

fenestrations (**Figure 2B**)(13). The endothelial cell cytoplasm is transfixed(pierced) by pores which stretch through its full thickness (8).These pores, fenestrations rather, contrary to continuous capillaries, make fenestrated capillaries more penetrable allowing conveyance of all substances omitting the largest plasma proteins such as albumin (13). Last but not least are the sinusoidal capillaries (13). These capillaries are a distinct type of fenestrated capillaries, they can be detected in the bone marrow and lymph nodes (13). The fenestrations of these capillaries are sizeable enough permitting passage of white and red blood cells alike (13).

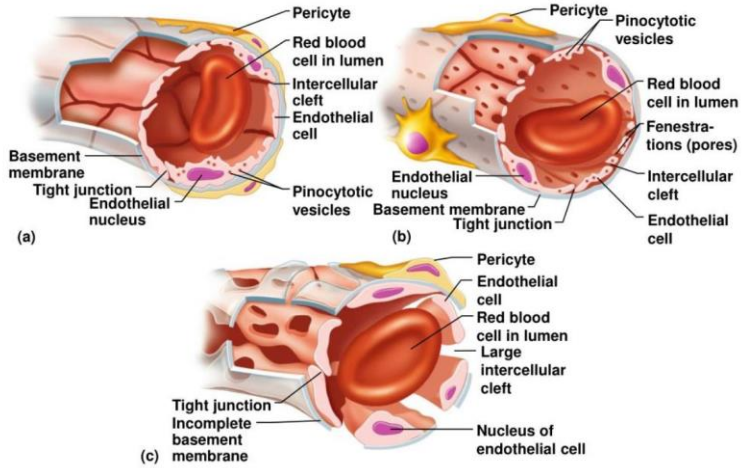

Figure 2: Overview of the tree main type of capillaries (A) continuous capillary (B) fenestrated capillary (C) sinusoidal capillary. *Continuous capillaries are commonly and substantially found in the skin and muscles. Their endothelial cells provide the capillary with a continual lining; adjacent cells are connected laterally by tight junctions which are largely incomplete. It is the least permeable of the three capillaries. The incomplete tight junctions leave gaps of unconnected membrane known as intercellular clefts, thus allowing limited passage of fluid and small solutes. Fenestrated capillaries are similar to continuous capillaries; they are characterized by the presence of pores, or fenestrations in their endothelial cells. Fenestrated capillaries are more permeable to fluid and small solutes than continuous capillaries, they are found in small intestine and kidneys. Sinusoid capillaries have large, irregularly shaped lumens, their endothelial lining has fewer tight junctions and lager intercellular clefts, allowing larger molecules and even blood cells to pass between the blood and surrounding tissues. Sinusoidal capillaries can be found in liver, bone marrow, lymphoid tissues, and some endocrine organs (14). Figure taken from 19.3 by Marieb & Hoehn (14).*

From capillaries, blood proceeds into venules and eventually into the veins, which gradually become larger as they draw closer to the heart (8). The circulatory network that conveys blood to the capillaries is known as the arterial system, while the network that transports blood away from the capillaries is named the venous system (8). Veins are, similarly to arteries, chronologically categorized into three classes in regard to the variable amount of smooth muscle in the tunica media and tunica externa respectively (12). Veins have variable sizes, the size variation are from less than 1 mm to 4 cm in diameter, they have a larger lumen and thinner wall in comparison with

arteries (8). Notwithstanding the fact that intimal, medial, and tunica external layers are present, they are however less distinctly delineated than in arteries (8). The indefiniteness of veins oftentimes makes it arduous to pinpoint where one layer ends and another begins (8). Unquestionably, it is the large veins that contain an adequate amount of smooth muscles in the tunica media, nonetheless, the thickest layer of the large veins is undoubtedly the tunica externa (12). Whereas, the small and medium veins contain a small number of smooth muscles with tunica externa being the thickest layer of these vessels (12). As noted earlier, venules and veins transfer blood to the heart (15). Of these two vessels, it is venules that are the collecting vessels, receiving blood from the capillary beds and eventually empty into the veins (15). Both the venules and veins are distinguished by their thin walls, which are collapsible and have low pressure (15). Furthermore, postcapillary venules, which are the smallest veins with a diameter of approximately 10-25μm in diameter, are the venules that drain the capillaries (8). Postcapillary venules lack smooth muscle cells and are instead covered with pericyte (16). These venules are capable of being distended and can act as blood repository; the venules are capable of expanding their blood volume by two to three times (15). When the circulation needs blood, the blood in venule reservoir is utilized, this happens by contraction of the smooth muscle in the muscular venules (15). Venous return to the heart therefore increases as a consequence of the contraction of the smooth muscle in the muscular venules (15). Postcapillary venules empty into larger collecting venules which are about 20-50 μm in diameter (8). Collecting venules on the other hand contain stellate periendothelial cells (16). As the collecting venules become larger bore the pericytes are incrementally replaced by smooth muscle cells (8). Consecutively, the smooth muscle cells form a layer one to two cells thick resulting in an identifiable fibro-collagenous tunica externa; these are muscular venules with a diameter of about 50-100μm (8). Eventually, the muscular venules empty into the smallest veins (8). Moreover, the veins, like the arteries, are found in practically every tissue of the body (11). The veins, in contrast to arteries, are larger and generally more numerous than the arteries; wherefore the entire capacity of the venous network is much grander than that of the arterial (11). Veins are charged with the assignment of carrying deoxygenated blood back to the heart (6). A great number of veins, contrary to arteries, have valves that are formed from saclike pockets of a single-cell lining endothelium, these valves hinders backflow of blood (6). The veins perform the function of conduits, conveying blood from venules back to the heart (17). Equally essential, veins serve as a major blood repository (17).

The pulmonary vasculature transfers blood through the entire output of the right ventricle of the heart by way of the pulmonary arteries and thereafter to the alveolar capillaries (18). Subsequently, the blood returns through the pulmonary veins and finally reaches the left atrium (18). Blood to be conveyed to the lungs is provided by the pulmonary and bronchial arteries and veins (8). The pulmonary artery transfers the venous blood from the right side of the heart to the lung (11). The blood provided to the lung via the pulmonary arteries is deoxygenated blood from the right side of the heart (8). This blood had previously provided the body's tissues with oxygen while concomitantly collecting carbon dioxide (8). The pulmonary artery is cleaved into two branches of approximately equal in size, the right, and the left pulmonary arteries (11). The right pulmonary artery is longer and larger in size than the left pulmonary artery (11). It runs horizontally outward, at the back of the ascending aorta and superior vena cava, to the root of the right lung (11). The right pulmonary artery is further bifurcated into two branches, of which the lower and larger provides the middle and lower lobes while the upper and smaller branch is distributed to the upper lobe (11). The left pulmonary artery is shorter and slightly smaller in size than the right pulmonary artery (11). The left pulmonary artery runs horizontally in front of the descending aorta and left bronchus to the root of the left lung where artery additionally bifurcate into two branches for the two lobes (11). The pulmonary arteries each come into the lungs at the hilum (8). The vessels terminate in the dense pulmonary capillary network in the interalveolar septa (8). Blood traverse through pulmonary capillaries in about 1 s, during which time the blood is oxygenated while excess carbon dioxide is withdrawn from the blood (9). The pulmonary veins begin in the pulmonary arteries and finally culminate into the left atrium of the heart (11). Pulmonary veins transport oxygenated blood which eventually is distributed to all parts of the body by the aorta (11). The bronchial circulation, although quite smaller, is thought of as the lungs' second circulation (19). This minor circulation derives from the thoracic aorta, (19) it supplies oxygenated blood to the larger unit of the bronchial tree (8), providing blood for the nutrition of the lung (11). The bronchial arteries endowing secondary blood supply which suffuses each lung at systemic arterial pressure providing it with, as previously stated, oxygenated blood (8). Subsequent traversing through supporting tissues, the bronchial arterial blood eventually drains into pulmonary veins and ingresses the left atrium (9).

Systemic circulation and pulmonary circulation differ in various significant aspects (18). The pulmonary circulation is a low-pressure, low resistance system in series with the systemic

circulation (9). The intravascular pressures in the pulmonary circulation are approximately one-fifth of those present in the systemic circulation (9). The pulmonary artery systolic pressure is 25 mmHg, conversely, whereas the systemic arterial systolic pressure lies between 110-135 mmHg (8). Despite that, the total blood flow conveyed through the lungs each minute equates to the amount conveyed through the systemic circulation (17). The low pressures of the pulmonary circulatory system are incommensurate with the lungs' demands, in view of the fact that all that is needed is to expose the blood in the pulmonary capillaries to oxygen and other gases in the pulmonary alveoli (17). Additionally, the low-pressure aids in preventing fluid from moving out of the pulmonary vessels into the interstitial space, thereby permitting the right ventricle to function and work at a low energy cost (20).The vessels of the pulmonary circulation system contrast considerably from those of the systemic circulation (8). For instance, pulmonary arteries have much thinner walls compared to the systemic arteries (18). In any case, the fundamental dissimilarity between the pulmonary and systemic circulation derives from the pressure difference (10).

The cardiovascular system of mouse and human has an exorbitant number of features in common; there are still, however, significant differences (3). Significant differences between the two species include the shape of the heart, location of the coronary arteries, structure of the heart valves, thickness of the pericardium, epicardium, and endocardium, and distinction of the cardiac skeleton(3). In humans, the heart inherently reposes on the diaphragm and is conical in shape with a flat inferior surface (3). In mice, the heart does not rest on the diaphragm (3). The heart of the mouse is typically oval and more effortlessly transportable within the pericardial sac (3). There are left and right cranial vena cavae and one caudal vena cava in mice, while the commensurate vasculature in humans comprises of only one superior vena cava and inferior vena cava (3). The pulmonary veins in mice coalesce before connecting the left atrium, in contrast, the four human pulmonary veins autonomously connect the left atrium (3). The mouse ordinarily has two major coronary arteries which originating in or marginally above the aortic sinuses supplying the left and right ventricles respectively (2, 3). The mouse coronary arteries ingress the myocardium, subsequent departing the aortic sinus, the arteries then crosses the heart within the myocardium (3). Humans also generally have two major coronary arteries that arise within the aortic sinus (3). Therefore, in distinction to humans, the coronary arteries of mice are intramyocardial and thus not easily detectable when investigating or analyzing the exterior of the heart (3).

Granting the fact that the anatomy, as well as histological architectural of the vasculature of the two species, have several features in common, they still have important distinctions, which include the thinner walls of mouse arteries and the pronounced presence of cardiomyocytes around mouse pulmonary veins (3).

1.2 Architectural anatomy and function of the lymphatic system

Mammals possess two mutually dependent circulatory systems, the blood circulatory system and the lymphatic circulatory system (**Figure 3**)(21). The lymphatic system serves as an accessory route in which fluid can flow from intestinal space back into the bloodstream (17). Thus it can be perceived as the "sewer system" of the body, as it plays an incredibly significant role in transporting tissue fluids and extravasates plasma protein back to the blood circulation (21).

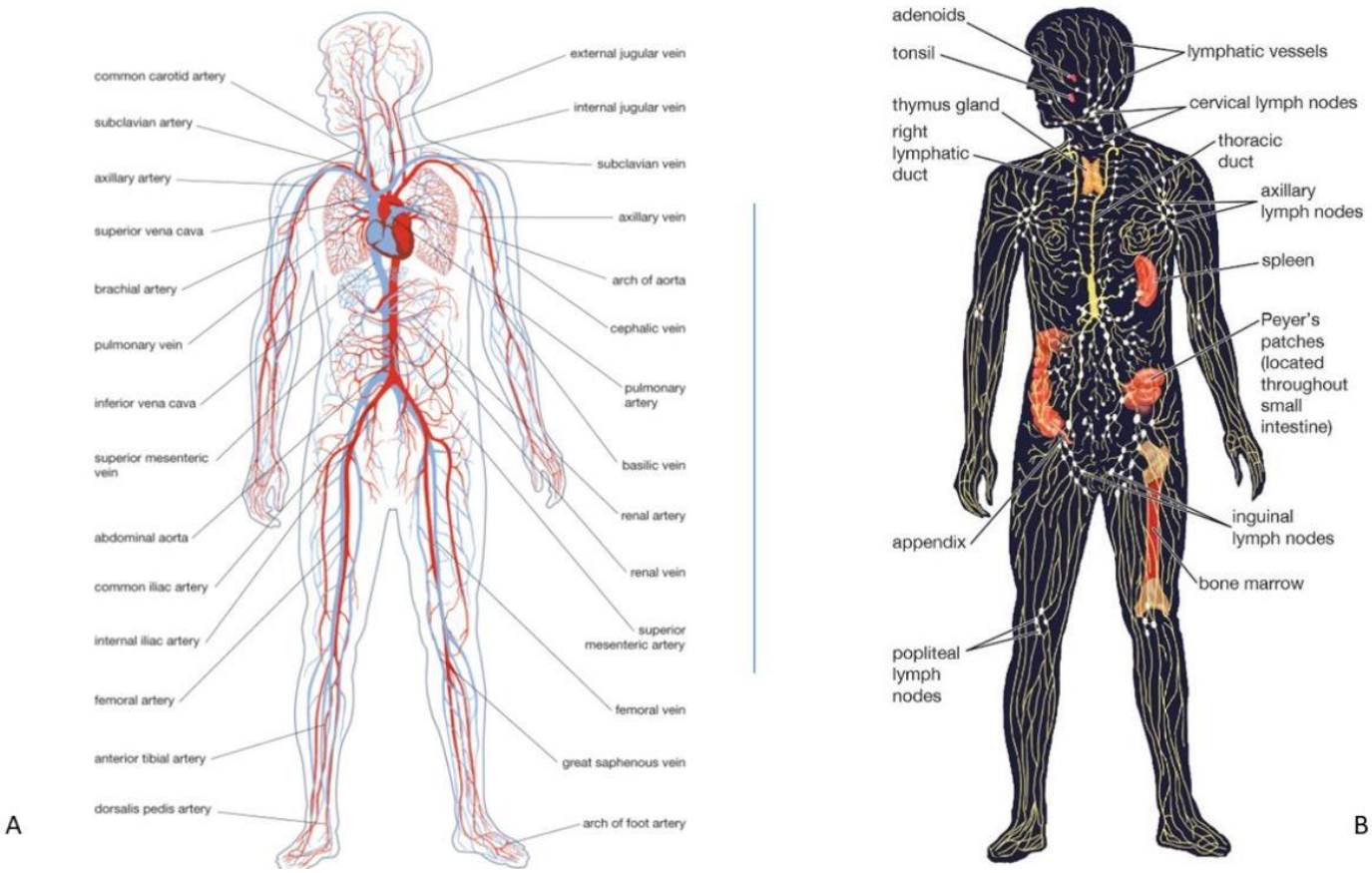

Figure 3:Overview of the circulatory system (A) and the lymphatic system (B). Figure is taken from Encyclopedia Britannica by Murray C (22)

In the course of embryonic development, mammalian lymphangiogenesis, or growth of mammalian lymphatic vessels occurs from preexisting blood vessels in a tightly regulated manner (23). It is a gradual process that needs the specification of lymphatic endothelial cell (LEC) progenitors in the embryonic veins (21). The succeeding budding of those LEC progenitors from the embryonic veins engendering to the primitive lymph sacs wherefrom the entire lymphatic system will ultimately stem (21).

The key role of the lymphatic system includes the maintenance of blood and tissue volume (23). The lymphatic system absorbs lipids from the intestinal tract, and it is in addition imperative for the immune response, it is one of the pre-eminent routes for the spreading of metastatic tumor cells (21). Moreover, the lymphatic system is remarkable in the sense that it is capable of collecting microbial antigens from their portal of entry and thereafter deliver the microbial antigen to the lymph nodes where they can stimulate the adaptive system (24). Another phenomenal reason that illustrates the significance of the lymphatic system is its efficiency to carry proteins, and large particulate matter, that cannot be removed by absorption, away from the tissue space into the blood

capillaries (17). The recrudesce of proteins to the blood from the intestinal space is a fundamental function with which we would perish within about 24 hours without (17). To accomplish these outstanding feats, the lymphatic system comprises a network of vessels of varying caliber (23). It is a conglomeration of freely permeable, thin-walled vessels that are spread throughout the entire body (25). The vessels are linked through a series of lymph nodes and other lymphoid organs (23). Lymph fluid drains into a network of tiny capillaries in tissue space that connects forming larger lymph vessels (6). Lymphatic vessels are closely involved in the maintenance of tissue homeostasis, immune cell trafficking, and transport of dietary lipids (23). The lymphatic vessels converge into afferent lymphatics that drain into the lymph nodes (24). Lymph nodes are the filtering and storage facilities of the lymphatic system, they are dispersed along the lymph vessel circuit (6). Moreover, the lymph drains out of the nodes through efferent lymphatics (24). Lymph nodes are linked in series by lymphatics, consequently, an efferent lymphatic that exits one node may act as an afferent vessel for another (24). The efferent lymph vessel at the end of the lymph node thereafter connects, with other lymph vessels, and conclusively empty in a large lymphatic vessel, the thoracic duct (24). The thoracic duct, in turn, drains into the blood venous system at the juncture of the left internal jugular vein and the left subclavian vein (17). Additionally, lymph fluid from the left side of the head, the left arm including parts of the chest region enters the thoracic duct prior emptying into the veins (17). By the same token, lymph from the right side of the neck and head, the right arm, and part of the right thorax enters the right lymph duct, finally drains into the blood venous system at the juncture of the right subclavian vein and internal jugular vein (17).

The initial lymphatic capillary has overlapping “flap-like” valves that advance the entry of intestinal fluid into lymphatics. Under normal conditions, however, these “flap-like” valves hinder reflux back into the tissue (26). LECs line lymphatic capillaries, and present loose overlapping intercellular junctions and anchoring filaments that support fluid seepage (21). When interstitial fluid cumulate within tissues, the extracellular matrix (ECM) swells and pulls the anchoring filaments (21). The anchoring filaments that pull the flaps open in the circumstance that interstitial fluid pressure arise (26), which results in the opening of the LEC junction thereby granting permission for the uptake of interstitial fluid (21). Whenever the interstitial fluid is high, the flaps are pulled open thus substantially facilitating the movement of lymph into the lymphatic channels (26). Lymph from initial lymphatics is thereafter transported within lymphatic collector vessels (26). Collecting lymphatic vessels exhibit intraluminal valves, that prevent lymph reflux, in

addition, they possess smooth muscle cells that consecutively contact propelling the lymph forward (21). The lymphatic collecting vessels maintain a monodirectional flow, and in this manner prevent backflow of lymph, a feat attributed to the presence of valves (26). Not only do the valves prevent the backflow of lymph, but they also separate the lymphatic vessels into functional units known as lymphangions (21). The lymphatics are equipped with valves at the very tips of the terminal lymphatic capillaries (17). Similarly, the lymphatics have valves, to some extent, along their larger vessels with which drain lymph fluid into the blood circulation (17). In some regions the lymphatic capillaries contain a fenestrated endothelium and a discontinued basement membrane (BM), allowing the access of larger molecules such as proteins, triglycerides, likewise some cells, especially cells of the immune system (8). Lymphangions are lymphatic segments that are bound by two unidirectional valves, compressed by rhythmic tissue compression formed by intrinsic phasic contractions and tonic contractions of specialized lymphatic smooth muscle cells (26). Under normal pathological conditions, lymphangions aid in propelling lymph forwards by their contractile action, lymph is, as a consequence, forced forward against a hydrostatic pressure gradient (26).

The active part of the lymphatic system is lymph fluid, which commences life as the interstitial fluid that accumulates between cells of the body (6). Interstitial fluid is inherently produced in all vascularized tissues by the movement of a filtrate of plasma out of capillaries (24). Virtually all tissue of the body possesses special lymph channels that drain surplus fluid directly from the interstitial space (17). There are, however, some exceptions which include the superficial portion of the skin, the central nervous system, the endomysium of the muscle, and unquestionably the bones (17). Surprisingly, even these tissues have minute interstitial channels termed pre-lymphatics, it is through these channels the interstitial fluid flows (17). This interstitial fluid subsequently percolates either into the lymphatic vessels or, as it is in the case of the brain, the interstitial fluid drains into the cerebrospinal fluid and eventually directly back into the blood (17).

The composition of lymph as it first enters the terminal lymphatics is virtually similar to that of the interstitial fluid (17). Customarily, lymph is a clear colorless fluid (8). Nonetheless, the discharging of lymph from the intestine during the absorption period is frequently milky in appearance (8). This milky fluid is called chyle, this appearance is indisputably caused by the high lipid content of the absorbed nutriment (8). The protein concentration in the interstitial fluid of

most tissues is approximately about 2 g/dl, and the protein concentration of lymph that flows from these tissues is nearby the same value (17). Lymph fluid that is produced in the liver has a protein concentration twice as high as that of the interstitial fluid, while lymph deriving from the intestines has a protein concentration as high as 3 – 4 g/dl (17). Typically, around two-third of all lymph emanates from the liver and intestines (17). For this reason, the thoracic duct lymph, which is a combination of all lymph from all regions of the body, has a protein concentration of 3-5 g/dl (17). The lymphatic system is one of the main routes for the absorption of nutrients from the gastrointestinal tract, particularly for the absorption of nearly all fats in food (17). As such, following a fatty meal, the thoracic duct lymph would occasionally have as much as 1-2 percent fat, hence the lymph's milky like appearance (17).

Lymph nodes are imperative to the body's defense system due to the fact that they indeed produce and accommodate immune cells (6). They are encapsulated, vascularized secondary lymphoid organs, possessing anatomical characteristics that favor the commencement of adaptive immune responses to antigens transported from tissues by lymphatics (24). Lymph nodes are a vital component of the secondary lymphoid organs (SLO) and serve as a unification unit of the lymphatic system (23). SLO include the spleen, lymph nodes, and Peyer's patches (27). SLO has a network of fibroblasts, vessels, and nerves that brace a large motile population of leukocytes that aid in immune surveillance and which react to harmful agents (27). SLO developed concomitantly with the evolution of an adaptive immune system in vertebrates with lymph nodes calculatedly allocated throughout the lymphatic system (27). This strategic allocation of lymph nodes provides a platform for congregating immune cells in well-defined zones (27). Thus allowing for a swift, effective, and methodical adaptive immune responses that exceed pathogen replication, spread, and pathology (27). Each lymph node is generally a mass of lymphatic tissue fragmented into compartments cleaved by connective tissues named trabeculae(6). Two regions within the lymph node are histologically prominent and distinguishable, these are the cortex and the medulla (**Figure 4**) (28). Lymph nodes comprise of multiple lymphoid lobules enveloped by lymph-filling sinuses (29). Each lobule is centered under its own afferent lymphatic vessel (30).

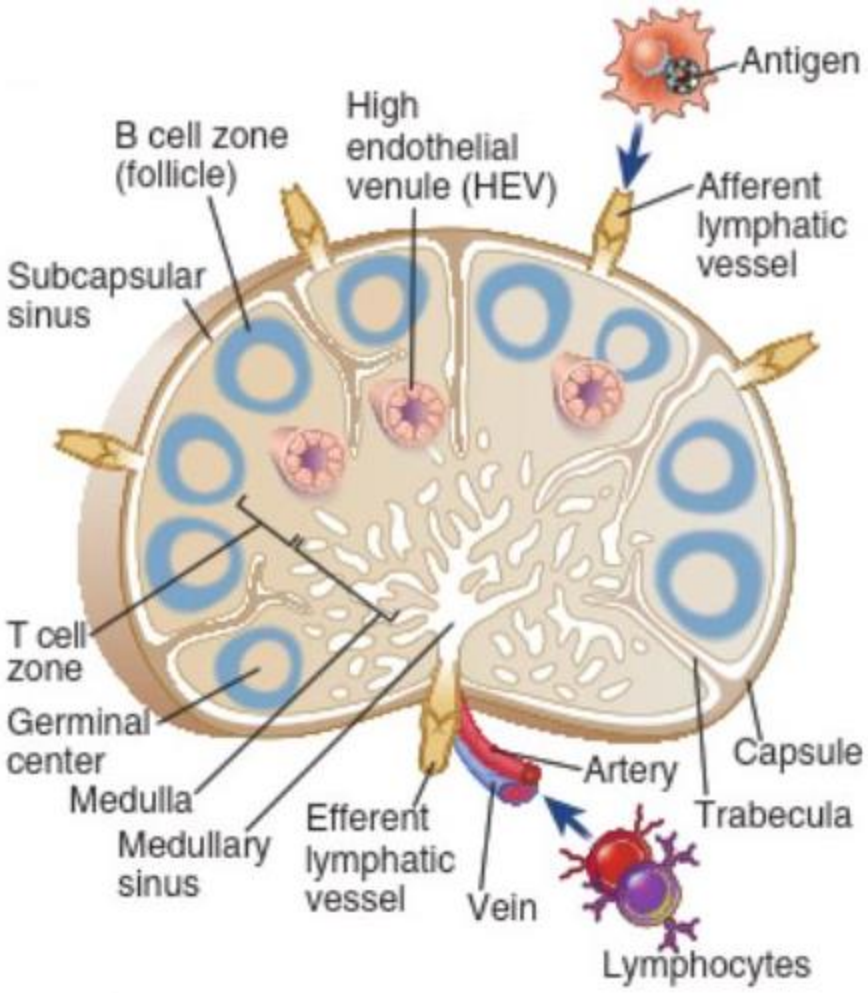

Figure 4:Organization of a lymph node. *A Schematic representation of the anatomical architectural of a lymph node displaying the capsule, trabecula, subcapsular sinus, medullary sinus, the medulla, the B-lymphocyte, and T-lymphocyte zones, HEVs, germinal center and the passage entry of antigens and lymphocytes. Most of the lymphocyte ingress the node from the circulation through the HEVs. Naïve lymphocytes ingresses the lymph node via an artery and exits the circulation via the HEVs. The B- and T-lymphocytes then migrates to their respective regions within the lymph node. Antigens gain access to the lymph node by way of the afferent lymphatic vessel, the antigen is drained into the subcapsular sinus which in turn drains into the cortical sinuses (not shown), through the medullary sinus, the antigen eventually leave the lymph node via the efferent lymphatic vessel. Figure is taken from figure 2.14 A by Abbas (24).*

Moreover, a lymph node is encapsulated by a fibrous capsule, underneath the fibrous capsule lies a sinus system which is lined by reticular cells, cross-bridged by fibrils of collagen as well as other extracellular proteins (24). The sinus system is filled with lymph, macrophages, dendritic cells, and other cell types (24). The macrophages within these sinuses ingest bacteria along with other unknown external matter and debris (6). Lymph fluid from the afferent lymphatic vessel spread over the lobule's apical surface in the subcapsular sinus, and maneuvers down the sides via transverse sinuses (30). The lymph fluid subsequently flows through medullary sinuses

encompassing the medullary cords, where it thereafter exits through the efferent lymphatic vessel in the hilum (30). Prior to exiting the efferent lymphatics the lymph fluid, collected from tissue and organs, is first and foremost filtered and cleansed in the lymph node (6). The efferent lymphatic, at the hilum, transfer lymph in the direction of larger collecting lymphatic vessels (8). These vessels drain, consecutively, into more proximal nodes preparatory to entering the blood by way of either the thoracic duct or the right lymphatic duct (8). The lymphoid lobule is the basic anatomical and functional unit of the lymph node (29). Each lymph node may contain a few or numerous lobules depending on the size of the lymph node (29). Lymphoid lobules are organized abreast and radiate capsad from the hilum (30). Lobules are embedded in the hilum by their vascular roots, they are despite that separated from the capsule by the subcapsular sinus (30). The lobule has a round ovoid apex and a base of slender medullary cords. The apex forms part of the nodal cortex and the base forms the nodal medulla (29). The nodal cortex is a structure consisting of two layers, the superficial cortex and the paracortex (30).

A lymphocyte-rich cortex is located below the inner level of the subcapsular sinus (24). The cortex is further furcated into the parafollicular or paracortex for short, and the superficial cortex (28). The superficial cortex, which is the outer cortex, holds aggregated cells termed follicles (24). A few follicles have central areas known as germinal centers (24). Follicles with germinal centers are named secondary follicles, whereas those lacking germinal centers are appointed primary follicles (24). The superficial cortex has spherical follicles that are encircled and parted by the interfollicular cortex (29). The paracortex consists of deep cortical units (DCUs), each lobule has a single DCU that can further be anatomically and functionally, divided into a central a DCU and a surrounding peripheral DCU (29). The peripheral DCU and interfollicular cortex are fashioned out of compacted paracortical cords (29). Paracortical cords are ampler than medullary cords, due to their ability to multiply alongside blood vessels which arborize widely in the paracortex (29). The paracortical cords encircle the central DCU and follicles like staves and barrel (29). The cords become distended and extended during an immune response and decrease in diameter if lymphocytes are exhausted (29). The interfollicular cortex in tandem with the peripheral DCU function as transit corridors for lymphocytes migrating from and to B and T-lymphocyte zones (29). Furthermore, B and T- lymphocytes are segregated in readily distinguishable regions within the cortex of the lymph nodes (24). Superficial cortex with its follicles home the B- lymphocyte zone (24). Within the primary follicles are mostly mature, naïve B- lymphocytes (24), where they

interact with follicular dendritic cells (FDC) for about 24 hours (29). Germinal center is developed when B- lymphocyte encounters and is stimulated by its antigen displayed on the FDC in the primary follicle (29). When the B-lymphocyte is stimulated it undergoes clonal expansion (29). The germinal centers are sites of astonishing B-lymphocyte cell proliferation, selection of B-lymphocyte cells capable of producing high-affinity antibodies, and generation of memory B-lymphocytes as well as long-lived plasma cells (24). The location of T-lymphocytes is mainly in the paracortical cords, right beneath and more central to the follicles (24). The paracortex is the region where circulating lymphocytes enter the lymph node, it is, in addition, the site where T-lymphocytes join forces with dendritic cells (DCs)(28).

The whole lymph node is filled with reticular meshwork, which is a delicate, porous, sponge-like tissue made up of stellate elongated fibroblastic reticular cells (FRCs) and their reticular fibers (29). The reticular meshwork forms the foundational structure of the lobules, it also intersects the lumens of the sinuses (29). Lobular reticular meshwork formed of stellate FRCs processes segments the lobule into countless narrow channels and interstices that are populated by lymphocytes, macrophages, and antigen-presenting cells (APCs)(29).

The T-lymphocyte rich region contains a network of fibroblastic reticular cells (FRCs)(24). The FRCs are organized in a manner that shapes the outer layer of tube-like structures known as FRC conduits (24). The surface of FRCs is layered with migration ligands, such as fibronectins, which enables lymphocyte adhesion and migration (29). Nonetheless, the FRC conduits commence at the subcapsular sinus, extending to both medullary sinus lymphatic vessels and cortical blood vessels, called high endothelial venules (HEVs)(24). HEVs are located at the center of each paracortical cords (28). HEVs are distinguished by their high cuboidal endothelial cells' appearance (29). A HEV is encompassed by layers of concentric pericytes which are FRCs (28). There is a small space between the BM of the HEV and the pericytes known as the perivenular channel (28). HEVs are the gateways that lymphocytes utilize to enter the reticular meshwork from the closed circulation (29). Consequently, they access and enter the stroma of the node via the HEVs (**Figure 4**) (24). Moreover, HEVs are equipped with a specialized cell receptor, the lymphocyte-homing receptor, which recognizes and binds circulating lymphocytes, thus facilitating their migration from blood into the lymph node (8). Naïve T and B-lymphocytes are transported to a lymph node by way of an artery, and subsequently, leave the circulation (24). Lymph node stromal cells secrete cytokines

in the B-lymphocyte zone as well as in T-lymphocyte zone (24). The anatomic separation of lymphocytes to their distinct regions, as a consequence, is cytokine dependent (24). It is the cytokines that redirects the migration of lymphocytes to their appropriate zones within the lymph node (24)

The medulla of the lymph node is a maze of lymph draining sinuses (28). The medulla mostly accommodates cell-rich medullary cords, wide medullary sinuses, large blood vessels, and their supporting trabeculae (8). The medullary sinuses are divided by medullary cords where plasma cells, some macrophages, and memory T-lymphocytes reside (28). The interstitial section of the medulla is supported by reticulin fibers, a small number of which cross the sinuses (8). Plasma cells are antibody synthesizing cells (8). Numerous of the plasma cell precursors transmigrate to the medullary cords (29). Within the medullary cords, the plasma cell precursors mature into plasma cells, upon maturation the plasma cells send forth, secrete rather, antibodies into the lymph (29). As previously stated, lymph travels through the subcapsular sinus over the lobule's apex (29). It then courses from the lobule's apex, down the periphery of the lobules by use of transverse sinuses where it finally courses the medullary sinuses (29). Lymph percolates through the medullary sinuses (8), and egresses through the efferent lymphatic vessel in the hilum (29). Lastly, the lymph fluid is thereafter transported back to the blood circulatory system succeeding traversing through the lymph node through the node (8). Unfortunately, the function of the medulla is regrettably poorly understood (28).

The function of lymph nodes in mice or murine models, analogous to that of human and are vital in facilitating immune reactions to external and internal stimuli (3). Nevertheless, lymph node in mice are normally quite small and quite difficult to identify within the adipose and other tissue (31). Mice have fewer lymph nodes compared to other species, these are small bean shaped structure joined to lymph vessels and are dispersed throughout the body (32). The peripheral lymph nodes are bilateral and include the mandibular, axillary, and popliteal lymph nodes (32). The largest of these are the mandibular and the mesenteric nodes (31). Central lymph nodes are located in the thoracic and abdominal cavities (32). Moreover, lymph nodes are vital components of the immune system in both species (3). Additionally, the mice microanatomy is similar in mice and humans (3).

1.3 Lymphoid organs

Lymphoid tissue is a type of connective tissue, it is characterized by a rich reservoir of lymphocytes (33). It dwells free within the regular connective tissue or it can be encircled by capsules by which the lymphoid organs are formed (33). The lymphoid organs are vital regulators of lymphocyte development and immune response (34). The lymphoid and hematopoietic system is made up of multiple tissues and organs which are allocated throughout the body (2). These systems are in charge of the development of the immune response, and the manufacturing of blood's cellular components (2). The lymphoid organs are made up of two tissue constituents, reticular connective tissue, and lymphatic tissues, comprised of lymphocytes, macrophages, and antigen-presenting cells (2). Through vertebrate development, primary lymphoid organs manifest earlier than secondary lymphoid organs (34).

Lymphoid tissues are practically constructed up of free cells, as consequence, they typically possess a rich plexus of reticular fibrils that support the cells and are primarily composed of type III collagen (33). In a lot of lymphoid organs, the fibrils originate or produced by a fibroblastic cell called a reticular cell, whose many processes rest on the reticular fibrils (33). The matrix of reticular fibrils of the lymphoid tissue may be of dense lymphoid tissue and thus capable of holding many free cells (33). Additionally, the matrix can also be of a loose lymphoid tissue type, with fewer but larger spaces (33). This type of matrix provides a conditions or environment for easy movement of the free cells (33). On the other hand, nodular lymphoid tissues are organized as spheres, often referred to as lymphoid nodules or lymphoid follicles, which chiefly encompass B-lymphocytes (33). Lymphoid nodules have various sizes, generally measuring a few hundred micrometers to 1 mm in diameter (33). They are ordinarily located free anywhere in the body within connective tissue or within lymphoid organs, such as lymph nodes, spleen, and tonsils except in the thymus (33). Moreover, they are never capsulated (33). Free lymphoid nodules are generally present in the lamina propria of miscellaneous mucosal linings, where combined with free lymphocytes, they comprise the mucosa-associated lymphoid tissue (MALT)(33). Furthermore, when lymphoid nodules are activated by the arrival of APC carrying antigens and recognition/stimulation of the antigen by B-lymphocyte (33). Subsequent antigen recognition/stimulation, the lymphocytes proliferate in the central portion of the nodule, which stains lighter and it is recognized as a germinative center (33). The germinative centers comprise

of a unique cell, the follicular dendritic cell, these bind antigens on their surfaces, and present the antigens to B-lymphocytes (33). Following termination of the immune response, the germinal center may vanish (33). Lymphoid organs such as the thymus, spleen, and lymph nodes are crucial components of the mammalian immune system (34). Moreover, lymphoid organs are subdivided into three classes; the primary, secondary, and tertiary lymphoid tissues/organs, each category with its own development and function as chronicled below (2).

1.3.1 Primary lymphoid organs

The primary lymphoid organs comprise the bone marrow, thymus, and the fetal liver (2, 35), the bone marrow and thymus are responsible for the production and maturation of the B- and T-lymphocytes (2). Primary lymphoid organs are needed for the evolution of lymphocyte effector cells (34). Primary lymphoid organs are, therefore, delineated as organs, or compartments within organs, where hematopoietic progenitors differentiate into a rich profusion of immune cells that are able to carrying out effector functions (35). In mammals, the thymus is the region of T-lymphocyte development, while the bone marrow is the site of B-lymphocyte development (34). B-lymphocytes are first produced in the fetal liver in mammals, and are later generated in bone marrow as it becomes hemopoietic (36). The adult bone marrow serves as a home for hematopoietic stem cells (HSC), mesenchymal stem cells (MSC), and endothelial stem cell progenitors (35). The bone marrows main functions are the production of blood cells, destruction of deteriorated red blood cells, and storage 8in macrophages) of iron from the breakdown of hemoglobin (33). Lymphocytes originate from lymphoblast, which arise from a pre-cursor colony forming unit-lymphocytes (CFU-L) cell (37). Larger lymphoblasts, approximately 15-20 µm in diameter, engenders smaller prolymphocytes (37). Some of the prolymphocytes differentiate and mature into B-lymphocytes within the bone marrow (78). Post maturation B-lymphocytes exits the bone marrow, enter the circulation, and migrate to the peripheral lymphoid organs such as the spleen and lymph nodes (37). Likewise, other prolymphocytes ingress the bloodstream during premature phases of embryonic and early post-natal life to populate the thymus gland (37). The cells in the thymus develop into T-lymphocytes (37). During their evolution, B-lymphocytes are subjugated to both positive and negative selection events that ultimately form the peripheral repository of antigen-reactive B-lymphocytes (38). Negative and positive signals coupling with B-lymphocyte activating factor (BAFF) dictate the future of B-lymphocytes (39). BAFF regulates B-

lymphocyte survival, additionally, the amount of BAFF influence the size of B-lymphocyte compartment (39).

The negative and positive selections are based on the expression and antigen specificity of the B-cell antigen receptor (BCR)(38). The formation of BCR by the change of the V, D, J gene segment in the heavy (H) and light (L) chain loci is the hallmark of B-lymphocytes evolution (40). Nevertheless, such random gene coupling events can regrettably lead to self-reactivity, for this reason, steps were put forth to as a safeguard to ensure as well as to reduce the number of self-reactive B-lymphocytes in the repository (40). The checkpoints depend on the interactions of the BRC with "self", thus the sensitivity of these interactions are strictly regulated in order to discern signals for positive versus negative selection (40). Only a small number of cells the immature, short-lived, B-lymphocytes are selected to enter the long-lived mature B-lymphocyte repository/repertoire in the periphery (41). The majority of all B-lymphocyte express one of two heavy (H) chain alleles and one of either (two κ six λ) light (L) chain alleles (41). Under B-lymphocyte development and upon ingress into the periphery, B-lymphocytes are, as stated above, screened against autoantibodies, either editing of L-chain expressing, by deletion or by inactivation through the initiation of anergy (41). Immune tolerance inhibits the potentially damaging responses of lymphocytes to the host tissue (42). For this reason, tolerance is regulated at the phase of immature B-lymphocyte development (central tolerance) by clonal deletion, comprising apoptosis, and by receptor editing (42). Self-reactive B-lymphocytes undergo receptor editing, by which current immunoglobulin (Ig) light chain is replaced by another light chain, resulting in secondary changes that can modify BRC specificity (42). Receptor editing gives room for several attempts at editing, thereby contributing to the vast diversity of the antibody repertoire (42). Mature B-lymphocytes express on their surface both IgM and IgD in different proportions on the same cells (41). IgM and IgD are the major immunoglobulins on the surface of B-lymphocytes, both of these two classes of immunoglobulins exist in two forms; membrane-bound and circulating form (33). IgM attached to the membrane of B-lymphocyte serves as its specific receptor for antigens (33). The corollary of this connection is the proliferation of additional differentiation of B-lymphocytes into antibody-secreting plasma cells (33). When secreted IgM is bound to the antigen, it becomes quite effective in activating the complement system (33).

The thymus is the venue of terminal differentiation and selection of T-lymphocytes. T-lymphocyte precursors, dedicated to producing T-lymphocytes, do not display the T-lymphocyte receptor on their surfaces and are on that account $CD4^-$ and $CD8^-$ (33). They originate in the fetal liver in early fetal life, thereafter they voyage from the bone marrow to the thymus (33). After entering the thymus, the T-lymphocytes precursors establish themselves in the cortex where they undergo cell division by mitosis (33). Within the cortex, these precursors T-lymphocytes are introduced to self-antigen that are attached to class I and class II MHC molecules present on the surface of the epithelial cells, macrophages, and dendritic cells (33). The maturation and selection of T-lymphocytes, including negative and positive selection take place within the thymus (33). Basically, T-lymphocytes whose T-cell receptor (TCR) lacks the ability to bind, or binds too robustly to self-antigens (approximately 95% of the total) are induced to die by apoptosis and devoured by macrophages (33). The surviving T-lymphocytes migrate to the medulla of the thymus (33). It is believed that only a small number of lymphocytes engendered in the thymus reach maturity (8). These are closes of T-lymphocytes that are capable to recognize external antigens (8). Those that recognize self-antigen, as mentioned above, are eradicated. This leads to immunological self-tolerance (8). Mature $CD4^+$ and $CD8^+$ T-lymphocyte with their respective TCR attached to their surface depart from the thymus, ingress the blood circulation, and are dispersed throughout the body (33).

1.3.2 Secondary lymphoid organs

Secondary lymphoid organs (SLO) consist of the lymph nodes, spleen, MALT, and Peyer's patches (PPs)(2, 35). The organogenesis of SLOs is completed during embryonic development in humans, and shortly post-natal in mouse (43). The way the peripheral lymphoid organs form and with such determined anatomical positioning has such a biological significance, here the cells of innate and adaptive immunity can communicate and work together in an efficient way for the eradication and removal of foreign pathogens (43). Members of the lymphotoxin (LT) family (LTα3 and LTα1β2) play a major role in the formation and maintaining of lymphoid organs through their production by $IL\text{-}7R^+CD4^+CD3^-$ lymphoid tissue inducer cells (LTis) (44). LTis interact with cells of mesenchymal origin, called lymphoid tissue organizer cells, which create chemokines that sequentially induce more LTαβ (44). The LTis express $LT\alpha_1\beta_2$ complex, a cytokine that is a vital determinant of SLO development (45). $LT\alpha_1\beta_2$ is a heterotrimeric complex

that consists of membrane-bound LTβ and soluble LTα (45). Combined they bind to the lymphotoxin-β receptor (LTβR) that is mainly expressed by mesenchymal stromal cells(45). The $LT\alpha_1\beta_2$ signals through LTβR to drive mesenchymal stromal cells to differentiate into lymphoid tissue organizer cells along with the up-regulation of chemokines such as CXCL13, CCL19, and CCL21 accompanied by adhesion molecule expression in the lymph node anlagen (45). Lymphoid tissue organizer differentiates into different non-hematopoietic stromal subtypes that exist in the mature SLO via LTβR signaling (45).

They are responsible for maintaining populations of mature lymphocytes and are the site of antigenic stimulation and clonal expansion (2). SLOs are strategically stationed within the lymph and blood, where they serve two fundamental functions (35). The main function is to filter pathogens and antigens from the circulation and lymph with antibodies and components of the innate immune system (35). Second, SLOs are positioned where adaptive B and T-lymphocytes mediated immune responses are initiated and controlled (35). Lymph nodes form at designates sites through the coordinated interaction of mesenchymal stromal cells and hematopoietic lymphoid tissue inducer cells (LTICs)(35). The dominant chemokine needed for the formation of lymph nodes is CXCL13, which is produced by stromal cells (35). CXCL13 mediates the employment of CXCR5-expressing LTICs to the appointed site of lymph node development (35). In mice lymph nodes and PPs are arranged or positioned into different sections; B-lymphocytes in follicles and T-lymphocytes in their zone (35). Severance of these lymphocytes in various compartments depends on specialized nonhematopoietic stromal cell populations that supply structural support and provide chemokines that organize immune cell positioning and function (35). B-lymphocyte follicles found in the lymph node, PPs, and in the spleen are regions of production of CXCL13 (35). CXCL13 is a selective chemoattractant for B-lymphocytes and T follicular helper lymphocytes that regulates cell positioning via interaction with CXCR5 (35). The stromal cells in the B-lymphocyte follicles, the follicular dendritic cells (FDCs), supplies the CXCL13 (35). The FDCs are able to exhibit antigen-antibody complexes on their surface and thus take part in B-lymphocyte affinity maturation (35). Fibroblastic reticular cells (FRCs) supply the population in the T-lymphocyte zone with chemokines such as CCL19, CCL21, and CXCL12, which direct T-lymphocyte migration and positioning (35).

Mature SLOs are distinguished by the anatomical coordination of lymphocytes in different compartments, the separation of these zones is facilitated by the aforementioned chemokines (27). The FRCs of the T-lymphocyte zone is located in the cortex within the lymph nodes and are typified by the expression of podoplanin as well as lack of the vascular marker CD31 (27). The FRCs are in charge of the recruitment, retention, and movement of the naïve T-lymphocytes and DCs through their expression of CCL19 and CCL21 (27). Equally important, FRCs create an extracellular network, establishing a system of microchannels that couple the subcapsular sinus with the paracortex and HEVs (27). Supplementarily, FRCs are an important reservoir of IL-7, CCL19 coupling with IL-7 plays a role in maintaining naïve T-lymphocyte survival withing the lymph node T-lymphocyte zone by modulating T-lymphocyte homeostasis (27).

1.3.3 Tertiary lymphoid structure

Organs are generally defined as a conglomeration of cells, with extracellular structure, and fluid, combined into an operational unit to perform a common function (27). The anatomical architecture of an organ is shaped by its structural elements, or resident stromal cells, which provide form and compartmentalization to the tissue (27). SLOs predominantly conform to this definition (27). Tertiary lymphoid organs (TLOs) have been observed in nearly every organ of the body, they are also recognized as tertiary lymphoid structures, ectopic lymphoid tissues, or tertiary lymphoid tissues (46). TLOs are aggregations of lymphoid and stromal cells that develop and organize at ectopic sites in response to chronic inflammation in autoimmunity, microbial infection, graft rejection, and cancer (46). Moreover, TLSs can be brought about experimentally by tissue-specific expression of some inflammatory mediators, including members of the lymphotoxin family, the exact cytokines that are vital for lymphoid organ development and maintenance (44). Often referred to as “TLOs” although as the name suggests, this term fails to conform to the proper definition of organs, as they lack a stable structural organization, including a capsule, therefore they are better categorized as TLS (47). Here TLOs will be referred to as tertiary lymphoid structure (TLS).TLS contrast the primary lymphoid organs and SLOs in that they emerge in response to inflammation or inflammatory signals, instead of emanating in ontogeny (46). TLSs generally lack a capsule, there are however contained within the boundaries of another organ yet are not confined to a set location in the body (46). Nonetheless, their structure, cellular composition, chemokine expression, and vascular and stromal foundation correspond with SLOs

and are the describing characteristics of TLS (46). B- and T-lymphocytes, APCs, FRCs, and other stromal cells and vascular elements, HEVs, and lymphatic vessels included, are archetypal components of TLSs (46). TLSs present other characteristics of SLOs such as divided T- and B-lymphocyte zones and exhibits the mechanisms to support local adaptive immune responses against locally exhibited antigens (47). Furthermore, TLSs can be distinguished from acute inflammation, as they normally incorporate few granulocytes, and are not essentially destructive, however, TLSs may convert into tissue-damaging substances (46). When inflammation persists and becomes chronic, the quantity of plasma cells and lymphocytes increases, lymphangiogenesis is induced (48). Subsequently, blood vessels develop features of HEVs specialized in permitting extravasation of lymphocytes (48). Occasionally, the chronic infest organizes into the accumulation of distinct T- and B-lymphocyte(48). TLSs are not present in embryonic life but are formed in adult life to support the accumulation of lymphocytes at the intended organ of disease (47). It has been implied that TLSs contrast SLOs by the lack of a capsule, nevertheless, TLSs in diverse chronic kidney diseases are in contact with fibrous capsule (44). The lack of a capsule may reflect the way that TLSs arise, compared with lymph nodes (44). While a lot of reports on TLS recount a certain degree of T- and B-lymphocyte division, vascular and stromal cell specialization and expression of lymphoid chemokines, the presence of a more intricate organization of the TLSs varies within and amongst diseases (47). The degree of TLS organization corresponds with tissue infiltration, demonstrating that vigorous TLS induction relies on abundant local immune cell activation (35). TLSs can be induced and also maintained during chronic infections and various autoimmune disorders (35). As disclosed above, TLSs generally develops during the progression from acute to chronic inflammation and disease (35). TLSs can unfortunately advance from a fairly benign to a calamitous stage and lose their lymphoid organ features (44). Furthermore, the formation of TLS is reversible once the inflammatory stimulus concludes or upon therapeutics, this feature makes TLSs the most placid lymphoid organs (35).

1.3.4 TLS ontogenesis

Development of TLSs at chronic inflammation sites shadows the many pathways utilized by lymphoid organogenesis antepartum (48). Inflammation is a physiological reaction to a pathological stimulus (49). It elicits response from tissue-resident cells as well as cells of the immune system with the objective allowing cells and proteins in the vasculature to ingress damaged of infected tissues and precipitate repair (49). Even though different infectious and immune or inflammatory triggers display the same degree of chronic inflammation and inflict similar damage, their ability to induce TLSs can widely differ (48).

TLS develop in peripheral tissues of adult organism in response to unresolved inflammation, including chronic infection, cancer, autoimmune disease, and a great number of other pathologies (50). There are two hypotheses concerning the ontogeny TLSs, one which is the *antigen-driven TLS hypothesis*, the other *inflammation- driven TLS hypothesis (50)*. One hallmark of many, but not all of the aforementioned conditions may be the appearance of autoantigens that are detected by the immune system as external or non-self-antigen, this will therefore trigger an immune response (50). Nevertheless, for several TLS-associated maladies, the presence of antigen triggered immune response, or antigen-triggered disease-causing immunity has not been established(50). The alternative notion concerning TLS ontogeny is the based on the *inflammation-driven TLS hypothesis* which postulate that TLSs develop in response to an inflammatory environment in the absence of antigens (50). It is plausible that chronic inflammation can be instigated by any form of unspecific, antigen-independent tissue injury, leading in the second phase, which subsequently leads to prolonged inflammatory tissue reaction that may eventually unmask previous hidden epitopes (50). It is still unclear, however, at which stage of chronic inflammation TLSs are brought about (50). Cytokines that are linked with inflammation may be enough, in many instances, to initiate and later to shape TLS phenotypes (50). Nevertheless, there is sufficient evidence that support the hypothesis that TLS form to provide an immune response against locally displayed antigens, suggesting that TLS formation is, not just an inflammation driven process, but also an antigen driven process (47). Normally, during an immune response, the antigens are collected by APCs in the periphery, the antigens are then moving through the complex plexus of lymphatic vessels, to be drained by lymph nodes (47). Lymph node space is pre-shaped during the embryonic development and is anatomically set prior production of immune response

to contain optimal interaction between APC, antigen, and immune cells (47). TLS organization on the other hand, is not anatomically prepared to organize such a response, therefore antigens presentation is frequently arranged by non-immune cells, such as stromal cells and epithelial cells (47). Deficiency in antigen drainage could automatically explain TLS formation (47). For example, TLS has been proposed to spontaneously form in the lungs if mice deficient in CC-chemokine receptor 7 (CCR7), which is a chemokine receptor needed for the migration of antigen-charged DCs to draining lymph nodes (47). Although the ontogeny and architecture arrangement of TLSs within inflamed tissues require homeostatic chemokines, lymphoid and inflammatory cytokines, and adhesion molecules, the knowledge of the cells responsible for giving rise to these events is still not clear, it is, nonetheless, evolving (50).

TLS tend to develop more easily in infants. Accumulating evidence postulate that TLSs represent a habituation or adaptation of the body to increased requirement for a localized immune response (48). A unique type of TLS termed isolated lymphoid follicles (ILFs), that develops postnatally in the intestinal wall, via epithelial recognition of nucleotide-binding oligomerization domain protein 1 (NOD1) ligands emanates from commensals (48). This conveys that in some cases, the formation or development of TLSs could be attributable to commensals (48).

1.3.5 TLS in autoimmune diseases

TLS functions differs, as it depends on the location, stimulus and kinetics of inflammation, and cellular activation (50). The most robust evidence that TLSs are injurious in exacerbating autoimmune disease comes stem from studies in rheumatoid arthritis (50). It appears that in some patients, evidence that somatic mutation and affinity maturation takes place in the region of the TLS in the joint provides evidence for a pernicious role leading to determinant spreading (50). The presence of regulatory T- lymphocytes in some TLSs propose that they can play a beneficial role by hampering inflammation (50). Autoimmune maladies such as SLE and rheumatoid arthritis are marked by chronic inflammation in end organs that can be connected with the progression of TLSs (51). In rheumatoid arthritis, TLSs are observed in the inflamed synovium of about half of the biopsies precured from patients and are linked with more sever joint and systemic inflammation (51). TLSs are further observed in other organs in other various autoimmune diseases, such as the salivary and lacrimal gland in Sjogren's syndrome, the central nervous system in multiple sclerosis (MS), the pancreas in diabetes, etc. (51). In infectious settings, TLSs have been postulated to be

protective, as it adopts SLO-like functions (51). TLSs developed in the lung of influenza infected mice can maintain and reactivate memory CD8+ T-lymphocytes and produce plasma cells and antiviral serum immunoglobulins (51). Remarkably, even though there is a slight delay in anti-viral immunity development, TLSs are enough for protection when the hosts have inadequate SLOs, accentuating the idea that TLSs can produce effector cells that provide effective host defense (51). TLSs developed in SLE kidneys have germinal centers that show clonal expansion and somatic hypermutation that are archetypical of germinal center responses in SLOs, demonstrating well-developed effector responses (51). Nevertheless, TLSs are strongly associated with the presence of immune complexes, implying that the locally generated autoantibodies to renal antigens can activate complement and therefore cause tissue inflammation and tissue damage (51). Comparably, B-lymphocyte responses correlated with TLSs in rheumatoid arthritis synovium, the salivary gland in Sjogren's syndrome(SS), and other target tissue demonstrate autoimmunity (51). Furthermore, SLE kidneys and rheumatoid synovium are also distinguished by the aggregation of T-helper 17 cells (Th17 cells), which have proinflammatory roles (51). Although IL-17 expressing cells could help to trigger the formation of TLS, the TLSs formed could in all probability also aid to support Th17 cell maintenance or acquirement of supplementary proinflammatory properties (51). B-lymphocytes in TLSs may be pathogenic, as it can stimulate autoreactive T-lymphocytes, which consecutively can contribute to the inflammatory environment in the affected end organs (51). In autoimmune diseases, TLSs can thereby be source of potentially pathogenic lymphocytes (51). Nevertheless, TLSs could in addition possess a protective role by sequestrating pathogenic lymphocytes thus hindering them form exiting the specific region or tissue compartment to cause further harm(51). For instance, in SLE, glomerular damage is unassociated to the degree of interstitial inflammation (51). Glomerular damage is instead associated with failure to sequestrate lymphocytes within the interstitial tissue, this could potentially result in the relocation of lymphocytes to the glomeruli thereby exacerbating glomerular damage (51). Sequestration of prospectively pathogenic cells may thus aid to limit the degree disease (51). Alternately, when TLSs are lacking, the lymphocytes could potentially ingress the circulation where they can quite possibly cause more damage to other organs external to the kidneys (51). Additionally, TLSs can have protective qualities if they provide a microenvironment that engenders regulatory or reparative cells that decrease or minimize the pathogenicity or inflammatory cells (51). When TLS evolves in response to viral infection it contributes to the

production of antiviral immunity and can thereby be regarded as beneficial for the host (52). TLSs that develop in autoimmune diseases may facilitate the activation of autoreactive cells (52).

DCs in TLSs frequently possesses an active phenotype, implying that they are the principal APCs stimulating autoimmunity(48). TLSs permits the secretion of naïve T-lymphocytes, allowing their differentiation into effector T-lymphocytes upon presentation to or upon contact with DCs (48). A significant constituent of TLSs are the B-lymphocytes that aggregate on the FDC plexus. Plasma cells are found near the TLSs and secrete antibodies specific for the pathogens that induced the TLS (48). The presence of TLSs in different models of chronic autoimmunity as well as in transplant rejection and their connection with tissue damage, has led to the proposition that they are paramount inductive zones for self-reactive T-lymphocytes, and antibodies that engenders pathology (48). When TLSs form at sites where autoantigens are perpetually being presented, they may lead to unwarranted tissue damage by facilitating the activation of autoreactive lymphocytes (52). This, for example, happens in non-obese diabetic (NOD) mice that spontaneously develop type 1 diabetes mellitus (T1DM) as a result of destruction of insulin secreting pancreatic islet cells by autoreactive T-lymphocytes (52). There is continuous development of TLSs in the pancreas during diabetes advancement in NOD mice (48).These TLS that develop in the pancreas provide a milieu for the proliferation of autoreactive T cells, thereby supporting the supposition that autoantigen is locally presented (52). Moreover, the formation of these TLSs seems to correspond with the development of diabetes, oppositely, when occluding or blocking their formation obviates the development of diabetes (52).The expansion of B-lymphocytes inside an single TLS around islets is regularly oligoclonal, which indicates the presence of autoantigen (48). TLSs in humans might contribute to the disease continuance in autoimmunity as well as in transplant rejection. In the lungs of patients with rheumatoid arthritis, B lymphocytes in the TLS produce rheumatoid factor (RF) and antibodies against deimination proteins, which are typical self-antigens in the rheumatoid arthritis (48). A study on SLE, conducted by Chang *et al*. reported a repertoire of B-lymphocytes expressing isotype-switched antibodies are deposited the basement membrane of the glomerulus (53). Additionally, TLSs have been discovered in the meninges of patients with secondary progressive MS, a more aggressive characteristic of SLE (48).

1.4 General architectural anatomy of Salivary gland and its function

The human salivary gland system is fractionated into two distinct exocrine groups; the major and the minor salivary gland (54). The major salivary glands are constituted of the paired parotid, submandibular, and the sublingual glands (54). The minor salivary glands which are subsets of the major salivary glands are largely dispersed in the oral mucosa and the posterior third of the tongue, cheeks, and palate (**Figure 5**) (1).

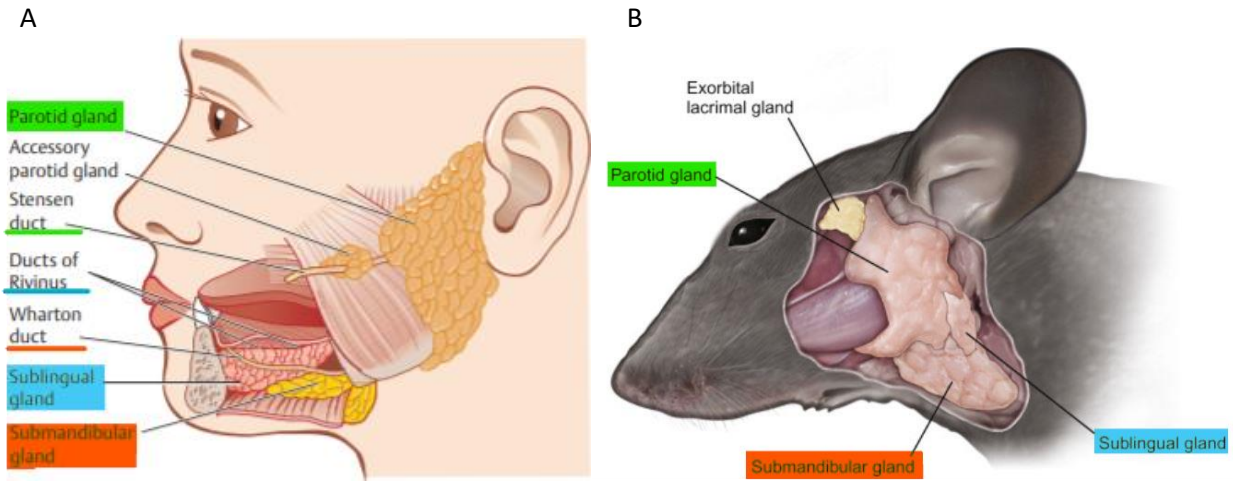

Figure 5: Anatomic overview of salivary gland. (A) *the position of the major glands in the human cranium.The parotid, sublingual, and submandibular glands with their corresponding ducts are delineated.* ***(B)*** *Overview of the mouse salivary glands, which are conjunctly situated in the cervical neck. The anatomical arrangement of the submandibular, sublingual, and paratoid salivary glands are illustrated. The submandibular salivary glands are located in the central region of the cervical neck, the sublingual salivary glands are positioned atop the submandibular glands while the parotid salivary glands are situated obliquely and outstretch to the base of the ear. Figure A is taken from Bradley PJ (1). Figure B is taken from Figure 2 by Treuting PM(55).*

The largest glands of the major salivary glands are the paired parotid glands, which weighs approximately 15-30 g (54). Situated in the preauricular region and along the posterior surface of the mandible. Each parotid gland is divided into two components by the facial nerve, a superficial and a deep lobe (54). The superficial lobe is the part of the gland lateral to the facial nerve, while the deep lobe is medial to the facial nerve and is situated between the mastoid process of the temporal bone and the ramus of the mandible (54). Stensen duct is the central duct of the paired parotid gland, this duct empties into the buccal cavity lateral to the second molar (1). The Stensen

duct secretes serous saliva into the chamber, or vestibula rather, of the oral cavity (54). From the anterior border of the gland, the serous saliva travels parallel to the zymogma, in an anterior direction across the masseter muscle(54). The serous saliva then turns dashingly and pierce the buccinator muscle where it finally enters the oral cavity across from the second upper molar tooth (54)

The submandibular gland is the second largest major salivary gland and weighs on average 7- 16 g (54). The gland is situated in the submandibular triangle, which has a superior boundary and inferior boundaries (54). The superior boundary is formed by the inferior edge of the mandible while the inferior boundaries are formed by the anterior and posterior bellies of the digastric muscle (54). The submandibular gland is fractionated by the mylohyoid muscle into superficial and deep lobes (1) where most of the submandibular gland is located posterolateral to the mylohyoid muscle (54). The main excretory duct of the submandibular gland is known as the Wharton duct, and it is located on the superficial portion of the gland (**Figure 5A**)(1). The duct of the Wharton duct is roughly 4-5 cm long (54). The ducts are attached around the mylohyoid muscle and proceed along the superior surface (1). The submandibular gland has both mucous and serous cells, these cells drain their precious commodity into ductules, which sequentially empty into the submandibular duct (54). The ducts eventually drain into the sublingual caruncles on either side of the lingual frenulum (1) through a papilla on the floor of the mount behind the lower incisor tooth (54).

The sublingual gland is the smallest of the major salivary glands, weighing approximately 2-4 g (54). The sublingual gland is a composite structure composed of one large segment and a group of 8-30 mixed minor glands, each possessing its own opening into the sublingual fold (1). The sublingual gland constitutes mainly of mucous acinar cells (54). The gland lies as a flat structure in a submucosal plane within the anterior floor of the mouth, superior to the mylohyoid muscle, and deep to the sublingual folds across from the lingual frenulum (54). The major glands are encircled by a connective-tissue capsule, while the minor glands have no capsule (1) but are instead concealed by oral mucosa (54). The minor sublingual ducts are acknowledged as the ducts of Rivinus while the main duct of the sublingual duct is well-known as the Bartholin duct (**Figure 5A**)(1). The sublingual gland produces mucus-rich saliva, which is rather more viscous and coats the oral cavity (1). The Bartholin duct coalesces the Wharthon duct to secrete through the

sublingual caruncle (1). Several ducts of Rivinus, on the other hand, either drain directly into the floor of the mouth or secrete into Bartholin's ducts which then goes on into Wharton's duct (54).

The anatomical structures of all three glands are substantially similar, all glands possess a ductal formation with a treelike branched architectural appearance (56). These ductal structures open into the oral cavity with secretory end segments, the acini, which are responsible for the saliva production (56). The acini, also called the salivary acinus, can be categorized into three main types; serous acini, mucinous acini, and mixed or preferably seromucous acini (54). Serous acini in the salivary gland are practically spherical and discharge via exocytosis a liquid-like protein secretion that is minimally glycosylated or non-glycosylated from secretory granules (54). The acinar cells that constitute the serous acini are pyramidal in shape, with basally located nuclei enveloped by sense cytoplasm and secretory granules that are most ample in the apex (54). Mucinous acini deposit a viscous, mucilaginous glycoprotein (mucin) within secretory granules, and upon release, the mucin becomes hydrated to form mucus (54). Mucinous acinar cells are generally simple columnar cells in structure with flattened, basally positioned nuclei and water-soluble granules which give it a clear intracellular cytoplasm appearance (54). The mixed, or seromucous acini, on the other hand, is an amalgam of both types containing components of both the serous and mucinous acini. Nonetheless, one type of secretory unit may dominate (54). Seromucous secretory units are, however, frequently distinguished as serous demilunes (half-moons) eclipsing mucinous acini (54). The acinar cells are encircled by an extracellular matrix, myoepithelial cells, myofibroblasts, immune cells, endothelial cells, stromal cells, and nerve fibers (56). The myoepithelial cells form a latticework and are endowed with cytoplasmic filaments on their basal side to assist in contraction and secretion of the acinus (54). As previously mentioned, the parotid gland contains only serous acini, while the sublingual and submandibular contains a mixture of both serous and mucous acini (1). Nevertheless, the submandibular gland has a ratio of serous acini to mucous acini of 7 to 3 (1). Whereas the major sublingual gland merely possesses a few serous acini that are scattered within the gland (1).

The salivary gland ducts are comprised of several well-defined segments, each with a segment with its unique morphology and function (1). These distinct segments of the salivary gland's duct system are responsible for electrolyte modification and transportation of saliva (54), before it is exuded into the oral cavity (56). The acini will first and foremost be secreted through microscopic

channels into the intercalated ducts (54). The intercalated ducts in succession drain into the striated ducts which lie within the glandular lobule (54). The striated ducts sequentially secrete into the larger collecting excretory ducts (1). The intercalated duct is distinguished by the cuboidal epithelium (1). The duct is quite small with rather prominent nuclei, the adjacent cells are linked by desmosomes (1). Bicarbonate is secreted into the segment, while chloride is absorbed from the acinar product within the intercalated duct segment (54). The striated ducts are highly polarized and possess short microvilli on the luminal surface, their nuclei are centrally located (1). Striated ducts have characteristic basal striations, this is due to the membrane invagination and mitochondria packed in between the membrane folds (1, 54). Striated ducts are lined by simple columnar epithelium with a large surface area (1, 54). These ducts play a role in the reabsorption of sodium from the primary secretion and accompanying secretion of potassium into the product (54). Chloride ions are, also, reabsorbed, while bicarbonate is secreted in this part of the duct, indicating that the electrolyte composition of the saliva is orchestrated or handle rather, in these ductal regions (1). The copious mitochondria presence is incumbent so the ducts can transport both water and electrolytes (54). Additionally, the striated ducts also function to secrete organic product, which is quite evident due to the presence of secretory granules in the duct cytoplasm (1). Collectively, the acinus, intercalated duct, and striated duct are known as a single secretory segment called a salivon (**Figure 6**)(54).

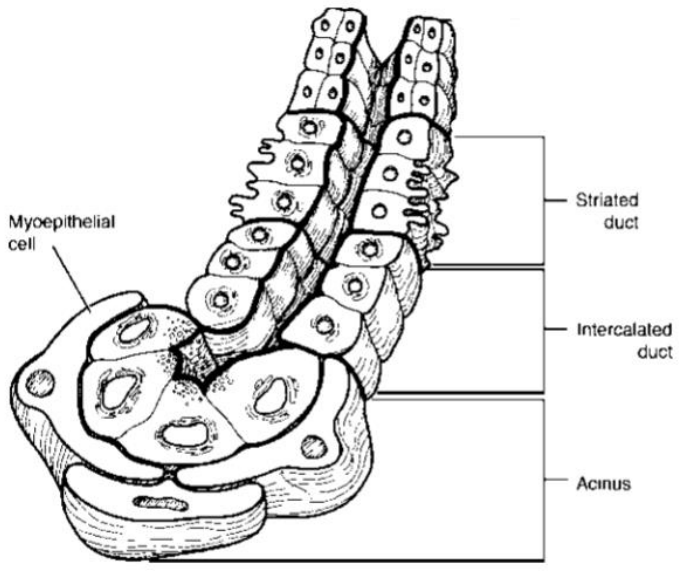

***Figure 6: Illustration of the acinus with the myoepithelial cell, the intercalated duct, and the striated ducts, collectively recognized as the salivon. The figure is taken from Myers & Ferris* (54).**

The next unit of the duct system is the excretory ducts, or collecting ducts, which is distinguished by the semblance of the interlobular excretory ducts within the connective tissue of the glandular septae (54). The epithelial lining constitutes of thinly dispersed gobbles cells scattered amidst the pseudostratified columnar cells (54). The epithelial lining composition transitions to a stratified columnar as the diameter of the duct increases (54). They further transition to nonkeratinized stratified squamous cells, within the oral cavity (54).

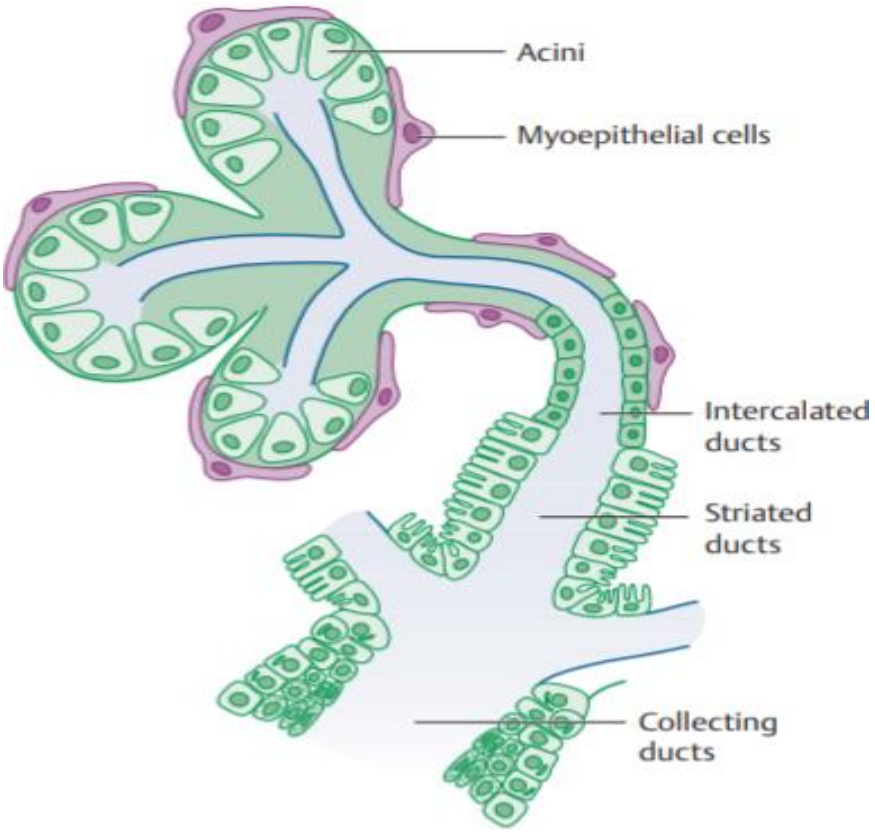

Figure 7: Illustrative representation of the salivary gland, delineating the acini, the salivon, and the arrangement of the collecting ducts. The figure is taken from Bradley et al.(1).

The distribution of acini and ducts varies within the salivary gland, as each gland has a different length of different duct types (1). The submandibular gland has rather shorter intercalated ducts and longer striated ducts compared to the parotid gland (1). The sublingual gland on the other hand has a less complex duct system, with either no striated ducts or only limited striated ducts (1).

The acini and intercalated ducts are enveloped by myoepithelial cells (**Figure 7**). Around the acini, the myoepithelial cells have a starlike, dendritic appearance, with long projections forming a

basket (1). The cells appear elongated around the intercalated ducts (1). It has been proposed that the myoepithelial cells have a contractile role and that they aid in saliva secretion by compressing the acini and thus speeding the outflow of saliva (1). Furthermore, the myoepithelial cells play a supporting role, by contributing to secretory pressure and reducing luminal volume (1).

The salient function of the salivary gland is naturally saliva production. It is essential and serves as a significant function in the process of digestion, lubrication (54). Not only does saliva possess a protective function, but it also cleanses the oral cavity, remineralizes the enamel of the teeth, stimulates wound healing, dissolves tastants, helps in the maintenance of taste buds, etc (1). Saliva aid in dissolving and transporting food particles away from taste buds to increase taste sensitivity (54). The lubrication of saliva serves to ease the swallowing processes and of the bolus migrating down the esophagus (54). Moreover, salivary lubrication is also quite imperative for speech (**Figure 8**) (54).

Figure 8:Schematic diagram of saliva functions. The figure is taken and modified from Bradley PJ (1).

Saliva is actively produced in high volumes corresponding to the mass of the salivary glands (54). Salivary production is practically entirely controlled extrinsically by both the parasympathetic and sympathetic division of the autonomic nervous system (54). Even though it is commonly thought that salivary secretion is exclusively under neural control, neoteric studies have unveiled that some gastrointestinal hormones do play a role in the controlling of secretion, thus influencing the responsiveness of glands (1).

Saliva plays a pivotal role in the digestion of carbohydrates and fasts through two chief enzymes, ptyalin, and lingual lipase (54). Ptyalin is an α-amylase in saliva, this enzyme splits the internal α-1,4-glysidic bonds of starches to yield maltose, maltotriose, and α-limit dextrins (54). The enzyme functions at an optimal pH of 7, and when exposed to a pH less than 4, the enzyme will quickly denature (54). A good example of this is when the enzymes come in contact with the acidic secretions of the stomach (54). However, approximately 75% of the carbohydrate content in a meal is fragmented by the enzyme within the stomach itself (54). The reason is that a big portion of an ingested meal remains unmixed with the oral region, and therefore it is delayed in the mixture of gastric juices in the food bolus (54). Nonetheless, the absence of ptyalin does not slow starch digestion, because pancreatic amylase is indistinguishable from salivary amylase and is therefore capable of breaking down all carbohydrates in the small intestine (54). The enzyme lingual lipase, from salivary glands of the tongue, has a function of breaking down triglycerides (54). Contrary to ptyalin, lingual lipase is very well functional within the acidic environment of the stomach and proximal duodenum due to the enzyme being optimally active at a low pH (54).

Saliva possesses besides antibacterial properties, which are due to its many protective organic constituents (54). The binding glycoprotein for immunoglobulin A (IgA), known as a *secretory piece*, forms a complex with IgA that is immunologically active against virus and bacteria (54). Furthermore, saliva also serves as a protective buffer for the mouth, it does so by diluting harmful substances and lowering the temperature of solutions that are very high in temperature (54). As well as this, saliva aid in washing out foul-tasting substances from the mouth (54). It also serves as a neutralizing agent, by which it neutralizes gastric juice to protect the oral cavity and esophagus (54).

In both mice and humans, there are three pairs of major salivary glands and several minor glands (3). The three major salivary glands that are grossly visible in both species are the parotid, submandibular, and sublingual gland (**Figure 5)**(3). The secretions of saliva may be serous, mucous, or mixed, and these salivary secretions have comparable functions in mice and humans alike (3). In mice, the submandibular (submaxillary) gland, located on the ventral midline of the neck, is the largest (**Figure 5B)**(3). The submandibular gland is multilobed and lobulated, it is rostrally encircled by the submandibular lymph node (3). Additionally, the submandibular gland abuts the sublingual gland and extends dorsally to the parotid gland (3). In contrast to mice, the

parotid gland is the largest of the salivary glands in humans (3). Nonetheless, the three major salivary glands in both species have a homogenous anatomic architecture (3). However, mice have a distinctive ductal organization in the submandibular gland, which constitutes the granular convoluted ducts coupling the intercalated to the intralobular ducts (3). Furthermore, this segment of the duct within the submandibular salivary gland has a characteristic sexual dimorphism in the mouse, which is testosterone dependent (3). The cells that line the duct are large, columnar cells that comprise distinct bright pink granules, in females, on the other hand, the cells are rather smaller with less prominent granules (3).

1.5 General architectural anatomy of pancreas and its function

The pancreas is an elongated organ, approximately 12-20 cm in length in adults (**Figure 9A**)(57). It has a thin conical formation extending from its head (58). The head occupies the space formed by the concavity of the duodenum, the tail is situated in the left hypochondrium near the hilum of the spleen (58). The main pancreatic duct nexus the distal end of the bile duct to open into the lumen of the duodenum at the ampulla of Vater (58). The pancreas, also known as an accessory organ of the digestive system, has both exocrine and endocrine functions (59). It has a thin connective tissue capsule and is arranged into lobules by connective tissue septa (60).

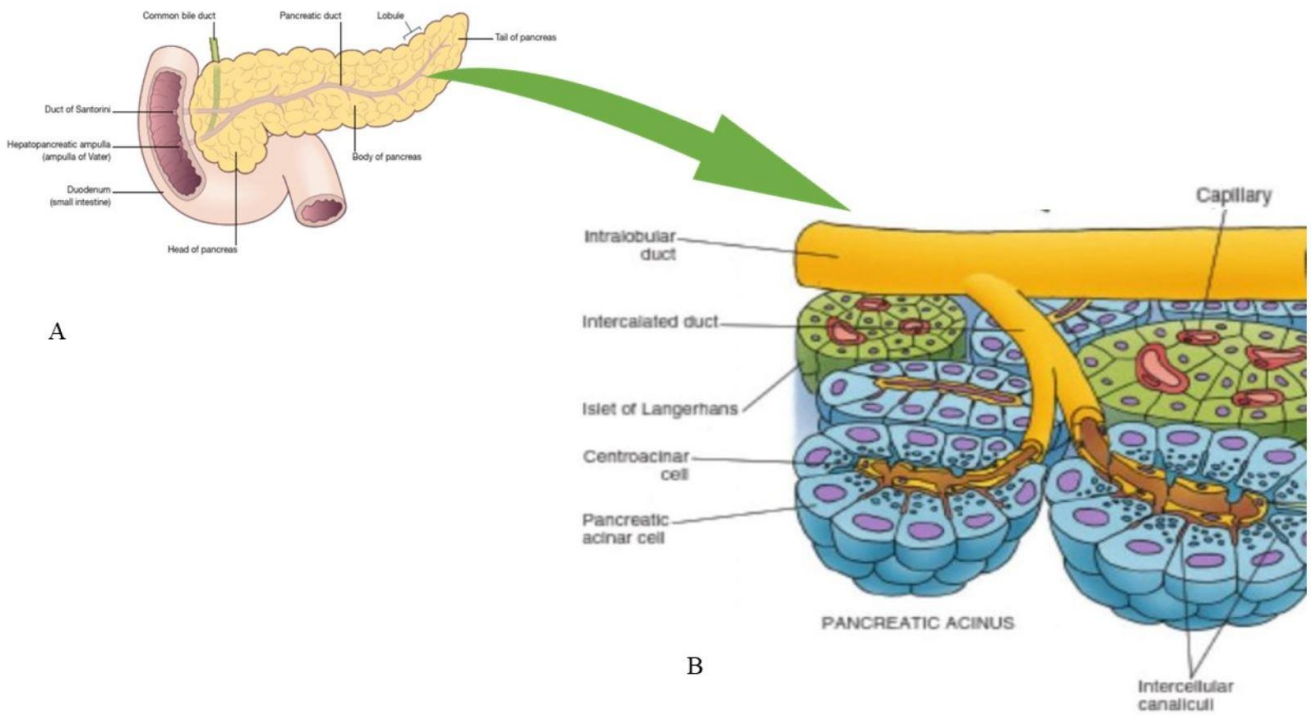

Figure 9: Diagram of the pancreas. ***(A)*** *exhibiting the pancreatic acinus* ***(B)*** *with their various cell types and the endocrine islets of Langerhans. Pancreas is also known as an accessory digestive gland, situated posterior wall of the abdominal cavity, its head is located in the concavity of the duodenum, while its neck, body and tail extends diagonally or obliquely to the spleen (37). Figure A is taken from figure 29.1 by Peate (61). Figure B is taken from figure 18-5 by Gartner (62).*

The exocrine pancreas comprises a collection of a conglomeration of compound tubule-acinar glands that drain into the system duct, which eventually empty into the duodenum at the hepatopancreatic ampulla (59). The exocrine cells are columnar epithelial cells, they are organized as acini or tubules (60). Each acinus consists of 45-50 pyramidal-shaped epithelial cells (59). The cells are in turn radially arranged around a central lumen and enwreathed by a basal lamina (59). The acini cells are composed of protein secreting cells (pancreatic acinar cells) which have a broad base and a narrow apical surface capped by a few short microvilli (58). The pancreatic acinar cells are rich in the rough endoplasmic reticulum (RER) and are primarily concentrated in the lower half of the cell (58). The copiousness of the RER is responsible for the cytoplasmic basophilia of the pancreatic acinar cells (58). The upper half of the pancreatic acinar cell close to the lumen consists of variable numbers of eosinophilic zymogen granules, which contain the pre-enzymes synthesized by the cell (58). The number of zymogen granules differs with food intake, it is highest

in fasted individuals (59). Each acinus is emptied by an intercalated duct, which is lined by light, low cuboidal cells called centroacinar cells (59).

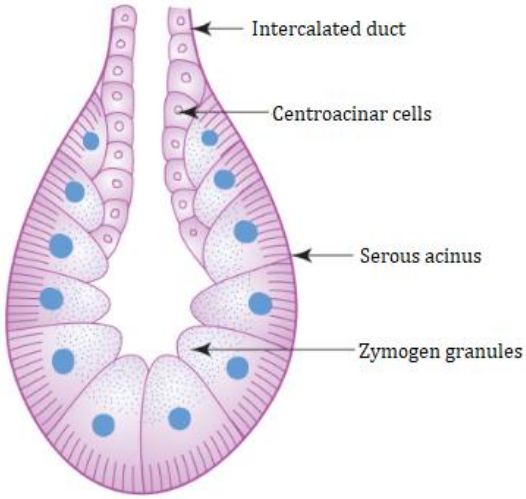

Figure 10: Schematic depiction of pancreatic acinus displaying the zymogen granules, centroacinar cells, and intercalated duct(59).

The centroacinar cells are the primary cells of the intercalated duct, they penetrate the lumen of the acinus and are the characteristic features of the exocrine pancreas (59). The centroacinar cells are lined by a simple monolayer of cuboidal epithelium, forming a complex network (**Figure 10**)(58). The pancreatic ductal system commences in acinus (58). The intercalated ducts from every isolated acinus will coalesce thus forming larger interlobular ducts (58). The interlobular ducts then run in the fibrocollagenous septa between the indistinct pancreatic lobules and are then lined by columnar epithelium (58). Ducts amalgamate within the lobules and, as beforementioned, they ultimately all concatenate and form a single pancreatic duct (60). As stated previously, the pancreatic duct then joins the bile duct and both the bile and pancreatic juices empty into the duodenum (60).

The endocrine part of the pancreas is composed of *islets of Langerhans,* they are more in the tail region of the pancreas (63). There are around 1-2 million *islets of Langerhans* and they amount to only 1-2 % of the gland and are dispersed among the acini of the exocrine pancreas (59). Each islet is a spherical aggregate of several hundred polygonal cells surrounded by a thin layer of reticular connective tissue (59). Cells are organized in irregular cord separated by fenestrated

capillaries(59). Moreover, each islet is only about 0.3 millimeter in diameter, and are structurally arranged around small capillaries by which its cells are capable of secreting their hormones (17).

The islets consist of three principal types of cells, alpha, beta, and delta cells (**Figure 11**). These cells are differentiated from one another by their morphological and staining attributes (17). The beta cells comprise 60% of all the cells of the islets (17). Beta cells are small cells with basophilic granules, they are mostly situated in the middle of each islet and secrete insulin and amylin (17, 63). Amylin is a hormone that is frequently secreted in parallel with insulin, unfortunately, its function is not fully apprehended and not well established (17). The alpha cells constitute about 25% of the total population (17). Alpha cells are large cells with eosinophilic granules, they are found for the most part at the periphery of the islet, and they secrete glucagon (63). Delta cells comprise 10% of the cell population and secrete somatostatin (17). Additionally, there exists another cell population, the *PP* cell, which represents a small number in the islets and secretes a hormone of unknown function called pancreatic polypeptide (17).

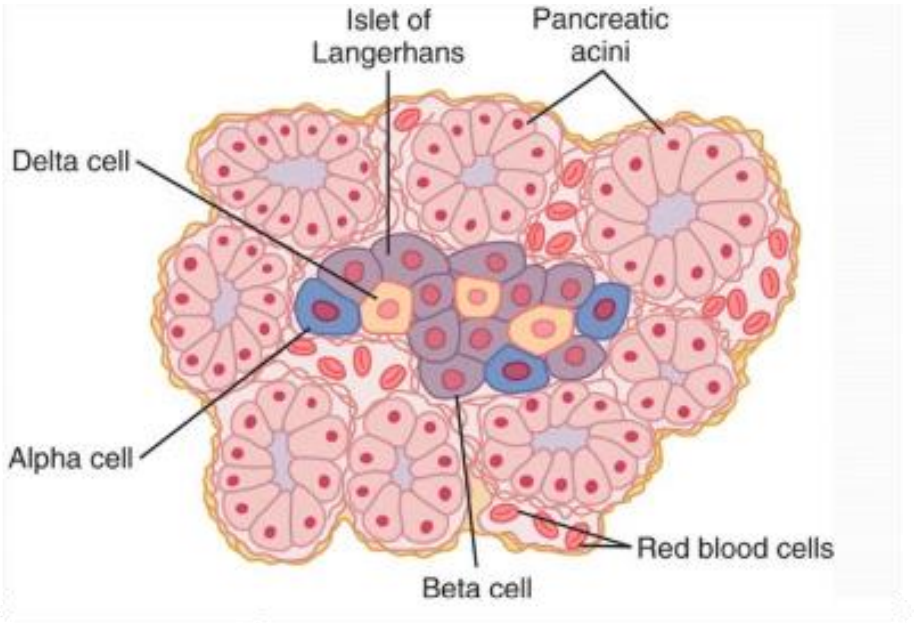

Figure 11: Diagram illustrating the anatomic organization of the Islet of Langerhans, the endocrine part of the pancreas(59).

The pancreas of the mice and humans have a lot of congruences than it does incongruity (3). A fundamental difference between the two species is that pancreas of the mouse is regionally

scattered throughout the mesentery abutting the duodenum (3). In humans, however, the pancreas, although ordinarily in the same locality, is compressed (3). Other important dissimilarities are the pancreatic islets; mice have larger and predominantly interlobular pancreatic islets in opposition to smaller, broadly intralobular islets observed in humans (3). Additionally, there are further marked species differences in the organization of the pancreatic ducts, as it intrudes into the duodenum (3). Moreover, the arrangement of the blood vascular system and the flow it takes to supply and egress the exocrine and endocrine segments of the pancreas also differs between the two species (3).

1.6 Architectural anatomy and function of the lungs

The respiratory system, in tandem with the circulatory system, is in charge of supplying all the cells of the body with oxygen, which is vital for the survival of the human body (6). The respiratory system is also responsible for removing pernicious carbon dioxide from the body (6). As the air enters the nostrils, occasionally through the mouth, it flows through the nasal cavity which cuts through the skull and finally enters the posterior of the pharynx (6). Only air is transported through the first portion of the pharynx, yet lower down, food and liquids pass through (6). The larynx, ordinarily known as the voice box, joins the pharynx to the trachea (6). Epiglottis, which is a flap of cartilage, is situated above the larynx, it descends over the opening of the larynx during ingurgitation, thus hindering food, liquids, and saliva from accessing the trachea (6). The human trachea has a total of 15-20 incomplete U-shaped cartilaginous rings, these are beneficial as they aid in supporting the trachea (31). The open aspect of the U-shaped cartilaginous rings is positioned caudally and is sealed by a thin fibromuscular membrane that connects the free ends of the rings (31). The cartilaginous aspect of the trachea provides robustness to the airway, preventing the trachea from collapsing, while the flexile caudal aspect allows the expansion of the esophagus as food traverse down to the stomach (31). The trachea is fractionated into two airways termed primary bronchi (6). One of the bronchi enters the left lung and the other the right lung, respectively (6). Each bronchus is further fractionalized into secondary and tertiary bronchi, which ultimately branches out into petite bronchioles (6). In humans, the right main bronchus is shorter, wider, and more vertical in direction than left bronchus (31). The right bronchus subdivides into three lobar bronchi that accordingly supply the three right pulmonary lobes (31). The human segmental bronchi, which contains cartilage, branches out into primary bronchioles that do not

possess any cartilage (31). The left bronchus on the other hand is segmented into two lobar bronchi (31). Each lobar bronchus further subdivides into different tertiary bronchi that supply the bronchopulmonary segments (31). The right lung has 10 bronchopulmonary segments and the left lung has about 8-10 bronchopulmonary segments (31). The bronchioles eventually transition into terminal bronchiole, which supplies the respiratory zone where gas exchange takes place (31). The part of the lung in which the terminal bronchiole supply is termed the acinu (31). The acinus represents the functional unit of the lung in which gas exchange transpire (31). Each respiratory bronchiole, in humans, engenders 2-11 alveolar ducts, from which stem about six alveolar sacs (31).

Although the whole respiratory system is fascinating, it is also a rather broad subject in itself. Therefore, this section focuses simply on the anatomy and function of the lungs.

Lungs are the significant organs of the respiration (11), the lungs are a duo and spongelike, filling a large part of the chest cavity (6). They are situated on each side of the chest, parted from each other by the heart and other components of the mediastinum (11). Structurally, each lung is cone-shaped consisting of an apex, a base, two borders, and two surfaces (11). The apex stretches into the root of the neck, reaching about 2.54 cm to 1.27 cm and a half above the level of the first rib (11). The base of the lung is wide, concave, resting upon the convex exterior of the diaphragm (11). Each lung is sectioned into distinct sections called lobes (61), an upper and a lower lobe, it is divided by a long and deep fissure (11). The fissure extends from the upper part of the back border of the organ, about 7.62 cm from its apex, downward and forward to the lower section of its anterior border, nearly piercing the root (11). The upper lobe of the right lung is somewhat fractioned by another and shorter fissure (11). The right lung is grander, heavier, broader in comparison to the left lung, the reason being the inclination of the heart to the left side (11). It is also shorter by 2.54 cm, as a consequence of the diaphragm ascending higher on the right side, as it provides accommodation for the liver (11). The root of the lungs is situated a bit above the inner surface of each lung, nearer to the back than the front border, and it is attached to the heart and the trachea (11). Structures that make up the root of the lung include the bronchial tube, the pulmonary artery, the pulmonary veins, the bronchial arteries and veins, the pulmonary network of nerves, lymphatics, bronchial glands, and are areolar tissue, all of which are contained by the pleura reflection (11).

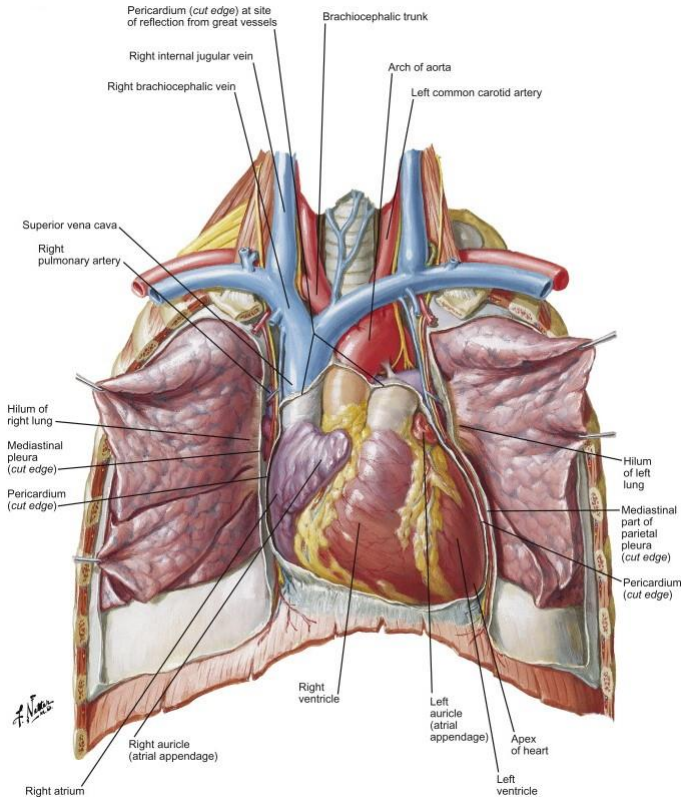

Figure 12: Reginal anatomical overview of the human lungs. *Overview of the lung displaying the right lung, which comprises three lobes, the left lung consisting of two lobes. Other constituent parts of the of the lungs are also displayed. Figure from ref (64).*

The root of the right lung lies in the rear of the superior vena cava and ascending part of the aorta and below the vena azygos major (11). In contrast, the root of the left lung goes below the arch of the aorta and passes in front of the descending aorta (11). Each lung is enveloped by two thin protective membranes, the parietal and visceral pleura (61). The parietal pleura covers the wall of the thorax while the visceral pleura lines the lungs (61). Between the two pleura is a thin film lubricating fluid that aids in reducing friction amidst the pleura as they glide over one another during the course of breathing (61).

Various anatomical and histological dissemblance exists between mouse and human (31). The majority of the dissemblance in mouse and human lungs are due to species differences in size, metabolic rate, and respiratory rate (31). Mice have a higher basal metabolic rate and an expeditious respiratory rate than humans (31). It is suggested that the mice's large airway caliber decrease the airway resistance that would, under other circumstances, occur in mice due to their rapid respiratory rate of 250-350 breaths per minute (31). The right lung in mice is subdivided into four lobes, while the left lung only has one lobe (**Figure 13**)(31).

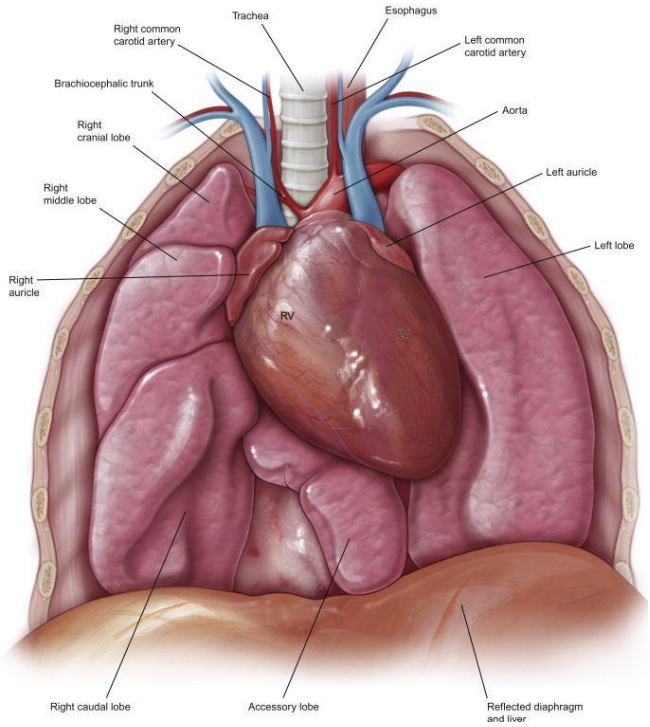

Figure 13: Reginal anatomical overview of the mouse lungs. *Overview representation of the structure the right lung, which comprises four lobes: accessory, caudal, middle, and cranial lobe. the left lung of the mouse consists of a single lobe. Figure taken form figure 1A from Suarez (65).*

The four lobes are the cranial, middle, caudal, and accessory lobe (32). The bronchi of the mice divide to form secondary bronchi, then bronchioles, terminal bronchioles, and finally alveolar ducts (32). The two extrapulmonary bronchi in mice ingress the right and left lungs where they then bifurcate into the intrapulmonary bronchi (31). The extrapulmonary bronchi in the mouse have cartilage rings, and intrapulmonary bronchi in mice do not have cartilaginous rings (32). Additionally, it is the intrapulmonary bronchus divides to supply the four lobes of the right lung, while the left intrapulmonary bronchus branches to purvey the left lung (31). Mice do not have distinct respiratory bronchioles, instead the terminal bronchiole in mice verge directly into the alveolar duct (32). In contradistinction to human, mice possess just a few or no respiratory bronchioles, which subsequently means that mice possess fewer airway generations than do humans (31). Furthermore, the parenchyma of mice lungs constitute a great portion of the total lung volume, 12 and 18% for humans and mice, sequentially (31).

1.7 Architectural anatomy of the spleen and its function

The spleen comprises a large encapsulated mass of vascular and lymphoid tissue located in the upper left quadrant of the abdominal cavity in the middle of the fundus of the stomach and the diaphragm (66). The spleen evolved as part of the vascular system in the part of the dorsal mesentery that suspends the evolving stomach from the body wall (67). The shape of the spleen is for the most part based on its relations to neighboring structures during the course of splenic development (66). The shape of the spleen, therefore, varies from a slightly curved wedge to a "domed" tetrahedron (**Figure 14**)(66). The superolateral aspect of the spleen is fashioned by the left dome of the diaphragm (66). The shape of the inferomedial aspect of the spleen on the other hand is influenced predominantly by the neighboring splenic flexure of the colon, the left kidney and, the stomach (66). Its long axis lies roughly in the plane of the tenth rib, its posterior border is around four cm from the mid-dorsal line at the level of the tenth thoracic vertebral spine (66). The weight and size of the spleen vary tremendously (68). Nonetheless, the average weight of the spleen in adults is estimated to be is approximately 180 g in adult males and around 140 g in adult females (69). Nevertheless, the normal range of the spleen is quite wide, ranging between 80 g and 300 g, the size is in part directly proportional to the amount of blood the organ contains (66). Moreover, the spleen is generally about 12 cm long and 7cm broad, it is nearly the size and shape of a clenched fist (68). The size and weight of the organ vary with age, sex (66), and the size and weight of the spleen generally decrease in older people and certain various conditions (69). In some diseases, the spleen can become enlarged weighing about 2000 g or more (69).

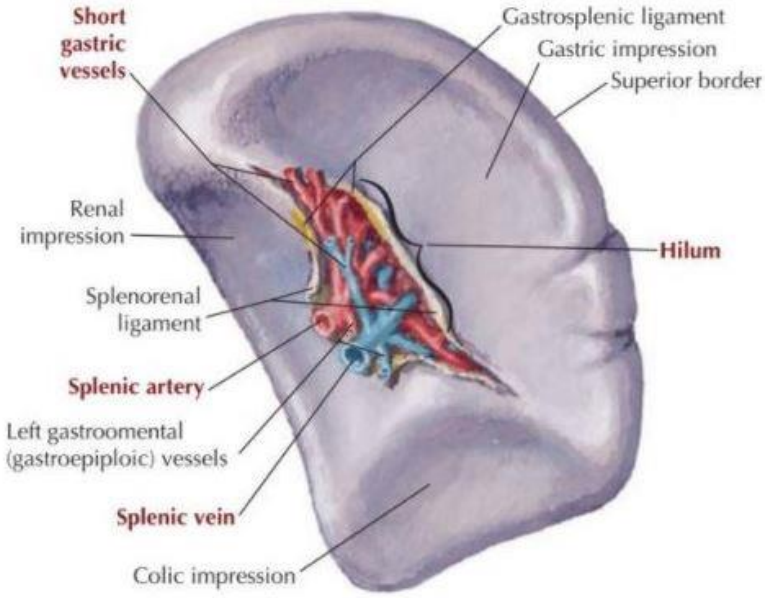

Figure 14:Diagram of the spleen. *Visceral surface of the spleen displaying the hilum, splenic artery, splenic vein, various ligaments as well as architectural components of the spleen(37).*

The whole spleen, except the hilum, is enveloped by peritoneum (68) that intimately adheres to its capsule. It is detached from the stomach and left kidney by recesses of the greater sac (66). The hilum of the spleen abuts against the tail of the pancreas (68). It is through the hilum that the vessels and nerves ingress and egress the organ (70). The spleen represents the largest aggregation of reticuloendothelial tissue in the body (70). The fibrous tissue of the capsule stretches out all the way into the spleen where it forms a series of trabeculae (70). The connective tissue capsule is a continuous layer of about 1.5 mm thick, possessing abundant type 1 collagen fibers and some elastin fibers (66). The capsule has an outer and inner lamina where the direction of the collagen fibers varies, which consequently intensifies its strength (66). Within the spleen, the trabeculae, which extends from the capsule (66), subdivides into small, interconnected compartments (69) which ultimately forms a supportive architectural plexus (66). The largest trabeculae ingress at the hilum, it supplies a conduit for the splenic vessels and nerves, sectioning into units/branches in the splenic pulp (66). Arteries, veins, and lymphatic vessels run through the trabeculae to supply each compartment with blood and nutrients (69). These vessels are abundant in the white and red pulp (69). These units or branches within the spleen become unceasing with a network of type III (reticular) collagen fibers (66). This network of type III collagen fibers fills both the red and white pulps and it is excreted by fibroblasts within its meshes (66). The spleen is, categorically, the

largest lymphoid tissues of the body (71). Even though the spleen's anatomical architecture is intricate, the organ still has several histologically unambiguous regions (71). The clearly defined regions, on a grand scale, are the red and white pulps (71). In addition to that, three other sites within the white pulp are easily identifiable; these sites include the marginal zone, the periarteriolar lymphoid sheath (PALS), and unequivocally, the follicle (71).

White pulp is lymphatic tissue that encircles the arteries within the spleen (69). The white pulp is segmented into three regions, the marginal zone, the PALS (72), and lymphoid nodules which include primary and secondary follicles (73). Altogether, the white pulp constitutes about 5-20% of the splenic parenchyma (73). In the spleen parenchyma, branches of the splenic artery penetrate the hilum within the trabeculae, furcating, and narrowing to arterioles (66). When the arteries and arterioles alike exit the trabeculae to enter the parenchyma (33), their connective tissue adventitia in the terminal is instantly encircled by a sheath of T-lymphocytes, the PALS (66). As these small arterioles branches out from the trabecular arteries, they penetrate the red pulp thus becoming central arterioles (72). Smaller arterioles branch from the central arterioles and supply the white pulp capillary beds (72). A few of these arterioles desist in the marginal sinus at the intersection of the white pulp and the marginal zone (72). Some, however, end within the marginal zone, while a few others stretch out beyond the white pulp desisting in the red pulp (72). Other smaller arterioles access to the lymphatic nodules where they engender capillaries that supply the red pulp (**Figure 15**)(69).

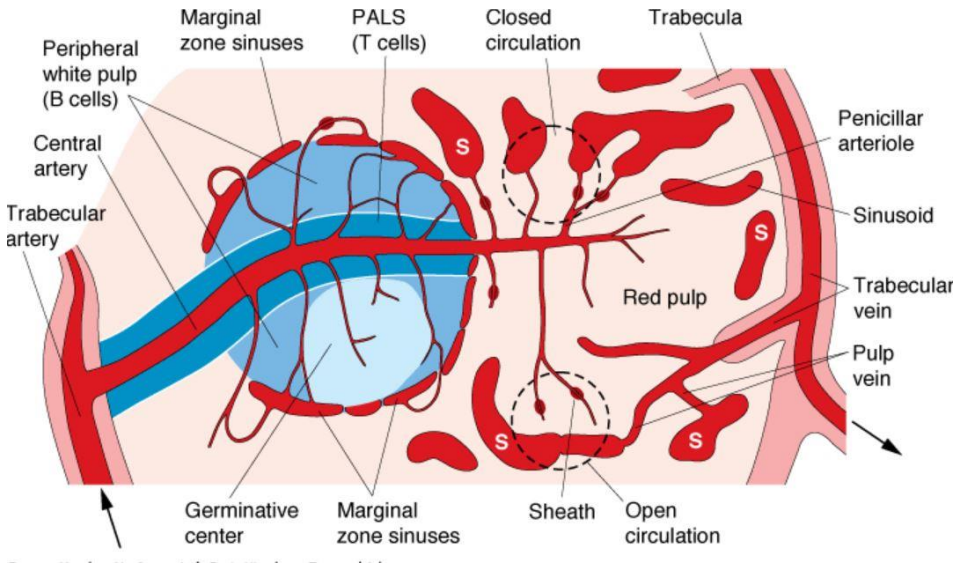

Figure 15: Schematic representation of the structural components of the spleen, with its two prominent splenic pulp, the white and red pulp. *The blood circulates from the trabecular artery, flows through the white and red pulp as it branches out into arterioles, eventually reaching the trabecular vein. Other identifiable regions are indicated, these include the PALS, germinative center, marginal zone sinuses, and the splenic sinuses. The figure is taken from Junqueira & Carneiro J. (33).*

Subsequent leaving the white pulp, the sheath of lymphocytes encircling the arterioles steadily thins (33). The aforementioned arterioles branches further out sidelong within the follicle forming a series of parallel terminal arterioles, known as penicillin, or penicillar arterioles (66). Near their terminal, some of these arterioles are enveloped by a thick sheath of reticular cells, lymphoid cells, and macrophages (33). After perambulating through the parenchyma for variable stretch (33), the PALS is widened in places by lymphoid follicles, which are the accumulation of B-lymphocyte (66). The PALS is made of diffuse lymphatic tissues that encompass arteries and arterioles which stretch out to lymphatic nodules (69). It is, additionally, comprised of a homocentric layer of reticular fibers and flattened reticular cells (72). The PALS is subdivided into the inner PALS and the outer PALS (72). The interior of the PALS is a T-lymphocyte dependent region, with mostly CD4+ T-lymphocyte (72). However, a smaller number of CD8+ T-lymphocyte subsets may also be present within the interior of the PALS (72). The exterior part of the PALS is occupied by small and intermediated B and T- lymphocytes, macrophages, including plasma cells when activated by antigenic stimulation (72). The PALS often encircle lymphoid nodules or follicles (73). These encircled lymphoid nodules/follicles are enriched with B-lymphocytes (73). The lymphoid follicles are chiefly positioned near the terminal branches of arterioles and generally emanate to

one side of a vessel, which consequently appears unconventionally positioned within the follicle (66). The splenic lymphoid follicles preponderantly consist of B-lymphocytes with a marginal center with the circumambient mantle zone and marginal zone (73). Germinal centers are comprised of B-lymphocytes, particularly a blend of centrocytes and centroblasts (73). An overabundant of centroblasts are located in the dark zone while centrocytes, macrophages, and plasma cells are situated in the light zone of the germinal centers (73). Additionally, a marginal zone is present within the splenic parenchyma, the marginal zone borders the lymphoid nodules (33). The marginal zone consists of a great quantity of blood sinuses and loose lymphoid tissue (33). It is located at the border between the white and red pulp (66). Further, the marginal zone is an essential region of appreciable functional significance, it is in this region where blood is delivered into the red pulp (66). Moreover, the marginal zone is where several lymphocytes exits the circulation and journey into their corresponding T- and B-lymphocyte zones within the white pulp (66). Not only is the marginal zone an entrance site in which lymphocytes access the spleen from the blood, but it is also residence to specialized macrophages (71), plasma cells, as well as interdigitating dendritic cells (73). Marginal sinuses are located peripheral to the marginal zone, they are lined by Mucosal Vascular Addresin Cell Adhesion Molecule 1 (MADCAM1) positive cells, which are sinus-lining endothelial cells (72). Circumferential to the marginal sinus, exists a broad outer band of the marginal zone (72). It is comprised of reticular fibroblasts, marginal zone macrophages, DCs accompanied by medium-sized marginal zone B-lymphocytes (72). The marginal zone of the white pulp eventually coalesces into the red pulp (72). Antithetical to the white pulp, the red pulp is consociated with veins (69). The red pulp comprises of the splenic cords and the venous sinuses (69). It further consists of a fibrous plexus, enriched with macrophages and red blood cells, and enlarged capillaries which links to the veins (69). The red pulp makes up the majority of the spleen, it constitutes about 75% of the entire splenic volume (66). The splenic cords fundamentally consist of a network of reticular cells that synthesize reticular fibers (69). The reticular cells lie around sinusoids, they produce the matrix components of the reticulum, they also synthesize collagen and proteoglycans, including their cytoplasmic processes compartmentalized the reticular space (66) The splenic cord also contains T and B-lymphocytes, macrophages, plasma cells, and other blood cells such as erythrocytes, platelets, and granulocytes (33). Splenic cords are parted by enlarged venous sinusoids that occupy the space between the parted splenic cords (69). The red pulp is composed of a plethora of venous sinusoids, which are disunited from one another

by a fibrocellular matrix (66). The fibrocellular matrix consists of small bundles of exquisite collagen type III fibers, the reticulum, and a great many reticular fibroblasts and splenic macrophages (66). Venous sinusoids are characterized as elongated ovoid vessels of about 50 μm in diameters (66). The venous sinusoids are lined by a distinguished incomplete endothelium that is quite distinctive to the spleen (66). Elongated endothelial cells lines the splenic sinusoids with the long axes collateral the long axes of the sinusoids (33). The passageway between the endothelial cells of the venous sinusoids are 2-3 μm in diameter or even smaller than (33). As a consequence of that only flexible cells can cross effortlessly from the red pulp cord and into the lumen of the venous sinusoids (33). The venous sinuses normally adjoin the trabecular veins, which merge to form vessels that exits the spleen to form the splenic vein (69).

As previously stated, the spleen is the largest accruement of lymphoid tissue in the body, it is also the only lymphatic organ interposed into the systemic vasculature (33). The spleen is enriched with phagocytic cells and therefore plays an imperative role in protecting the body against antigens that manage to reach the blood circulation (33). Another pivotal role the spleen plays is to sustain a normal immunity and also maintain normal hematopoiesis (73). The spleen is also where senescent red blood cells are eradicated (33). Not only that, but the spleen also filters the blood, during which poorly ill-shaped red blood cells are removed from the circulation (73). Particles from circulating red blood cells like nuclear remnants, insoluble globin precipitate, and endocytic vacuoles are also removed (73). The spleen being a lymphopoietic organ plays a crucial role in antibody formation and T-lymphocyte and B-lymphocyte proliferation (73). It is after all the production regions of activated lymphocytes, which are further transported to the blood (33). Additionally, the spleen function as a storage, sequestering roughly one-third of the total amount of platelet, and a large proportion of granulocytes (74). As blood flows into the spleen, it enters the white pulp via the splenic artery (61). The white pulp is an invaluable production region of lymphocyte (33). Within the white pulp, B and T-lymphocytes screen the blood that streams through the spleen (61). While T-lymphocytes aids in recognizing and attack pathogens that have entered the bloodstream, the B-lymphocytes produce antibodies that aid in preventing infections from developing (61). Blood circulates from the white pulp and into the red pulp of the spleen, where it eventually reenters the blood circulation (33). The removal of senescent and defective red blood cells takes place within the interior of the red pulp (61). Macrophages in the red pulp cords engross and break down the degenerating and old red blood cells (33). Hemoglobin contained within the red blood cells are

broken down into various parts and recycles (61). The protein, globin, is hydrolyzed to amino acids, they are recycled and used in protein synthesis (33). Iron is freed from heme, it is thereafter combined with transferrin and finally conveyed in the blood to the bone marrow. It is then recycled/reused in the production of red blood cells (33). As previously stated, one-third of the body's supply of platelets are stored in the spleen, more precisely, in the red pulp of the spleen (61). When severe bleeding transpires, the additional supply of platelets can be released and utilized to stop the bleeding (61).

The spleen, in both species, is situated in the left upper quadrat of the abdomen abutting the great arc of the stomach (31). The spleen of mice is more extended than in humans and it weighs approximately 100-200 mg in 2- to 4- month old mice (31). The spleen is surrounded by a capsule composed of fibrous tissue, elastic fibers, and smooth muscle, with and a thin covering of mesothelial cells (31). In both species, vessels ingress and exits the spleen at the hilum (31). Blood ingress the spleen via the splenic artery and exits through the splenic vein, which then drains into the portal vein (31). Seldom, an accessory spleen may be detected in both species (3). The spleen displays comparable general anatomical architectural in both species (3). The spleen functions in filtering the blood and mediating immune responses in both species (31). Additionally, in mice only does the spleen also function as normal site of hematopoiesis throughout life and can thereby provide a hematopoietic response to different stimuli such as various diseases and infectious agents (31).

1.8 Systemic lupus erythematosus overview

The systemic lupus erythematosus (SLE), as the name indicates, is a multisystemic autoimmune disease (75). It is a chronic, relapsing malady with protean manifestation where, unfortunately, almost any organ system can be inflicted (75). SLE is a miscellaneous autoimmune disorder with various arrays of clinical manifestations (76). The malady is characterized, as above stated, by a broad spectrum of clinical features, profuse immunological and laboratory aberrations, and a mercurial course and outcome (77). In addition, loss of tolerance against nuclear autoantigens, lymphoproliferation, polyclonal autoantibody production, immune complex disease, and multiorgan tissue inflammation is indeed also contributing characteristic features of this complex autoimmune disease (78). This perplexing autoimmune disorder emanates from the defect of multitudinous immunologic elements of the innate and adaptive immune system, respectively (79).

Furthermore, there are other implicated culprits resulting in this complex disease, these include altered immune tolerance mechanism, hyperactivation of T and B-lymphocytes, the attenuated capability to remove immune complexes and apoptotic cells, and incompetence of multiple regulatory networks (79). The precise etiology and pathogenesis of SLE is, regrettably, still obscure, and rather elusive as it involves intricate number of factors such as genetic, epigenetic, hormonal and environmental factors, which ultimately leads to loss of self-tolerance (80). As SLE can result in serious multi-system organ damage, early detection is therefore critical considering that it can have significant implications for morbidity and management of the malady (76). It is probable that immunological abnormalities antecede the onset of clinical disease by many years, ultimately making the disease rather difficult to study (79). In fact, due to the diverse manifestation of SLE and their progression over time can make the disease hard to diagnose (76). There exist some criteria that has to be present for a clinical diagnosis of SLE (79). These standard criteria originate from the 1997 updated version of the 1982 validated classification criteria developed by the American College of Rheumatology (ACR)(77). Eleven criteria were distinguished for SLE clinical presentation, and at least four of these criteria have to be met prior to diagnosing a patient with SLE (79).

Table 1: The 1982 adjusted criteria for categorization of SLE

1. Malar rash
2. Discoid rash
3. Photosensitivity
4. Oral ulcers
5. Arthritis
6. Serositis
7. Renal disorder
8. Neurologic disorder
9. Hematologic disorder
10. Immunological disorder
11. Antinuclear antibody

The requirement for SLE diagnosis is based on whether the patient presents with or meet four out of the eleven criteria during the progression of the disease. The table is modified from table 2 by Tan et al(81).

Nevertheless, SLE is a multiorgan autoimmune disorder with a vast range of autoantibodies circulating about (82). When these autoantibodies come in contact with antigens, they produce immune complexes which are further deposited in various organs (82). The deposition of the immune complexes can cause damage in the organs subsequent to activating the complement (82). The multiorgan manifestation of SLE makes it difficult to make a clear assessment of the SLE activity (82), as there is no single test that provides a sufficient measure of disease activity in a complex disease such as SLE (83). As the comprehension of SLE expanded over time, it became imperative to measure disease changes (75). There are various activity indices that have been utilized over the years. A few of these activity indices are used nowadays (75). These activity indices are utilized to evaluate the spectrum of the manifestations of the disease activity in SLE (83). The British Isles Lupus Activity Group instrument (BILAG), the SLE Disease Activity Index (SLEDAI), and the Systemic Lupus Activity Measure (SLAM) are the activity indices used nowadays (83). These have been thoroughly studied and it has been shown that the instruments have convergent and construct validity when related to the clinician's findings (83). SLAM and SLEDAI provide an overall measure of disease activity, and BILAG provides an individual organ/system assessment scale capable of assessing disease activity in single organs (84). BILAG is a computerized index that measures clinical disease activity in SLE(85), the index score was developed to reflect the physician's "intention to treat" (83). The instrument, or index rather, assigns scores to each of the eight organ-systems, where "rate-of-change" in disease activity is the foundation that would lead a physician to change the patient's treatment (83). A total score is not given, instead, alphabetic scores from A to D are distributed to each of the eight organ-systems (83). Furthermore, disease activity is measured without referring to the patient's current treatment (83). The given alphabetic score determines severity and what kind of treatment the patient will receive (83).

Table 2: Scoring of disease activity of the classical BILAG

BILAG score	BILAG score definition
A	Require urgent disease-modifying therapy
B	Demanding close attention, often symptomatic therapy
C	Stable, SLE controlled on current therapy
D	No involvement

BILAG scoring system with scoring definitions, established in 1988, based on the principle of physician's "intention to treat". Table inspired by ref (83).

The original version of the BILAG was published in 1988, it was updated to BILAG-2004, and was published in 2005 (86). The updated version assigns disease activity into five alphabetic distinctive levels from A to E, contrary to the classical version (86). SLEDAI is a rating system that includes 24 variables that are significant in clinical and laboratory evaluation of disease activity (83). The SLEDAI scoring system weighs the 24 clinical and laboratory variables of nine organ systems (86), of the 24 variables 16 are clinical and 8 are based on laboratory findings (87). The SLEDAI is a global index, designed on the grounds of clinician global evaluation or judgment (86). Each manifestation is registered absent or present at 10 days before and during the period of assessment, despite the severity of the disease or even if it has improved or exacerbated (87). Individual item scores range from 1 to 8 while the total global score for all 24 variables ranges from 0 to 105 (87).

SLAM was first issued in 1988 and updated in 1991, SLAM measures global disease activity in the last month (86). It was established on the principle of domain sampling theory (86). This index includes both clinical and laboratory manifestations weighted according to the graveness of the disease (88). The revised version of SLAM, SLAM-R, is more frequently utilized, and in this version, the disease activity spans from a minimum of 0 to a maximum of 84 (88). SLAM-R is predicated on the assessment of 30 variables concerning 11 organ-systems and 8 laboratory manifestations (88). SLAM-R and SLAM alike do not include immunological parameters, nevertheless, laboratory manifestations such as the haematocrit, white blood cells, lymphocyte count, platelets, serum creatinine, urinary sediment, etc. are habitually measured at each clinic visit (88). The occurrence of organ damage in SLE due to disease activity, treatment, and/or comorbidities is another grisly outcome of SLE (75). Systemic Lupus International Collaborating Clinics (SLICC) in conjunction with the ACR, therefore developed a damage index for SLE (77),

damage is assessed with the SLICC/ACR damage index (SDI) which encompass irreversible changes transpiring in 12 organ-systems post SLE diagnosis (75). Furthermore, the SDI score also prognosticates mortality (77). The damage index is thereby an essential outcome measure for assessing the prognosis and long-term effect of SLE disease activity and treatment (77).

Some common clinical manifestations of SLE include skin disease and arthritis, nevertheless, any organ can be affected to a various degree (77). Neuropsychiatric dysfunction and renal disease are two of the grave acute SLE manifestations (77). Likewise, fever, fatigue, and weight loss are some recurrent but nonspecific manifestations of SLE, as they can result from other medical conditions (77).

SLE can present at an early age or late in life, it commonly appears between 15 and 45 years of age (89). The Childhood-onset of SLE constitutes about 10-20 % of the cases, the female to man ratio is almost equal in the very early onset of SLE(77). SLE has a clearly noticeable female predisposition (75), female prevalence in SLE exists across all ages with about 2:1 female-to-male ratio prior to puberty and post menopause (89). In child-bearing years the female to male ratio is 9:1, the increased risk in females has been postulated to be related to factors such as sex hormone levels, particularly that of oestradiol, epigenetic changes, environmental exposures, and risk alleles on the X chromosome (75). With regard to hormones, oestradiol and similar hormones can have various effects on the immune system (75). The most acute effect, concerning SLE, is that these hormones can enable autoreactive B-lymphocytes to escape deletion during B-lymphocyte ontogeny (75). Pertaining to epigenetics, the dormant or suppressed X chromosome in women is excessively methylated than the expressed X chromosome, and can therefore be antigenic (75). There is a definite pattern that has presented itself from various reports, notwithstanding the fact that SLE incidences varies significantly, nevertheless, a pattern obtained from various reports has presented itself (90). It seems race and ethnicity are deciding components in determining whether one develops the autoimmune disease (75). Furthermore, women of African origin appear to have the highest incidence and prevalence rates reported worldwide (75). They are, in addition, the ethnic group that develops SLE at a younger age, with a more severe disease, with an expeditious accrual of damage, and higher mortality rates (89). In USA studies, women of African origin had a very high prevalence rate compared with white women (196.2/100,00 vs 59.0/100,000 in Georgia, and 186.3/100,00 vs 86.7/100,000 in Michigan)(75). Other groups with a high prevalence

of SLE include American Indians and Alaska Natives(178/100,00), and Aborigines from Australia(73.5-92.8/100,000)(75). Mortality in patients with SLE has remarkedly ameliorated over the past decades, regrettably, mortality remains significantly higher in the general population (80).

1.8.1 Pathogenesis of SLE

The pathogenesis and the exact etiology of SLE are sadly not yet uncovered thus remaining a rather puzzling enigma (91). There are, however, several risk factors that might be a stimulus for the development or initiation of SLE (**Figure 16**)(89). There is not just one risk factor but instead, it is a complex interplay that presumably instigates the development of SLE (89). The pathogenesis of SLE has been shown to stem from multifactorial interplay between genetic, hormonal, epigenetic, and environmental factors that result in loss of self-tolerance (77, 80).

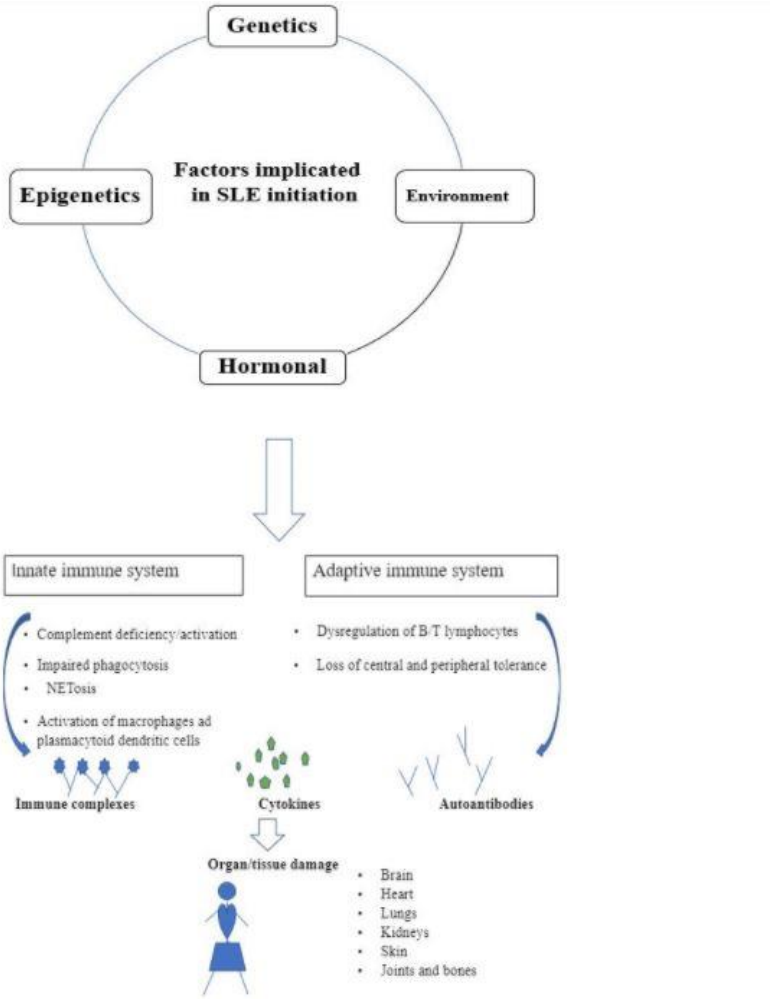

Figure 16: Overview of the pathogenesis of SLE. A plethora of factors are implicated in the development of SLE. This figure was modified from "Figure 2.1 by Gordon(75).

SLE is a polygenic disease as it is influenced by more than one gene, it can sadly manifest in individuals without a family history of the disorder (77). Nonetheless, siblings of affected individuals have a much higher chance and are more likely to develop SLE (77). Moreover, monozygotic twins (24-57%) present with a higher risk than dizygotic (2-5%), demonstrating that genetics plays a central role in the susceptibility of the development of SLE (91).

It is a disease with polygenic inheritance, thus individuals inflicted by this illness can obtain multiple predisposing genes, nonetheless, these predisposing genes alone would sadly not predict the disease (77). Furthermore, certain genetic variants and pathological mechanism in SLE occurs often in other autoimmune maladies such as type 1 diabetes, rheumatoid arthritis, and MS (77). These aspects construct evidence for genetic predisposition, on which the presence of other appurtenances and accumulative factors essentially facilitate or promote the development of the

disease (77). For instance, certain infectious agents play a major role in SLE as they might promote particular inaugural steps in the disease pathogenesis (77, 92). It has been established that pathogens promote lupus autoimmunity and clinical SLE through various means of interaction with the immune system (77, 92). For instance through mechanisms such as molecular mimicry, functional mimicry, altered apoptosis of the host cells, pathogenic invasion of immunocompetent cells, disruption of immunoregulatory mechanism, etc. (77, 92). All of these mechanisms can engender to a dysfunctional of the immune system (92). Pathogens that have been established to be associated with SLE pathogenesis include Epstein-Barr virus (EBV), cytomegalovirus (CMV), parvovirus B19, as well as human herpesvirus (HHV) 6, 7 and 8 (80). Infections commonly lead to ephemeral, low-level production of autoantibodies by stimulating activating of cytokine pathways, differentiation, and activation of immune cells, and exposure to autoantigens (77). In most people, however, these alterations have no significant consequence and do not give rise to autoimmune diseases because the immunoregulatory mechanism is not compromised (77). The immunoregulatory mechanism can therefore reinstate tolerance to self-antigen thereby suppressing inflammation after the infection is cleared (77). Contrariwise, in people who are genetically predisposed to SLE, subjection to certain pathogens can alter the immune system toward a dysregulated state, consequently permitting the commencement and progression of autoimmune disease (77).

Some environmental elements including biologic, physical, or chemical agents can accelerate the development of SLE in individuals who already are susceptible to SLE (77). One of the well-recognized biological agents is the aforementioned Epstein-Barr virus (75). The physical agents, a well-known risk factor, associated with SLE pathogenesis is exposure to ultraviolet light (77). Ultraviolet light is, amongst other things, detrimental to DNA as it can harm the molecule, ultraviolet light can also amplify cell apoptosis and the presentation of self-antigens to immune cells (77). Silica dust which can be found in a lot of construction materials such as cement, bricks, including drywall, has been affiliated with the inception of SLE in some individuals (75). Silica dust is acknowledged to be a component capable of inducing oxidative stress, a key element in the development of tissue disease in SLE (75). Equally important, cigarette smoke, air pollution, as well as exposure to elemental mercury are also another vitally important inducer of oxidative stress (75). Smokers have a greater risk for SLE and the development of anti-double-stranded DNA (anti-dsDNA) antibodies, potentially because smoke escalates cellular necrosis (77). Lastly, drugs have

been acknowledged to cause side effects which ultimately result in iatrogenic forms of SLE (77). Some drugs induce epigenetic alterations within DNA in T-lymphocytes by decreasing the level of DNA methyltransferase 1 (Dnmt1)(75). The consequence of disrupting DNA methylation is that gene expression in T-lymphocytes is altered which transmutes a healthy immune response into an auto-reactive cascade (75). Luckily effects of these drugs dissipate and are reversed upon withdrawal (77).

More than 100 distinct autoantibodies have been characterized in SLE. Regardless, the most predominantly associated with SLE is none other than anti-DNA, and anti-chromatin, and anti-nucleosomes in lupus nephritis (77). These autoantibodies together with their correspondent antigen form immune complexes that can be internalized by local plasmacytoid dendritic cells (pDCs)(77). Nonetheless, autoantibody production and disease activity in SLE is not essentially connected to one another (77). Immune complexes, which comprise complement and phagocytes, can play a vital role in determining disease severity (77).

The identification of risk alleles in SLE has been established by single nucleotide polymorphism (SNP) genotyping and genome-wide association studied (GWAS) that have identified risk loci (77). GWAS have discovered over 50 gene loci associated with the development of SLE, nevertheless, only a few of these genetic variants present a very high risk for SLE when inherited by itself(75). More than 60 genetic regions have been documented as strongly related to SLE (77). Most of these genes can be categorized according to their involvement in the three immunological processes relevant to the pathogenesis of SLE:

1. Activation of toll-like receptor (TLR) and type I interferon (IFN) production, and nuclear factor kB (NF-kB) signaling
2. Clearing of apoptotic cells and immune complexes
3. Dysfunctions in lymphocyte signaling (77, 79).

Herein I shall describe only a few of the key elements implicated in the SLE predisposition (75). Genetic predisposition to SLE is evidently a paramount element in the development of malady (75). A few specific gene polymorphisms display or present a higher association with SLE than others, there is therefore not only one single “SLE gene” (75). Instead, patients inherit various high-risk alleles, which in combination with epigenetics and environmental triggers causes manifestations of clinical symptoms of the disease (75). There are gene mutations that present with

a higher risk of disease development than others, however, these are rare (75). Of these mutations are the homozygous deficiencies of complement protein/component 1q (C1q), an early complement component; mutations of three prime repair exonuclease 1 (TREX1) and DNase1, responsible for regulating DNA breakdown; and ACP5 and SPP1 polymorphisms, which induce the increased activity of interferon-alpha (75). As previously stated, only a few of the genetic variants identified by GWAS are associated with high risk for SLE when exclusively inherited (75). For instance, 93% of patients who are deficient in C1q will develop a lupus-like syndrome (75). C1q is a complement protein in charge of clearing immune complexes as well as apoptotic cells, therefore immunodeficiency of this component is highly associated with the development of SLE (75). TREX1, a protein-coding gene, is in charge of DNA degradation (75). A missense mutation in TREX1 has been connected to neuropsychiatric lupus, where 25% of the patients with the mutation develop the disease (75). Sadly, most patients inherit a number of gene polymorphisms (75). Each mutation plays a small part, but when combined they are affiliated with the instigation of diseases and increase disease activity (75). The most typical site of susceptible genetic alleles in SLE originate within the major histocompatibility complex (MHC), also recognized as the human leukocyte antigen (HLA) region(75). The HLA region is subdivided into three smaller regions, where regions I and II encode the prominent ubiquitous reported HLA genes (HLA-A, -B, -C, -DR, -DQ, and -DP) which participate in antigen presentation to T-lymphocytes (**Figure 17**)(75). These molecules are highly expressed on antigen-presenting cells (APC), such as DCs and B-lymphocytes, and display peptides for CD4+ helper T-lymphocytes (93).

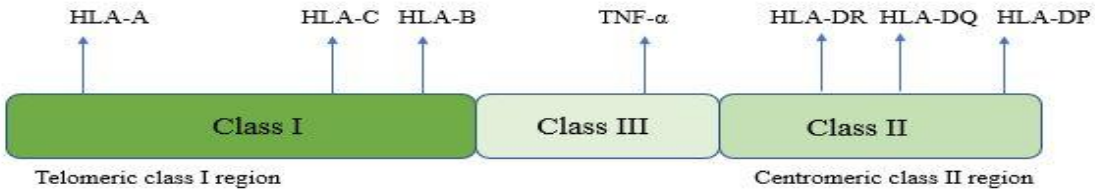

Figure 17: Overview of the various HLA regions*. Telomeric class I region with HLA-A, -B, and -C genes represent the widely expressed genes on HLA. The centromeric class II region contains the HLA-DR, -DQ, and -DP genes. Figure modified/inspired by figure 1 from Ka, Sojeong, et al. (94).*

Region III encodes for early complement components (C2, C4, factor B), cytokines such as TNF-α, and heat shock proteins. Moreover, approximately 75% of SLE patients have at the minimum one predisposing HLA gene polymorphism (75). Class III region is located between class I and II region, as illustrated in (**Figure 17**), this region encompasses several immune-related genes (93). Some of these genes include the cytokines TNF- α, lymphotoxin- α, and the complement components C2, C4, and Factor B (93). HLA-class II antigen-presenting alleles DR and DQ are linked with susceptibility to SLE as well as the production of lupus-related autoantibodies (93). Polymorphism within HLA-DR2 and HLA-DR3 alleles have been strongly associated with SLE, and it is well observed in primarily European populations (77). In two large independent replication cohort studies about genotyped HLA class II in a multi-center US Caucasian SLE family, performed byGraham *et al,* it was demonstrated that specific HLA-DR2 and DR3 class II haplotype, exclusively and in combinations, are strong contributing factors of autoantibody production and disease predisposition in human SLE (93). Furthermore, cumulative studies have documented the association of HLA class II alleles with autoantibody production, particularly that of HLA-DR3 with anti-RO/La antibodies (77).

Cytokines which are low-weight soluble proteins originate from different cells in the innate and adaptive immune system (95). They play a significant role in the differentiation, maturation, and activation of diverse immune cells (96). Not only are cytokines embroiled in immune dysregulation of SLE, but they are also involved in the local inflammatory response which conclusively leads to tissue injury (96). A few cytokines can even serve as biomarkers to detect disease activity as well as a predictive tool to prognosticate disease severity (96). Furthermore, the manipulation of cytokines may represent a potential novel therapeutic approach for the treatment of SLE(96). Various evidence demonstrates that IL-10 implication in SLE susceptibility (97). IL-10 is a vital immunoregulatory cytokine that hinders or impedes T cell function by suppressing the expression of proinflammatory cytokines such as TNF-α, IL-1, IL-6, IL-8 including IL-12(97). IL-10 possesses both immunosuppressive and immunostimulatory properties and has been found elevated in sera from SLE patients (77). The elevation of IL-10 in sera corresponds with disease activity. T- and B-lymphocytes, monocytes, and macrophages extensively express IL-10 (77). In addition to the inhibitory activity, IL-10 enhances B-lymphocyte proliferation, survival, and immunoglobulin class switch, consequently prompting antibody secretion (96). Increased production of IL-10 could thereby elucidate B-lymphocyte hyperactivity and autoantibody

production (97). Enhanced antibody secretion has the capacity of infiltrating extravascular compartments where they can promote inflammation in SLE (96). B-lymphocyte hyperactivity as well as autoantibody production are two of the chief hallmarks of immune dysregulation in SLE(97). TNF- α, which is a cytokine that plays a vital role in the regulation of inflammation and programmed cell death (apoptosis)(97). TNF- α is a proinflammatory and immunoregulatory cytokine, it has a differential effect on T and B-lymphocytes including dendritic cells (98). Additionally, TNF- α has a differential effect on the mechanism of apoptosis (98). The molecule stimulates the production of inflammatory cytokines, it increases neutrophil activation and expression of adhesion molecules (97). In addition to this, TNF- α acts as a costimulatory for T-lymphocyte activation and antibody production (97). TNF- α polymorphisms have been implicated in the pathogenesis of SLE, as well as other autoimmune diseases such as rheumatoid arthritis, etc. (99). Zuniga et al reported that the connection between polymorphism of the TNF- α positioned at -238 and SLE and that the TNF- α -238 could play a pivotal role predisposition of the disease (99).

1.8.2 Role of autoantibodies, and immune complex in the pathogenesis of SLE

In patients suffering from SLE, autoantibodies are the main culprits' effector of the commencement of the disease (75). Pathogenic subsets of autoantibodies and immune complexes are deposited either in or on tissues (75). Deposition of these factors in tandem with released cytokine, chemokines, and proteolytic enzymes, consequently results in organ inflammation, cell death, and tissue damage (75). In SLE, tissue damage often transpires from the aforementioned production and widespread deposition of immune complex, which particularly are deposited in the kidneys, the vascular system, the brain, and the skin (100). The pathogenicity of circulating immune complexes predominantly depends on their capability of activating the complement system (100). When the complement system is activated, vasoactive substances and mediators of inflammation are released (100). Immune complexes are structures produced by the binding of autoantibodies and antigens (95). These formed complexes stimulate macrophages to express TNFα, which promotes inflammation (95). The site of inflammation can be a source of cell death (necrosis), as well as the source by which new autoantibodies are formed (95). High TNFα expression levels in tissues of patients with SLE can therefore be linked with inflammation and consecutive tissue damage (95). Moreover, autoantibodies precede the first symptoms of the disease by an average of 2-3 years in 85% of SLE patients (75). In patients with SLE, a temporal

echelon of expression of autoantibodies exists, where antinuclear antibodies (ANA) emerging first, ensued by anti-DNA and antiphospholipid antibodies, which are further followed by anti-smith (anti-Sm), and anti-ribonucleoprotein antibodies (anti-RNP)(75). ANAs are present in about 95-99% of patients with SLE, serologically, the hallmark of SLE is a high elevated level of ANA (77). Nevertheless not all ANAs have been proven to be pathogenic, as 13.8% of the normal population were found to be ANA positive (75). Up to 10-80% of patients with SLE present with anti-dsDNA antibodies during the course of the disease (75). There are several different theories postulating how anti-dsDNA antibodies bind to tissues, activate complement ultimately inducing inflammation (75). One theory hypothesized that anti-dsDNA form complexes with free-floating dsDNA or nucleosomes, thereafter the immune complex is deposited in different tissues (75). Other propose that the complexes are formed amongst nucleosome fragments and anti-dsDNA antibodies are since there are miniscule free-floating dsDNA in human serum(75).

ANAs can bind to nucleic acids (DNA or RNA), they can in addition bind protein and complexes of DNA or RNA with proteins (101). ANAs production is not exclusive or prototypical to just SLE, nonetheless, the pattern of autoantibodies expressed by patients with SLE is rather highly distinctive (101). It, therefore, permits the utilization of serology for screening, classification, diagnosis, prognosis as well as the staging of SLE (101).

ANAs can be distinguished by their antigenic target, disease association, or by the acknowledged role they play in the pathogenesis of the disease (101). The most noteworthy ANAs in SLE tend to bind to either nucleosome components or RNA-binding proteins (RBPs)(101).

Nucleosomes are the conformation in which DNA is found in the cell nucleus (101). It comprises of DNA wrapped around a core octamer of histone proteins-, the DNA amid nucleosomes is known as linker DNA (101). Thus, in SLE, ANAs can attach to DNA, histones, or DNA-histone complexes, those tethered to DNA-histone complexes are known as anti-nucleosome or anti-chromatin antibodies (101). Anti-DNA antibodies are the most characteristic among the anti-nucleosome antibodies, antibodies that bind dsDNA are unique for the classification and diagnosis of SLE (101). Of the anti-RBP antibodies, just anti-Sm antibodies constitute a marker for SLE classification(101). The formation of these antibodies implies that there is a pathological disturbance in the mechanism that otherwise ought to prevent B- and T-lymphocyte reactivity to self-antigens (101).

The formation of immune complex is a key mechanism by which ANAs mediate inflammation in SLE (101). This can be accomplished either by accumulation in tissue or by stimulating cytokine production by cells of the innate immune system (101). Nuclear self-antigens can derive from cell death (101). Defects in the clearance mechanism can increase the availability in the amount of extracellular nuclear debris, which ultimately gives rise to nuclear self-antigens (101). Regarding DNA, insufficiency of nucleases such as DNase 1 and DNase 1-like 3 (1L3) can boost the quantity of self-antigen that can form immune complexes (101).

Self-tolerance is in part compromised by impairment in cell death pathways and impairment in the clearance of cellular debris (102). As previously stated, changes or modification of cell death pathways, which also include apoptosis and neutrophil specific kind of death known as NETosis, can set forth a possible source of autoantigens (102). When these autoantigens are exposed to the immune system they can ultimately result in an autoimmune response (102).

Therefore, inadequate clearance of cellular debris plays a role in the breakdown of self-tolerance, which leads to the onset of an autoimmune response mainly directed against nuclear autoantigens (102). Clearance deficiency also plays a role in the perpetuation of chronic inflammation by supplying autoantigens that activate and enhance local inflammatory responses mediated by autoantibody (102). Complement activation is required for a proficient phagocytic breakdown of apoptotic cells by macrophages, thus deficiencies in the early components of the complement pathway would suggest that there is impairment in the clearance of apoptotic cells (103). Botto *et al*. discovered glomerular apoptotic cells in C1q-deficient mice compared with controls, ultimately the mice developed lupus-like malady (104). Some SLE patients have reduced clearance of apoptotic cellular remnants, as demonstrated by an increased number of apoptotic cells in their germinal centers (105). Both in vitro and in vivo experiments have demonstrated and support the idea that the early complement components are needed for the clearance of apoptotic cells (105). The high frequency of SLE in patients with C1q, C4, and C2 deficiency may partially be explained by the defect in the clearance capacity (105). These discoveries are in congruent with the hypothesis that C1q deficiency causes autoimmunity as a result of impairment in the clearance of apoptotic cells (104), proving that complement does indeed play a role in the clearance of apoptotic cells in vivo (103). This could elucidate why humans with early complement component deficiencies develop SLE (103).

1.9 The Aim of the thesis

TLS are formed during the course of chronic inflammation; they are produced directly at the site of inflammation (52). TLS formation and is for the most part associated with tissue damage and are significant inductive regions for self-reactive T- and B-lymphocytes as well as plasma cells generating autoantibodies that contribute to the state of malady (106, 107).TLSs are habitually detected in target organs of autoimmune diseases (47). The observation of these structures in tissues is frequently affiliated with poor prognosis of disease, production of autoantibody and the evolution of malignancy (47). Insight into the mechanism involved in the formation of TLSs is pivotal for hindering TLSs from manifesting at site of tissue damage, as well as for inducing their formation at sites where they contribute to a continues immune response and clearance of pathogens (52). TLS have been described in various human chronic inflammatory maladies, nevertheless the cells and molecules critical for the development of TLSs are yet to be uncovered (52). A recent study by Dorraji *et al* discovered that the formation of TLS in the kidney of lupus-prone New Zealand black x New Zealand white (NZB/W) mice frequently occurs within the pelvic wall of the medulla, larger arteries and larger veins these (108). These TLS are described to be organized in large, interconnected plexus of immune aggregate within the kidneys of lupus prone mice (108). Additionally, the article reported the TLS structured possessed all cells necessary to function as a as region for regulating T- and B-lymphocytes (108).

Previous studies on TLS in kidney have elucidated, to some extent, the correlation between and SLE, nevertheless cells responsible for TLS formation have yet to be recognized. This indicates that the process of TLSs development needs to be further investigated in order to uncover and better understand their function and immunoregulation in autoimmune diseases. Further comprehension of TLSs and evaluation of these structures can potentially aid in the development of immunotherapy. The aim of this study is:

- To detect TLS in various tissues such as the pancreas, spleen, lung, salivary gland at different stages of SLE development in lupus prone murine models.
- Investigate the presence of TLS using antibodies markers for T and B- lymphocytes as well as analyze gene expression.

2 Material and Method

Material sections deal with equipment that was utilized and their purpose. The method deals with all the procedures and the method used for scoring of IHC results.

2.1 Materials

The materials utilized in the study are listed in Appendix TableA1A1. An overview of the materials used for each method are listed in Appendix Table A2.

2.2 Methods

2.2.1 Animals

Mice are invaluable model organisms; the mouse has been a substantial valuable force in the unravelment of the genetic basis of human physiology and pathophysiology (109). Mice and humans share ~ 99% of their genes, and therefore also share common diseases (109). It is, therefore, no wonder that mice are common and premier model organism for the genetic basis of human disease due to its small size, short gestation period (~19-20 days), and the fact that it can be maintained cost-effectively (109).

A quotidian mouse model that has been and still is quite significant in the study of SLE is the New Zealand Black/White F1 mouse (NZBWF1) (110). The NZBWF1 mouse is a hybrid strain from a cross between the New Zealand Black and New Zealand white strains (110). The NZBWF1 hybrid exhibit a lupus-like phenotype including B-cell hyperactivity, development of anti-nuclear antibodies (ANA), and immune complex-mediated glomerulonephritis (110).

For IHC the NZB/W J mice were used (**Table 3)**. While for qPCR the NZB/W P-mice and F-mice were used. An overview of the murine models utilized in the qPCR experiments of this thesis is itemized in **Table A3 and A4** in the appendix.

Table 1: Overview of the various mice used for IHC study

Mouse name	Strain	Supplier	Age (w.o)	Anti-dsDNA Ab	Proteinurea
J1	NZBWF1/J	JAX	22	Ab -	1+
J2	NZBWF1/J	JAX	25	Ab?	1+
J3	NZBWF1/J	JAX	25	Ab +	1+
J4	NZBWF1/J	JAX	25	Ab -	2+
J5	NZBWF1/J	JAX	25	Ab +	2+
J6	NZBWF1/J	JAX	28	Ab +	4+
J7	NZBWF1/J	JAX	32	Ab +	2+
J8	NZBWF1/J	JAX	29	Ab +	1+
J9	NZBWF1/J	JAX	32	Ab +	2+
J10	NZBWF1/J	JAX	28	Ab?	4+
J11	NZBWF1/J	JAX	33	Ab +	1+
J12	NZBWF1/J	JAX	35	Ab?	2+
J13	NZBWF1/J	JAX	27	Ab +	4+
J14	NZBWF1/J	JAX	31	Ab?	4+
J15	NZBWF1/J	JAX	30	Ab +	4+
J16	NZBWF1/J	JAX	30	Ab +	4+
J17	NZBWF1/J	JAX	34	Ab +	3+
J18	NZBWF1/J	JAX	34	Ab +	3+
J19	NZBWF1/J	JAX	33	Ab+	3+/4+

2.2.2 Immunohistochemistry

Immunohistochemistry (IHC) is a technique for localizing specific antigens in tissues or cells (111). The method is purely based on antigen-antibody cognizance (111). The IHC method exploits the meticulous specificity provided by the binding of an antibody with its corresponding antigen at a light-microscopy level (111). IHC is a robust investigative technique that can provide auxiliary information to the routine morphological assessment of tissues (112). IHC is utilized to study cellular markers that define specific phenotypes (112). The use of IHC has bestowed significant diagnostic, prognostic, and predictive information respective to the status of malady and biology (112).

The quality of immunohistochemical staining depends on many factors (113). Several factors, steps rather, must be optimal to obtain quality immunohistochemical staining, these include

fixation, washing, incubation conditions as well as mounting of cell and tissue specimens into slides (113). An appropriate fixative has a significant impact on the quality of immunohistochemical staining (114). Fixation should therefore be sufficient to maintain the integrity of the tissue section throughout the entire immunostaining methodology (114). Preserving the morphology of the sample is imperative for optimal immunostaining. Fixation should thus not be too harsh that it damages the specimen and the antigen of interest. (114). Tissue sections utilized in this experiment were fixed in formalin and embedded in paraffin (6). The advantages of utilizing formalin is that it is an outstanding fixative that preserved the morphological detain of the tissue due to inducing molecular cross-links in proteins (6). A combination of formalin fixation and embedment of tissue in paraffin not only enable easy storage but also excellent preservation of morphological tissue detail and resolution (6).

The IHC technique can be furcate into three phases: pre-analytical (phase 1), analytical (phase 2) and post-analytical (phase 3) (115). Pre-analytical phase commences with tissue sample collection, fixation of the sample, trimming, and embedding, and concludes with sectioning of tissue sample utilizing a microtome (115). The analytic phase begins with deparaffination of the tissue sections, retrieval of antigen, blocking of nonspecific activities, incubation with the primary antibody, labeling of the antigen-antibody reaction subsequent counterstaining and covering the tissue sections with coverslips (115). The post-analytical phase includes result interpretation by microscopy (115). IHC is, as previously mentioned, a technique based on the specific binding of antibodies to their respective antigens. The method of detecting antigen of interest can be made through direct and indirect immunostaining (116). The antigen detection method employed in this IHC experiment followed an indirect method (116). The indirect method comprises of an unlabeled primary antibody that binds to the antigen and a labeled secondary antibody that binds to the primary antibody (117).

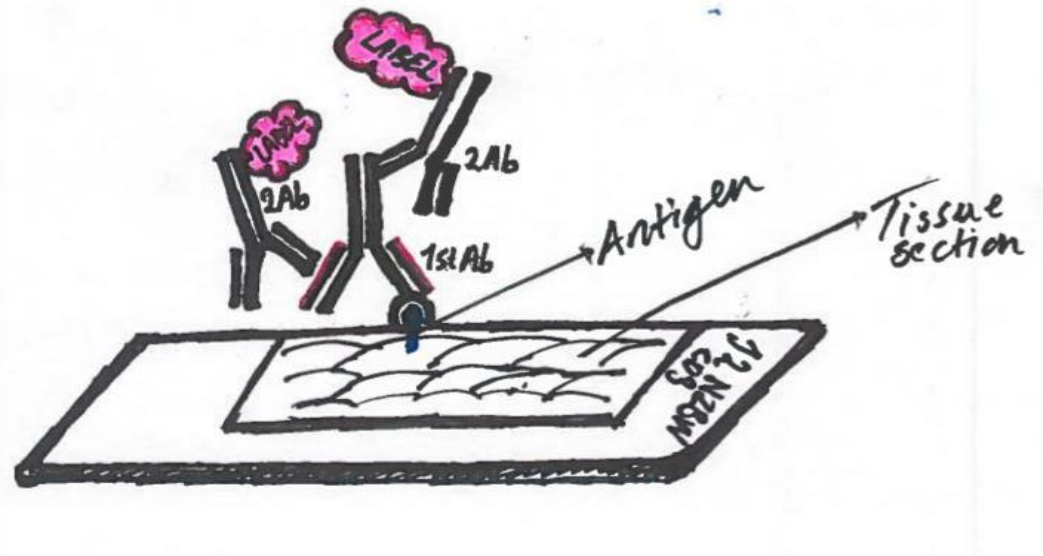

Figure 18:Delineation of indirect immunostaining method. *Figure illustration is modified from figure 4.2 by Buchwalow &, Böcker (114).*

The indirect immunostaining method is the most commonly utilized method (114). One advantage of utilizing the indirect immunostaining method is that it is a sensitive consequently signal amplification through a number of secondary antibodies binding to various antigenic sites (114).

2.2.2.1 Objective of IHC

The objective of IHC in this study was to examine protein expression of CD3, B220 and Meca 32 to detect T-lymphocytes, B-lymphocytes and endothelial cells in lung, SG, pancreatic tissue of NZB/W mice at different ages and disease progression.

2.2.2.2 Method

Formalin fixed sample from lung, pancreas and SG embedded in paraffin were utilized in this part of the study. The samples were routinely cut using the "Microm cool-cut", 4µm section were cut and floated out on water at 45 ºC. The sections were thereafter collected on +glass slides and were further incubated at 60 ºC cabin overnight. Deparaffination and rehydration/dehydration of the tissue samples were done under the biosafety cabinet **(Figure 19)**. The slides were deparaffinized in two changes of xylen (10 minutes each) subsequent four changes of decreasing ethanol concentration**:** two baths in absolute ethanol baths for 2 minutes each and two baths of 96% of ethanol baths 2 min each and finally under running deionized water for about 2 minutes.

Figure 19: Depicting the deparaffinization (left) and dehydration (right)with decreasing and increasing ethanol solution, sequentially.

Deparaffinization and preheating of the antigen retrieval machine "PT-link "was performed simultaneously. The PT-link (Dako, Glostrup, Danmark) machine was filled with sodium citrate buffer (pH6) (Appendix Table A6) and preheated to 65 ºC prior placing the formalin fixated section in the machine for antigen retrieval. The sodium citrate buffer was thus heated to 97 ºC and the section were incubated at this temperature for 20 min. After 20 min incubation time, the citrate buffer was cooled down to 65 ºC. All procedures were performed at room temperature, unless stated otherwise.

The slides were placed in 1 x PBS, sections were outlined with a hydrophobic pen (PAP pen). Blocking of endogenous peroxide was done with 100 µl of 3% hydrogen peroxide for ten min. Sections were then rinsed in three changes of 1xPBS baths for 5 minutes. Blocking of nonspecific protein binding was performed with a thirty-minute incubation in 10% normal serum (Goat serum). Slides were drained for a few second and excess fluid was wiped away around section using a gassbind. Primary antibody was diluted prior to incubation (**Table 4**).).

Table 2: List of Antibodies used in this study

Primary Antibody	Reactivity	Dilution factor	% Normal serum added	Secondary Antibody	Detection system	Source
CD3	T-cells	1:200	10% goat serum	Labelled polymer HRP anti-rabbit	Envision + System-HRP(DAB) Labelled polymer K4011 kit	Dako
B220	B-cells	1:600 (1) 1:800 (2)	10% goat serum	Poymer -HRP anti-rat. Rat antibody enhancer	Pollnk-2 plus HRP (DAB) detection kit (D46-15)	GBI Labs
MECA 32	Endothelial cells	1:100	10% goat serum	Poymer -HRP anti-rat Rat antibody enhancer	Polink-2 plus HRP (DAB) detection kit (D46-15)	GBI Labs

Two dilution factors were used for B220 to assess which yielded a better IHC staining. (1) The first dilution factor used for B220 was 1:600. (2) Second dilution factor used for B220 was 1:800. Dilution factor of 1:800 yielded a better IHC staining and was utilized throughout the IHC procedure.

Sections were incubated for 30 minutes with 100 µl of primary antibody which was diluted in 10% normal serum (diluted in 1XPBS buffer). All sections were subsequently rinsed three times in changes of 1xPBS baths for 5 minutes. The slide incubated with CD3 primary antibody were further incubated with 100 µl of secondary rabbit antibody for an additional 30 minutes. For sections with CD3 as primary antibody, the secondary antibody Labelled polymer HRP anti-rabbit from Dako Envision system-HRP (DAB) (Kit 4011 kit) was used. Section incubated with B220 and MECA 32 primary antibodies were incubated with 100 µl Rat antibody enhancer first for 10 minutes and rinsed with three changes of 1xPBS baths for 5 minutes. 100 µl of polymer-HRP for rat was applied to all sections and incubated for a consecutive 10 minutes subsequent three washes in 1xPBS baths for 5 minutes. For sections with B220 and MECA32, the secondary antibody Polink-2 plus HRP anti -Rat DAB detection kit (D46-15) rat antibody enhancer was used.

Adequate amount of newly prepared chromogen solution, 100 µl, from the two detection kit was added to each section and incubated for 5 minute with the polilink-2 plus HRP anti-rat DAB detection kit (D46-15) and for 10 minutes with the Labelled polymer HRP anti-rabbit from Dako Envision system-HRP (DAB) (K 4011) kit. **Table 4** lists an overview of concentration of normal serum added and dilution factor of each antibody used, and detection kits used for the different antibodies. Addition of chromogen was performed under the biosafety cabinet. The sections were counterstained with hematoxylin for thirty seconds, rinsed in running deionized water until clear. The sections were blued Scott's solution for 15 seconds and thereafter rinsed in running deionized

water prior dehydration. The sections were dehydrated in increasing ethanol solution (twice in 96% alcohol and twice in absolute ethanol, for 30 seconds each). The PAP pen marker was removed as the slides were cleared in two changes of xylen baths, 30 seconds each, and mounted with histokit.

2.2.3 Scoring system and quantification of in situ protein expression

IHC is conventionally method utilized for the monitoring of protein expression and localization in the context of tissue morphology (118). This technique uses antibodies for the detection and examining of protein expression in the native tissue (118). TLS are considered to supply a site that enables immune cell interactions which lead to local antigen specific T- and B-lymphocyte activation, priming, and differentiation into effector cells (118). These activities initiate or generate an adaptive immune response which aggravate autoimmune disease (118). Additionally, IHC is an entrenched tool utilized to aid in identification of a wide spectrum of specific pathogenic processes (119). Post analytic variable of IHC analysis involves reporting of results as well as result interpretation (119). Moreover, misinterpretation of positive and negative, inappropriate morphological context, unclear scoring systems, and insufficient statistical analysis make it hard to perceive any data and compare it to equate scientific information (119). However, utilizing a clear scoring definition will meliorate comprehension of presented data which will, additionally, increase repeatability of scoring system (119). Scientists design an individual scoring system for many IHC markers, as a widely scoring system for IHC does not yet exist (119). Qualitative scoring system for data interpretation are commonly utilized amongst scientists (119). For this study, I have devised a scoring system which will be implemented in data evaluation and interpretation.

Detection of TLS was made possible by utilizing IHC technique where two specific B- and T-lymphocyte markers, CD3 and B220, were investigated. These markers made the investigation of TLS aggregates clearly visible under the light microscope. IHC result are based on qualitative microscopic assessment of antibodies staining of the various tissues under investigation. Three scoring systems are utilized for the assessment of CD3, MECA 32 and B220 expression. One for assessing the immunostaining intensity and background staining as well as a descriptive morphological assessment of tissues (**Table 5**). Qualitative scoring of antibody expression where

the overall IHC-positive stained cells are evaluated (**Table 6**). Lastly is the qualitative assessment of TLS, this is simply done by observing the presence or lack of TLS within the various tissues.

Table 3: Qualitative scoring of immunostaining results

Score	Score description
Optimal	An optimal score is given only if the antibodies clearly stain the cells it ought to stain, at the same time as they do not stain cells that the antibodies are not supposed to stain. If the staining gave background color that disturbed the assessment to such an extent that it was difficult to assess whether a cell was positive or negative, then there were withdrawals in the score. It is important that the morphology is well preserved after unmasking during the immunohistochemical procedure. Deduction in scores were only made if background staining made, as well as morphology of the tissue made it difficult to assess what kind of cells were positive or negative.
Moderate/Good	Withdrawal in score is given if the tissue stained more cells than it should or less than it should. Deduction in scores were given for weak immune staining, if background staining made, as well as morphology of the tissue made it difficult to assess what kind of cells were positive or negative.
Suboptimal	This score was given when the immunostaining is at such a level that the whole examination is of little help. Additionally, when cells that were not supposed to be stained were stained or when background staining as well as tissue morphology made it difficult to assess the tissue rendering the examination useless.

Table 4:Qualitative scoring of CD3, B220 expression

Score	Score description
-	No positive staining
+/-	One or few positive stained cells. Less than one twentieth of cells are positively stained
+	Less than one fifth of cells are positively stained
++	Two fifth of the cells are positively stained
+++	Three fifth of cells are positively stained
++++	More than three fifth of cells are positively stained

2.2.4 RNA extraction/Isolation

Isolating good quality RNA is a fundamental and a prerequisite step in all gene expression studies (120). Obtaining purified intact RNA is the primary and elementary step of many molecular biology techniques such as northern blotting and quantitative polymerase chain reaction (qPCR) (121). A typical mammalian cell contains approximately around 10^{-5} µg of RNA where ribosomal RNA (rRNA) constitute about 80 to 85% (121). Smaller species, however, such as transfer RNA (tRNA) comprise around 10 to 15 % while messenger RNA (mRNA) constitute a meagre 1 to 5% (121).

Isolating high quality RNA from cells grown in culture is an easier to accomplish that, it is more challenging that attempting to isolate high quality RNA from tissue samples (122). The predominant reason for this adversity in precuring high quality RNA is due to the three-dimensional architecture of the tissue (122). The challenge occurs when the three-dimensional architecture of tissue must be deconstructed and removed compared to disruption of a cell monolayer (122). There are important factors to consider when isolating RNA from tissues, these includes the tissue mass, cell types involved, the age of the tissue, the status of the tissue (whether is fresh, flash-frozen, formalin-fixed, animal or plant) (122). It is important to take into account that each tissue type possesses distinctive qualities that make the RNA isolation technique unique to the sample (122). Another challenge when isolating high quality RNA is compounded by the

ubiquity and robust biochemical nature of ribonucleases (RNase) (121). RNase occurs naturally in all cells and will to expeditious degrade RNA (121). RNase are unfortunately also present on the skin which also gives room for contamination (121). Failure to eliminate potential sources of RNase contamination will in general yield a useless and degraded RNA sample (123).

2.4.4.1 Objective of RNA isolation

Isolate total RNA for reverse transcriptase translated into cDNA and analyses of gene expression using quantitative polymerase chain reaction (PCR).

2.4.4.2 Methodology of RNA isolation

Tissue sample from spleen, lung and pancreas were removed from RNAlater using forceps, each tissue sample were then meticulously dissected and measured (on ice). All procedures were performed at RT, unless stated otherwise. Each tissue sample were thereafter transferred to their correspondent marked 2mL Magna Lyse beats tubes.

Tissue sample were lysed in 600µl of TRI Reagent ™ and homogenized in the homogenizer "Precellys 24 (Bertin Technologies, Montigny-le-Bretonneux, France) "at 6000rpm 2x for 10 seconds. After homogenization, the supernatant was transferred into 1.5mL RNase- free tube where equal volume of absolute ethanol was added to the supernatant and the tubes were mixed thoroughly. The mixtures were transferred into their marked Zymo-Spin™ IIC column in a 2ml collection tubes, which was then centrifuged at 13 000rpm for 1 minute. The flow-through was then discarded. 400µL of RNA wash buffer was added to each sample and centrifuged for 1 minute at 13 000rpm. The flow through was decanted. A mixture of DNase I and DNA digestion buffer were directly added to the column matrix and the samples were incubated for 15 minutes. After incubation time, 400µL of Direct-zol™ RNA prewash was added to the column and centrifuged for 1 minute at 13 000rpm. The flow through was decanted and the step was repeated. 700µL of RNA wash buffer was added to each column and centrifuged for 1 min at 13 000rpm, the flow through was discarded. The marked Zymo-Spin™ IIC column were thus equipped with new collection tubes and centrifuged for 1 min at 13 000rpm. The columns were carefully transferred into 1.5 mL RNase-free tubes and 30 µL of DNase/RNase-free water was directly added to the column matrix and centrifuged. The columns were thus discarded and the eluted stock RNA in the 1.5 mL RNase-free tubes were put on ice. The concentration of the isolated RNA stock solution

was measured using the Nanodrop® ND 1000 spectrophotometer, the stock RNA was then stored frozen at ≤ -70ºC.

2.2.5 Agilent; qualitative analysis of total RNA

The Agilent RNA 6000 Nano kit quick start guide was used in the quantitative control analysis of the extracted/ isolated RNA**.** RNaseZAP and RNase-free water were both routinely used for cleansing of electrode, while RNaseZAP was also used for decontamination of electrode. Prior sample analysis, the Agilent 2100 had to be adjusted by two washing steps, once with RNaseZAP and a second wash with RNase-free water The first step in the calibration process, 350µL of RNaseZAP was added to the first washing chip labeled "electrode cleaner", the chip was placed into *the Agilent 2100 bioanalyzer* for one minute. The RNaseZAP was thereafter discarded. RNase-free water was added in another chip and placed into the *Agilent 2100 Bioanalyzer* for one minute, the RNase-free water was discarded and the *Agilent 2100 bioanalyzer* calibrated and ready for use.

To prepare the gel, 550µL of RNA gel matrix was added into a spin filter and centrifuged at 1500g for 10 minutes at room temperature. Post centrifuging, 65µL aliquot of filtrated gel was transferred into a 0.5 RNase-free microcentrifuge tubes. RNA dye concentrate was vortexed for 10 and 1µL of the dye was added into the 65µL aliquot of filtered gel. The tube was vortexed and centrifuged at 13000 f for 10 min at room temperature.

Prior loading the Gel-Dye mix, the RNA chip was put on the chip priming station, and then 9µL of gel-dye mix was pipetted in the well labelled **G**. The plunger was positioned at 1mL and then the chip priming station was closed, the chip was released after 30 seconds. After 5 seconds of waiting, the plunger was slowly pulled back and repositioned to the 1mL position. The chip priming station was reopened and 9µL of gel-dye mix was pipetted in the wells marked **G**. The remaining gel-dye mix was thereafter discarded.

5µL of RNA marker was pipetted in all 12 sample wells and in the well labelled with a ladder on the RNA chip. 1µL of prepared ladder was pipetted in the well-marked with a ladder, and 1µL of the sample were loaded to each of the sample wells. For the unused sample wells, 1µL of water was added. The chip was put horizontally in the IKA vortexer and vortexed for 1 minute at 2400 rpm. The chip was run in the Agilent 2100 Bioanalyzer instrument for analysis.

2.2.6 Reverse transcription and Real Time PCR

Reverse transcription (RT) is a fundamental/principal methodology for gene expression analysis utilizing DNA microarray or real-time quantitative polymerase chain reaction (qPCR)(124). RT-PCR is used to amplify RNA sequences of interest, it's a process by which a reverse transcriptase reaction occurs (125). Reverse transcriptase reaction uses mRNA or another RNA template with random or poly(dT) primers to create complementary DNA (cDNA)(125). This step is preformed to transmute the labile mRNA to more stable DNA and also in order to incorporate the fluorescent label. The cDNA can furthermore act as a template in conventional or other variant PCR reaction (125). The cDNA is utilized to amplify specific products and compare their copiousness with respect to reference genes to normalize the expression (126).

The conversion of RNA to cDNA is accomplished by help of retroviral enzyme reverse transcriptase (127). Reverse transcriptase, which is an RNA-dependent DNA polymerase, synthesizes DNA on an RNA template. For the enzyme reverse transcriptase, a short RNA primer is necessary for the initiation of DNA synthesis and catalyzes polymerization in the 5'-to-3' direction, in addition divalent cations such as Mg^{2+} or Mn^{2+} are incumbent for activity (128). The primary result of DNA synthesis on an RNA template is a DNA-RNA hybrid (128). Some reverse transcriptase therefore possesses RNase H activity (128). The RNase H activity grants the reverse transcriptase ability to degrade the RNA strand of the DNA-RNA hybrid (128). Degradation of the RNA strand gives rise to a cDNA that will be synthesized on the newly formed strand. As a consequence a double stranded complementary DNA (ds cDNA) is produced (128). In this experiment, the primary yield of reverse transcription, the cDNA synthesized from RNA template, was an essential prerequisite step for qPCR.

The qPCR is one of the modern methodologies by which gene expression levels can be measured or rather quantified (129). The method is used to determine gene expression over and above size and sequence information. It allows to quantitate nucleic acids precured from cells or tissues, to compare the variable states of infection, to determine gene expression level of samples and so much more (130, 131). Quantification of RNA expression levels serves as a prime indicator of the physiological status of a cell or tissue (132). Quantitative measurement of specific gene expression

utilizing qPCR is pivotal for comprehension of basic cellular mechanism (131). It is also necessary for detection of modification or alteration in gene expression levels in respond to biological stimuli such as for example growth factor and the like (131).

The major advantages of utilizing qPCR are that it can utilize small amount of template, the method is highly sensitive with an ability to detect products during the reaction (126). The qPCR allows for immediate detection of amplified products at any given cycle using a quantitative relationship with the sequence of interest at the beginning of reaction (132).

The principle behind qPCR is monitoring of the accumulated PCR product or amplicons in "real time" (133). The PCR product formation are continuously monitored throughout the reaction by use of a fluorogenic reporter (134). This is accomplished by measuring the change in emission of fluorescence from either fluorescent DNA-binding dyes or target-specific fluorescently labeled primer or probes added to the PCR (133). All detection methods utilizing fluorescent probe technology are dependent on a process known as fluorescence resonance energy transfer (FRET)(131). It is a process by which transfer of light energy amidst two adjacent dye molecules occurs (131).

The probes that are utilized in qPCR are oligonucleotides of different sizes, they are attached to one or more fluorophores (135). In this experiment hydrolysis probes from TaqMan were employed. These probes are target-specific probes (133). The TaqMan probes are designed with a fluorescent label at the 5' end, a quencher at 3' end and a complementary DNA sequence sandwiched between the two (136).

When the fluorophore and the quencher are unbound and are in close proximity, the quencher is able to reduce is able to reduce the reporter fluorescence intensity by FRET, and therefore no fluorescence is detected (131). When, however, the quencher and the fluorophore are not in close proximity nor in direct contact, the quencher is no longer able to suppress the fluorescence of the fluorophore and thus light is emitted (136).

As the primers are extended in the course of PCR, the probe is encountered, the probe hybridize with its complementary nucleotide sequence (133, 136). Hydrolysis probes uses the 5' exonuclease activity of the Taq polymerase molecule (136). Consequently, during PCR the probes are degraded

by the 5’ exonuclease activity of the polymerase molecule, thereby releasing and separating the 5’ fluorescence reporter dye from the 3’ quencher dye, enabling fluorescence emission (131, 133).

2.2.6.1 Objective

The aim of the aforementioned experiments, hitherto, were to prepare cDNA from the extracted RNA product by means of reverse transcriptase reaction. In these experiments, the “High-capacity cDNA reverse transcription kit” was utilized to perform the reverse transcription. The cDNA product obtained served as a template in qPCR by which can gene expression can be studied.

The genes of interest analyzed were inflammatory cytokines such as interleukin 1beta (*IL-1B*), interleukin 18 (*IL-18*), tumor necrosis factor alpha (*TNFα*). The L-selectin, *CD62L*, which participates in leukocyte homing, furthermore the CD62l mediates the primary binding and rolling of leucocytes on endothelial surfaces (137, 138). Growth differentiation factor 3 (*GDF3*), The polymeric immunoglobulin receptor (*Pigr)*, a is transmembrane protein, G-protein-ccoupled receptor 132 (*Gpr132*), a protein coding gene, another protein coding gene *Relt, Emr4* and TATA-Box binding protein *TBP* which was used as a housekeeping/reference gene.

2.2.6.2 Reverse transcription

The procedures in preparing cDNA were performed on ice, unless stated otherwise. A 2x reaction master mix was prepared antecedent reaction plate preparations, this was accomplished by using High capacity cDNA reverse transcription kit components. **Table 7** depicts the components of the 2x reaction master mix. The required volume, withholding the reverse transcriptase, was pipetted into a 0,5 mL Eppendorf PCR tube. Prior reverse transcription addition, 9µL of was withdrawn from the master mix, to ensure a control without reverse transcriptase. The reverse transcriptase enzyme was subsequently added the master mix.

Table 5: Illustrates the procedure and components of the 2x reaction master mix for the reverse transcription reaction for samples with and without the reverse transcriptase enzyme.

Reagents 2x Reaction Mastermix	Components with reverse transcriptase		Components without reverse transcriptase
	1 sample µL added	44 samples µL added	1 sample µL added
10x Reverse transciption buffer	2µL	88µL	2µL
25x dNTPs	0.8µL	35.2µL	0.8µL
10x random primers	2µL	88µL	2µL
Multiscribe reverse transcriptase (50U/µl)	1µL	44µL	0µL
Nuclease -free water	4.2µL	184.8µL	5.2µL
Total volume	10µL	440µL	0.1µL

The cDNA archive reaction was prepared by pipetting 10µL of the master mix into a 0,5mL Eppendorf PCR test tubes, in addition, 10µL RNA sample was added to the tubes. Two negative controls were prepared, one without reverse transcriptase (denoted RT-) consisting of 10µL master mix without reverse transcriptase 8.1 µL of nuclease free water and 2,9 µL of RNA stock solution, one without RNA (denoted RNA -) comprised 10µL master mix with reverse transcriptase and 10µL of nuclease free water. The tubes were vortexed and briefly centrifuged as a mean to spin down content and eliminate bubbles.

The thermae cycle was programmed for the ideal conditions for the reverse transcription reaction. The reaction was incubated at 25 ºC for 10 min, followed by a 2-hour incubation at 37 ºC and cooling down step at 4 ºC. Subsequent reverse transcription completion, the yielded reaction product, cDNA, was stored at -20 ºC.

2.2.7 Real time quantitative PCR

Prior real time qPCR, the cDNAs were diluted with 180 µL nuclease free water. All preparation steps were conducted on ice, unless expressed otherwise. The master mix solution was prepared as delineated in the procedure in **Table 8**. A volume of 7,5 µL of the master mix and 2,5 µL of the diluted cDNA was pipetted in each well of the 96 well plate, which brough the total reaction volume to 10 µL/well. All reactions were run in duplicates with exception of the two

aforementioned negative controls (RT-, RNA-). A final negative control, comprised simply of nuclease free water, was incorporated. The plate was covered with optical adhesive cover and briefly centrifuged to steer clear of bubbles. The plate was subsequently put into the LifeCycler®96 system real time PCR machine.

Table 8: Provides an overview of the procedure, reagents and volume concentration master mix for qPCR

Master mix reagents	volume/reaction	volume/reaction
	1 sample	***n* sample**
Universal master mix	5 µL	5• *n* µL
Primer/probe mix	0,5 µL	0,5• *n* µL
Nuclease-free water	2 µL	3• *n* µL
Total Volume	7,5 µL	7,5• *n* µL

The LightCycler®96 software version 1.1.0.1320 was utilized in programming the conditions for real time qPCR LightCycler®96 analysis machine, all the wells were identified in the software with sample ID and primer/probe of interest. The thermal cycling parameters were programmed for 95 °C for 10 min (Taq activation), 95 °C for 15 seconds for denaturation, and 60 °C for 60 seconds for annealing and extension (**Table 9**)(139).

Table 9: Depicts thermal cycling parameters made in LightCycler®96 software for real-time qPCR

Program	Temperature (°C)	Time (s)
Taq activation	95	600
Denaturation (40 cyles)	95	15
Annealing/extension	60	60

All the raw data were compiled and organized in Microsoft Excel. The real time qPCR data were normalized utilizing a housekeeping/reference gene TATA box binding protein (TBP). The delta quantitative cycle (ΔCq) values were calculated by normalizing the average quantitative cycle (Cq) of the targeted gene by subtracting the average Cq of the housekeeping/reference gene. ΔΔCq was calculated by subtracting the ΔCq value from the average control ΔCq calculated from the young mice (5 weeks old). The Fold change was calculated by using ΔΔCq value for each sample. Equation 1-3 illustrate the statistical calculations mentioned above.

Equation 1 $\Delta Cq = Cq\ target\ gene - Cq\ housekeeping\ gene\ (reerence\ gene)$

Equation 2 $\Delta\Delta Cq = \Delta Cq - average\ control\ \Delta Cq$

Equation 3 $Fold\ change = 2\text{^} - \Delta\Delta Cq$

3 Results

3.1 Immunohistochemistry and assessment of immune cell infiltration in salivary gland, pancreas, and lungs of NZB/W lupus prone mice.

IHC results were assessed and described based on microscopic images and scored according to the criteria listen in Tables 5 and 6. Representative images of different grading were selected and presented in **Figures 20-26**. A short description of each image is given based on tissue morphology, presence, or lack of TLS in tissue as well as a qualitative scoring system of antibody expression. Qualitative assessment of results is based on microscopic assessment of how the different antibodies stain the various tissues. At least two independent investigators scored all the samples. The result from scoring of B and T- lymphocytes in various organs from the different mice are listen in **Table 10.** For the IHC study, three different tissue types of 19 different NZB/W mice were selected for immunostaining. The tissue types of each mice were categorized in 3 categories; lung, salivary gland, and pancreas, of which two slides from each category were prepared to be stained with either a T-cell marker or B-cell marker, CD3 and B220, respectively. Total number of samples were 114, excluding the 6 controls. The immunostaining yielded a vast range of results, ranging from a score of – which denotes that no immune cells were present in the tissue to a scoring of ++++ which signified the presence of abundant immune cells in the tissue. Of the selected NZB/W mice, four yielded a score of – (**Figure 20**) , seven mice yielded a scored of +/- (**Figure 21**) , fourteen mice yielded a score of + (**Figure 22**), twelve mice yielded a score of ++ (**Figure 23**), sixteen mice yielded a score of +++ (**Figure 24**) and 5 mice yielded a score of ++++ **(Figure 25** and **26).**

Table 6: Result overview of immunostaining score in lung, pancreas, and salivary gland tissue of lupus prone NZB/W-J mice

Mouse ID & Strain	Antibodies	Pancreas	Lung	SG	TLS
J1 NZB/W	CD3	+		++	-
	B220	+		+/-	
J2 NZB/W	CD3	+	+++	++	-
	B220	-	+	+	
J3 NZB/W	CD3	+/-	+	+++	SG
	B220	+/-	++	+++	
J4 NZB/W	CD3	+	++	++	-
	B220	-	++	+/-	
J5 NZB/W	CD3	++	+++	+++	SG
	B220	+/-	+	++	
J6 NZB/W	CD3	+	++	++	SG
	B220	+ /-	++	+	
J7 NZB/W	CD3	++	+++	++	-
	B220	+/-	++	+/-	
J8 NZB/W	CD3	+	+++	+	-
	B220	+/-	++	+ /-	
J9 NZB/W	CD3	+++	+++	+++	PA and SG
	B220	+++	+	+++	
J10 NZB/W	CD3	+	+ ++	+++	SG
	B220	-	+	+++	
J11 NZB/W	CD3	++++	+++	++++	PA and SG
	B220	+++	+	+++	
J12 NZB/W	CD3	+	++	+++	SG
	B220	+ /-	+	++	
J13 NZB/W	CD3	++++	++++	++++	PA, Lung, and SG,
	B220	+++	++++	++++	
J14 NZB/W	CD3	+	+++	++++	-
	B220	-	+++	++++	
J15 NZB/W	CD3	+++	+++	+++	PA and SG
	B220	+++	+++	+++	
J16 NZB/W	CD3	+++	+++	+++	PA
	B220	+++	++	+	
J17 NZB/W	CD3	+	++++	+++	Lung
	B220	+	++++	++	
J18 NZB/W	CD3	++++	++++	++++	PA, Lung, and SG,
	B220	+++	++++	+++	
J19 NZB/W	CD3	+++	+++	+++*	PA
	B220	+++	++	+++*	

*TLS: tertiary lymphoid structure. SG: salivary gland. PA: pancreas - no positive cells, +/ extremely few positive cells + few scattered/or few positive cells ++ moderate amount to great deal of positive cells +++ great deal of positive cells ++++ abundant positive cells. *Lymphom SG?*

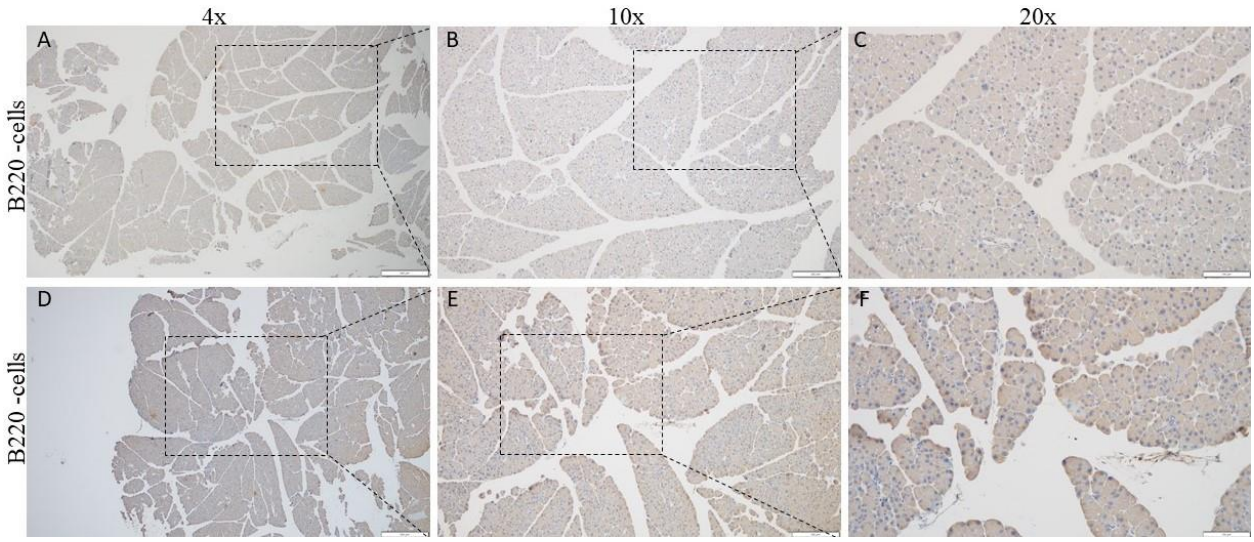

Figure 20:Representative picture of B-cells in pancreatic tissue of proteinuric NZB/mice.(*A-C)B220 negative B cells within pancreatic tissue of a 25-week-old proteinuric NZB/W mouse, with an overall score of -. (D-F) B220 negative B cells within pancreatic tissue of a 31-week-old proteinuric NZB/W mouse, with an overall score of -. Tissue morphology was optimal in both tissues. Scale bars: (A and D) 500µm, (B and E) 200µm, (C and F) 100µm.*

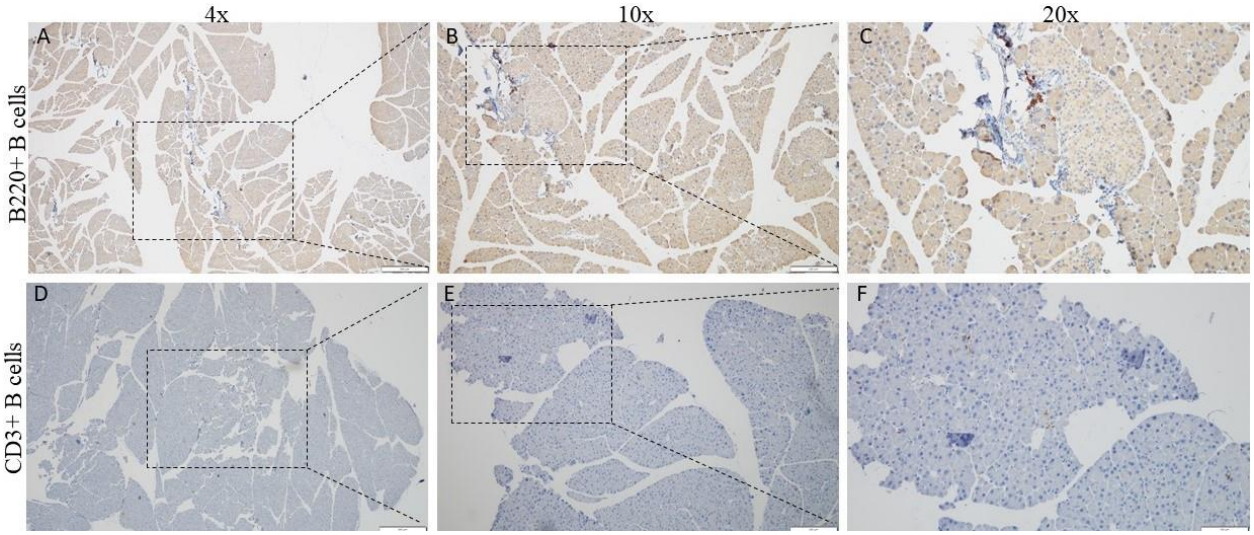

Figure 21: Representative picture of B and T cells in pancreatic tissues of proteinuric and anti dsDNA positive NZB/W mice.(*A-C) B220 positive cells (brown) detected within pancreatic tissue of a 25-week-old proteinuric, anti dsDNA positive NZB/W mouse, with an overall score of +/- (D-F) CD3 positive cells (brown) detected within pancreatic tissue of a 25-week-old proteinuric, anti dsDNA positive NZB/W mouse, with an overall score of +/-. Tissue morphology was optimal in both tissues. Scale bars: (A and D) 500µm, (B and E) 200µm, (C and F) 100µm.*

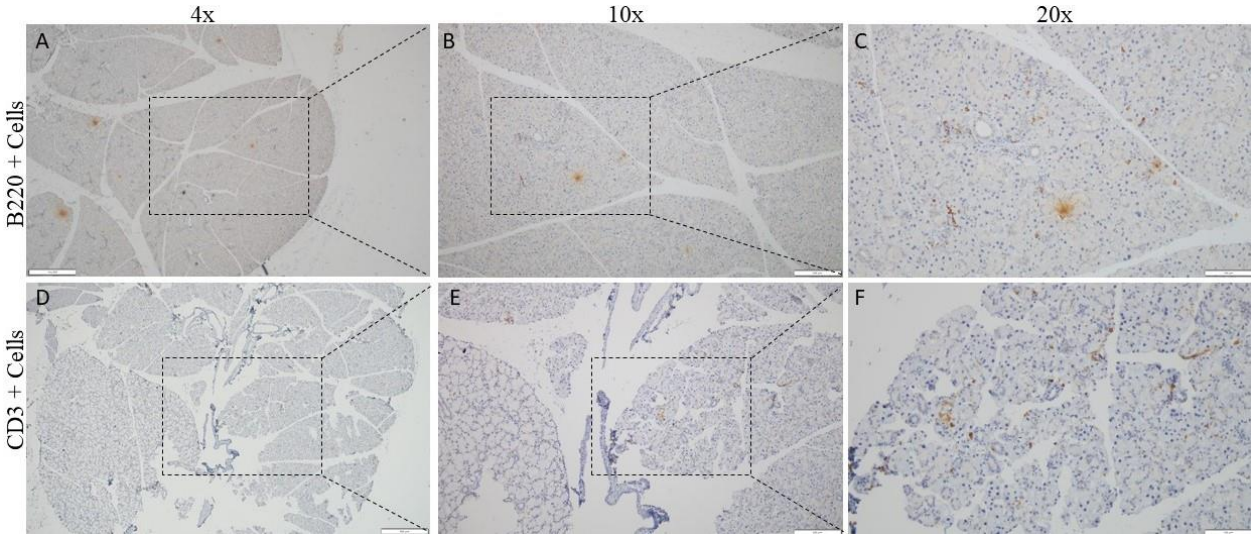

Figure 22:Representative picture of B and T cells in salivary gland tissue of proteinuric NZB/W mice. *(A-C) B220 positive cells (brown) detected within salivary gland tissue of a 25-week-old proteinuric NZB/W mouse, with an overall score of +. (D-F) CD3 positive cells (brown) detected within salivary gland tissue of a 29-week-old proteinuric, anti dsDNA positive NZB/W mouse, with an overall score of +. Tissue morphology was optimal in both tissues. Scale bars: (A and D) 500µm, (B and E) 200µm, (C and F) 100µm.*

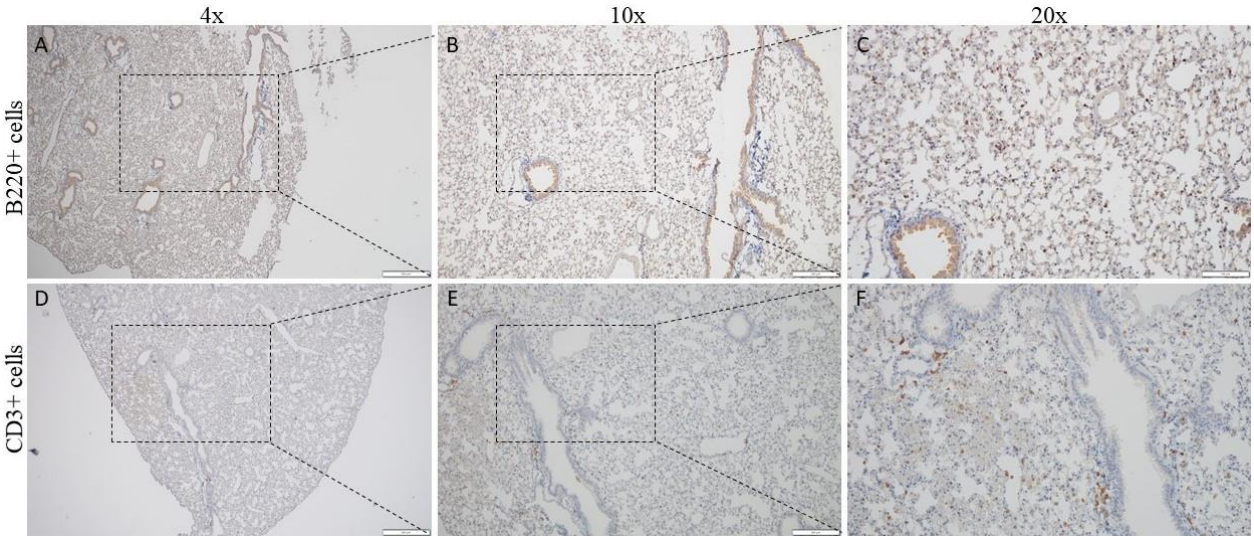

Figure 23: Representative picture of B and T cells in lung tissue of proteinuric NZB/W mice. A*-C) B220 positive cells (brown) detected within lung tissue of a 25-week-old proteinuric NZB/W mouse, with an overall score of ++. (D-F) CD3 positive cells (brown) detected within lung tissue of a 32-week-old proteinuric, anti dsDNA positive NZB/W mouse, with an overall score of ++. Tissue morphology was optimal in both tissues. Scale bars: (A and D) 500µm, (B and E) 200µm, (C and F) 100µm.*

(

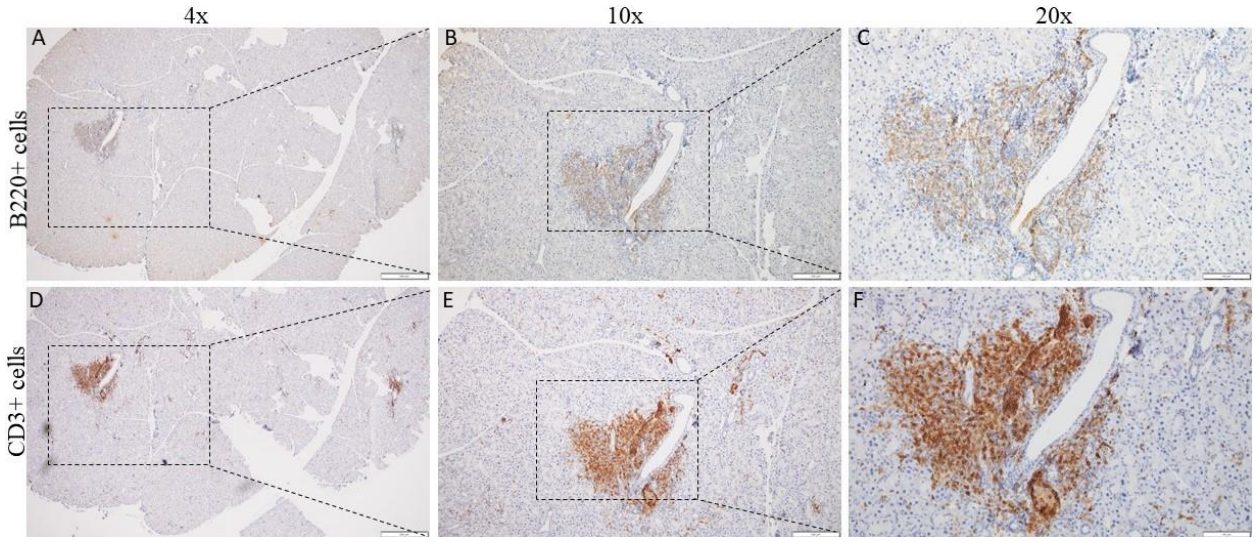

Figure 24: Representative picture of B and T cells in salivary gland tissue of proteinuric NZB/W mice. *(A-C) B220 positive cells (brown) detected within salivary gland tissue of a 28-week-old proteinuric NZB/W mouse, with an overall score of +++. (D-F) CD3 positive cells (brown) detected within salivary gland tissue of a 28-week-old proteinuric NZB/W mouse, with an overall score of +++. Tissue morphology was optimal in both tissues. Scale bars: (A and D) 500µm, (B and E) 200µm, (C and F) 100µm.*

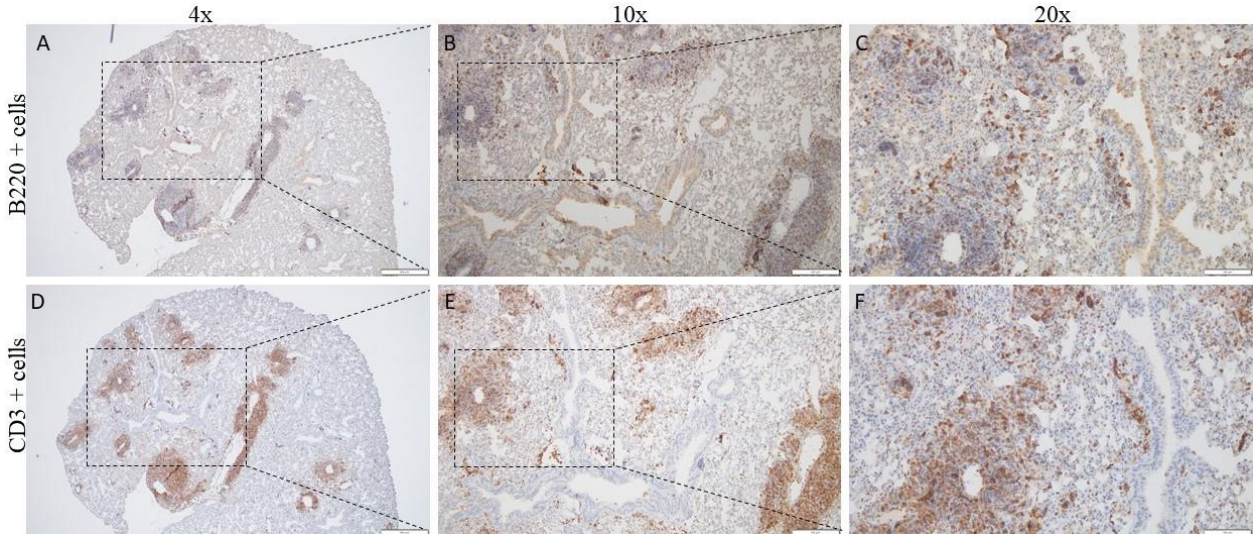

Figure 25: Representative picture of B and T cells in lung tissue of proteinuric, anti dsDNA positive NZB/W mice. *(A-C) B220 positive cells (brown) detected within lung tissue of a 27-week-old proteinuric, anti dsDNA positive NZB/W mouse, with an overall score of ++++. (D-F) CD3 positive cells (brown) detected within lung tissue of a 27-week-old proteinuric, anti dsDNA positive NZB/W mouse, with an overall score of ++++. Tissue morphology was optimal in both tissues. Scale bars: (A and D) 500µm, (B and E) 200µm, (C and F) 100µm.*

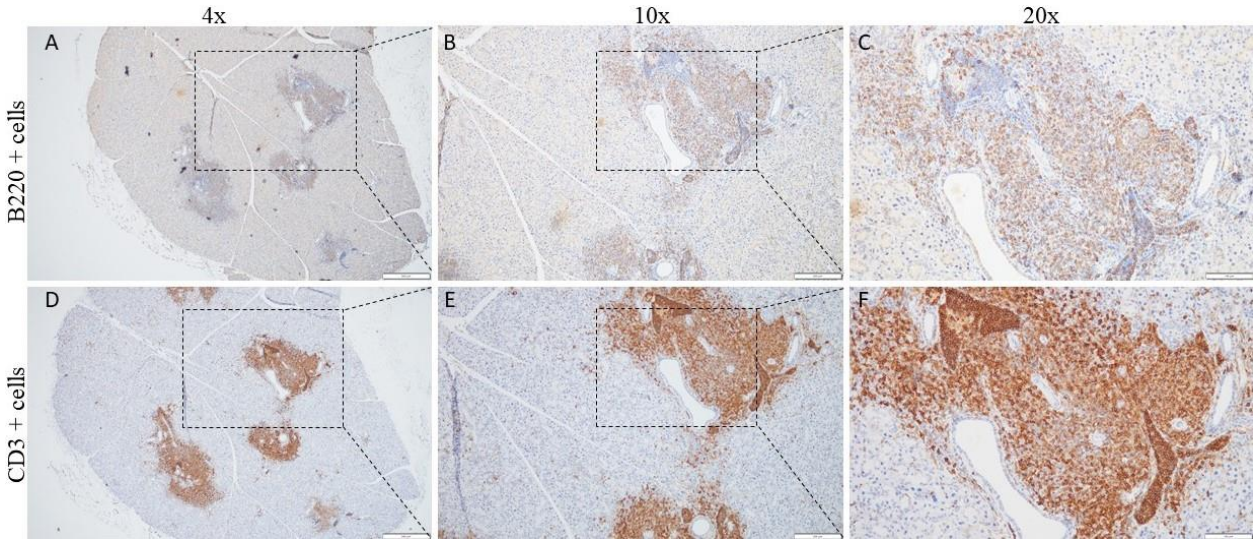

Figure 26: Representative picture of B and T cells in salivary gland tissue of proteinuric, anti dsDNA positive NZB/W mice. *(A-C) B220 positive cells (brown) detected within salivary gland tissue of a 27-week-old proteinuric, anti dsDNA positive NZB/W mouse, with an overall score of ++++. (D-F) CD3 positive cells (brown) detected within salivary gland tissue of a 27-week-old proteinuric, anti dsDNA positive NZB/W mouse, with an overall score of ++++. Tissue morphology was optimal in both tissues, (A-C) weaker immunostaining. Scale bars: (A and D) 500µm, (B and E) 200µm, (C and F) 100µm.*

3.2 Tertiary lymphoid structures in salivary glands, pancreas, and lungs of NZB/W lupus prone mice

All sections were further assessed for the presence of TLS, defined as aggregates of B and T cells. Of the 19 NZB/W mice, a total of 12 mice displayed TLS within the various tissues (**Table 10**). Additionally, 11 out of the 12 mice displaying TLS were proteinuric and anti-dsDNA Ab positive, nonetheless the age of these mice varied between 25- 35-week old (**Table 10**). **Figures 27-32** show representative pictures of TLS in the different organs. Some mice had TLS only in SG (**Figure 27**), some mice displayed TLS in both SG and pancreas (**Figures 28** and **29**, respectively), while some had TLS in both SG, pancreas and lung (**Figures 30, 31** and **32**, respectively). An overview of the different mice, including age, proteinuria, anti-dsDNA antibodies, immunostaining of different organs, as well as TLS depiction is presented in **Table 11**. A Spearman correlation matrix comparing the different parameters listed in **Table 11**, is shown in **Table 12**. The Spearman correlation disclosed no significant statistical correlation between TLS and age. Moreover, there were no correlation between proteinuriaproteinuria and TLS. There were, however, significant statistical correlation between the weeks Ab+ and TLS in kidney and pancreas. TLS in lung and SG did not display any significant statistical correlations. Ab+ showed a correlation with T and B-lymphocyte infiltration in lung tissue. Additionally, there was a statistical correlation with Ab+ and T-lymphocyte infiltration in SG, and B-lymphocyte infiltration in SG correlated with age.

Table 7: Overviews of clinical parameters and overall result of immunostaining of the lungs, pancreas, and salivary glands including TLS results overview of lung, pancreas, salivary gland, and kidney of NZB/W lupus prone mice

Mouse ID	Strain	Weeks old	anti-dsDNA ab	Protein in urin	TLS Kidney	B220 Immune cells Pancreas	CD3 Immune cells Pancreas	TLS PA	B220 Immune cells SG	CD3 Immune cells SG	TLS SG	B220 Immune cells Lung	CD3 Immune cells Lung	TLS Lung
J1	NZB/W	22 wo	neg	1+		+	+		+/-	++		+	++	
J2	NZB/W	25 wo	?	1+		-	+		+	++		+	+++	
J3	NZB/W	25 wo	1w Ab+	1+	Y	+/-	+/-		+++	+++	Y	++	+	
J4	NZB/W	25 wo	neg	2+		-	+		+/-	++		++	++	
J5	NZB/W	25 wo	3w Ab+	2+	Y	+/-	++		+++	++	Y	+	+++	
J6	NZB/W	28 wo	12w Ab+	4+	Y	+	+/-		++	+		++	++	
J7	NZB/W	32 wo	4w Ab+	2+		+/-	++		++	+/-		++	+++	
J8	NZB/W	29 wo	1w Ab+	1+		+	+/-		+/-	+		++	+++	
J9	NZB/W	32 wo	2w Ab+	2+	Y	+++	+++	Y	+++	+++	Y	+	+++	
J10	NZB/W	28 wo	?	4+		-	+		+++	+++	Y	+	+++	
J11	NZB/W	33 wo	14w Ab+	1+	Y	+++	++++	Y	+++	++++	Y	+	+++	
J12	NZB/W	35 wo	?	2+		+/-	+		++	+++	Y	+	++	
J13	NZB/W	27 wo	11w Ab+	4+	Y	+++	++++	Y	++++	++++	Y	++++	++++	Y
J14	NZB/W	31 wo	?	4+		-	+		++++	++++		+++	+++	
J15	NZB/W	30 wo	6w Ab+	4+	Y	+++	+++	Y	+++	+++	Y	+++	+++	
J16	NZB/W	30 wo	11w Ab+	4+	Y	+++	+++	Y	+	+++		++	+++	
J17	NZB/W	34 wo	16w Ab+	3+	Y	+	+		++	+++		++++	++++	Y
J18	NZB/W	34 wo	16w Ab+	3+	Y	+++	++++	Y	+++	++++	Y	++++	++++	Y
J19	NZB/W	33 wo	14w Ab+	3+/4+	Y	+++	+++	Y	+++	+++	Y	++	+++	

Table 8:Spearman correlation matrix showing correlations coefficient of comparisons of clinical parameters, Tertiary lymphoid structure, T-lymphocytes and B-lymphocytes in kidney, lung, pancreas, and salivary glands of NZB/W mice.

	Age	Weeks Ab+	Proteinuria	TLS kidney	TLS lung	TLS Pancreas	TLS SG	T cells Pancreas	B cells Pancreas	T cells SG	B cells SG	T cells Lu	B cells Lu
Age		**0,821**	0,251	0,216	0,110	0,381	0,281	0,442	0,314	0,447	**0,464**	**0,570**	0,424
Weeks Ab+	***<0,001***		**0,611**	**0,706**	0,371	**0,522**	0,314	**0,523**	**0,492**	**0,523**	0,465	**0,638**	**0,632**
Proteinuria	*0,300*	***0,012***		0,305	0,246	0,344	-0,010	0,284	0,287	0,050	0,082	0,292	0,400
TLS kidney	*0,376*	***0,002***	*0,204*		0,293	**0,651**	**0,596**	**0,564**	**0,635**	**0,663**	**0,600**	0,363	0,379
TLS lung	*0,653*	*0,157*	*0,311*	*0,224*		0,094	0,018	0,089	0,102	0,310	0,271	**0,468**	**0,610**
TLS Pancreas	*0,108*	***0,038***	*0,150*	***0,003***	*0,703*		**0,587**	**0,939**	**0,910**	**0,536**	**0,625**	**0,574**	0,413
TLS SG	*0,244*	*0,237*	*0,967*	***0,007***	*0,941*	***0,008***		**0,590**	**0,565**	**0,856**	**0,905**	0,185	0,258
T cells Pancreas	*0,058*	***0,038***	*0,239*	***0,012***	*0,717*	***<0,001***	***0,008***		**0,862**	**0,549**	**0,629**	**0,611**	**0,541**
B cells Pancreas	*0,191*	*0,053*	*0,233*	***0,003***	*0,677*	***<0,001***	***0,012***	***<0,001***		**0,498**	**0,601**	**0,484**	0,398
T cells SG	*0,055*	***0,038***	*0,838*	***0,002***	*0,197*	***0,018***	***<0,001***	***0,015***	***0,030***		**0,891**	0,304	**0,471**
B cells SG	***0,045***	*0,070*	*0,738*	***0,007***	*0,262*	***0,004***	***<0,001***	***0,004***	***0,007***	***<0,001***		0,342	0,389
T cells Lu	***0,011***	***0,008***	*0,226*	*0,126*	***0,043***	***0,010***	*0,449*	***0,005***	***0,036***	*0,205*	*0,152*		**0,709**
B cells Lu	*0,071*	***0,009***	*0,090*	*0,109*	***0,006***	*0,079*	*0,286*	***0,017***	*0,092*	***0,042***	*0,099*	***0,001***	

Cursive numbers: P values; Bold numbers: statistical significant correlations coefficient

Of the tree tissue analyzed from NZB/W mouse J3, only SG resulted in TLS with an overall score of +++ (**Figure 27, Table 10**). The pancreatic tissue had only few scattered positively stained cells yielding a score of +/- for both B220 and CD3 (Data not shown). For CD3 of the lung, there were few scattered cells thus yielding a score of +, the lung tissue with B220 antibody moderate number of positive cells and resulted in a score of ++ (Data not shown).

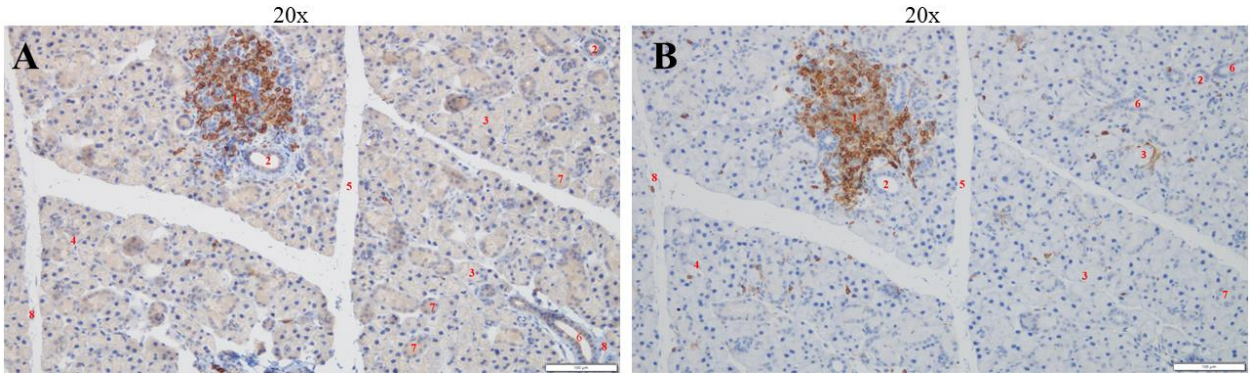

Figure 27: Depict TLS in salivary gland tissue of a 25-week-old, proteinuric and anti-dsDNA positive J3 NZB/W mouse.*(A)Positively stained B220 cells (brown), (B)positively stained CD3 cells(brown). (1) TLS, (2) Interlobular duct, (3) Mucous acini, (4) Lobule, (5) Septum, (6) Interlobular excretory duct, (7) Serous acini, (8) Connective tissue. Tissue morphology: Optimal. Scale bars: 100µm.*

TLS was discovered in two types of tissues from NZB/W mouse J11, in pancreatic tissue and salivary gland (**Table 10**). Cells that were positively stained with B220 in salivary gland were mostly concentrated in the area of TLS, while there were no B220 positively stained cells throughout the whole tissue, the overall score was therefore +++ (**Figure 28**). Cells that were positively stained with CD3 in salivary gland were concentrated in aggregates (TLS) but there were also positively stained CD3 cells throughout the tissue section, the overall score for salivary gland with CD3 antibody was therefore ++++ (**Figure 28**).

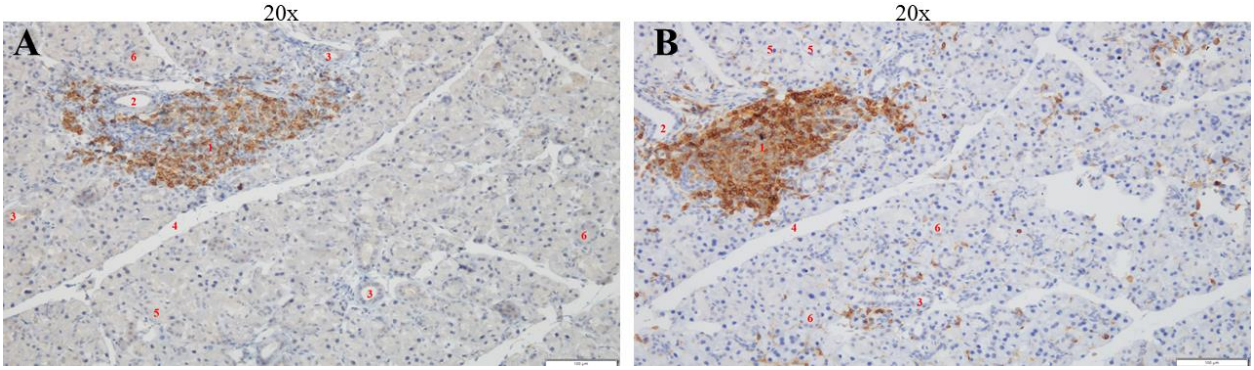

Figure 28:Depict TLS in salivary gland tissue of a 33-week-old, proteinuric and anti-dsDNA positive J11 NZB/W mice. *(A)positively stained B220 cells (brown), (B)positively stained CD3 cells(brown). (1) TLS, (2) Interlobular excretory duct, (3) Intralobular duct, (4) Septum, (5) Mucous acini, (6) Serous acini. Tissue morphology: Optimal. Scale bars: 100µm.*

Cells that were positively stained with B220 in pancreas were mostly concentrated at the site of aggregated (TLS), while there were no B220 positively stained cells throughout the whole tissue, the overall score was therefore +++ (**Figure 29A**). Cells that were positively stained with CD3 in pancreas were concentrated in aggregates (TLS) (**Figure 29B**). There were, however, positively stained CD3 cells throughout the tissue section thus the overall with CD3 antibody was therefore ++++. The lung tissue on the other hand displayed very few positive B220 cells that were scattered withing the tissue, the overall score was + (Data not shown). CD3, in the lung, displayed more positive stained cells and had an overall score of ++ (Data not shown).

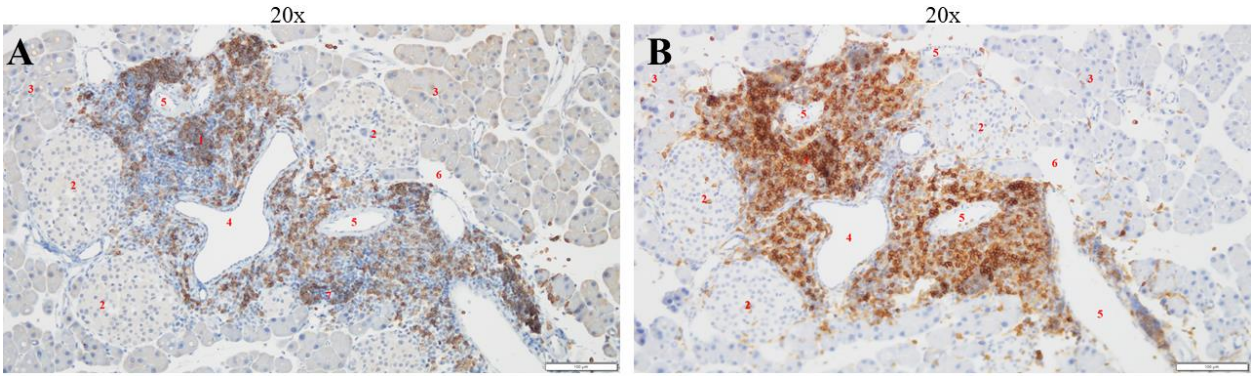

Figure 29: Depict TLS in pancreatic tissue of a 33-week-old, proteinuric and anti-dsDNA positive J11 NZB/W mouse*. (A)positively stained B220 cells (brown), (B)positively stained CD3 cells(brown). (1) TLS, (2) Islets of Langerhans, (3) Exocrine secretory acini, (4) Interlobular duct, (5) Artery, (6) Vein, (7) Lymph vessel. Tissue morphology: Optimal. Scale bars: 100µm.*

TLS was discovered in all tissues type of J18 NZB/W mouse (**Table 10**). Cells stained with B220 in salivary glands were mostly concentrated in the zone where TLS aggregate was located, only a very few cells were stained positive for B220 throughout the tissue (**Figure 30A**). The overall score for salivary gland stained with B220 was +++ (**Table 10**). Cells stained with CD3 were concentrated in the zone where TLS aggregate was located, there were, additionally, positively stained CD3 cells throughout the whole salivary gland tissue (**Figure 30B**). The overall score for salivary gland stained with CD3 was ++++.

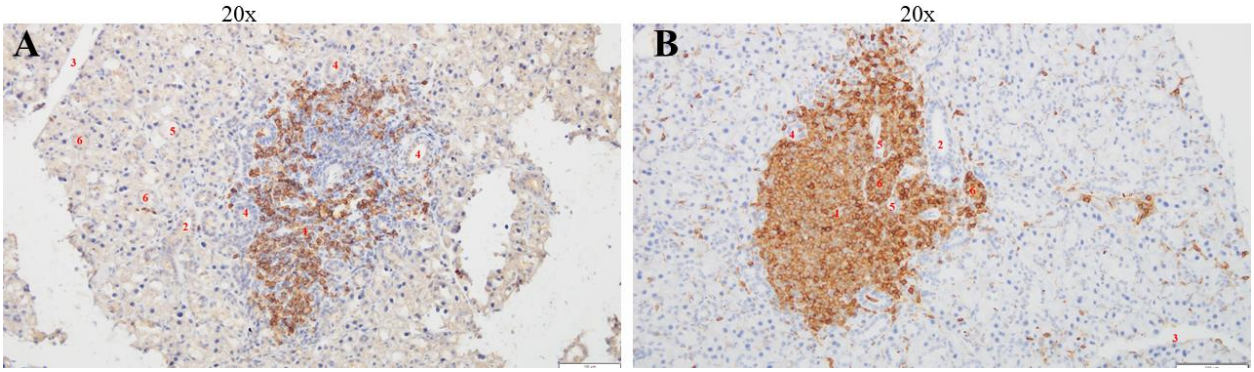

Figure 30:Depict TLS in salivary gland tissue of a 34-week-old proteinuric and anti-dsDNA positive J18 NZB/W mouse*. (A) positively stained B220 cells (brown), (B)positively stained CD3 cells(brown). (1) TLS, (2) Interlobular excretory duct, (3) Septum (4) Intralobular duct, (5) Artery (6) Lymph vessel. Tissue morphology: Optimal. Scale bars: 100µm.*

Cells stained with B220 in pancreas were mostly concentrated in the zone where TLS aggregate was located, only a very few cells were stained positive for B220 throughout the tissue (**Figure 31A**). The overall score for the pancreatic tissue stained with B220 was +++ (**Table 10**). Cells stained with CD3 were concentrated in the zone where TLS aggregate was located, there were,

additionally, positively stained CD3 cells throughout the whole tissue of pancreas (**Figure 31B**). The overall score for pancreas stained with CD3 was ++++ (**Table 10**).

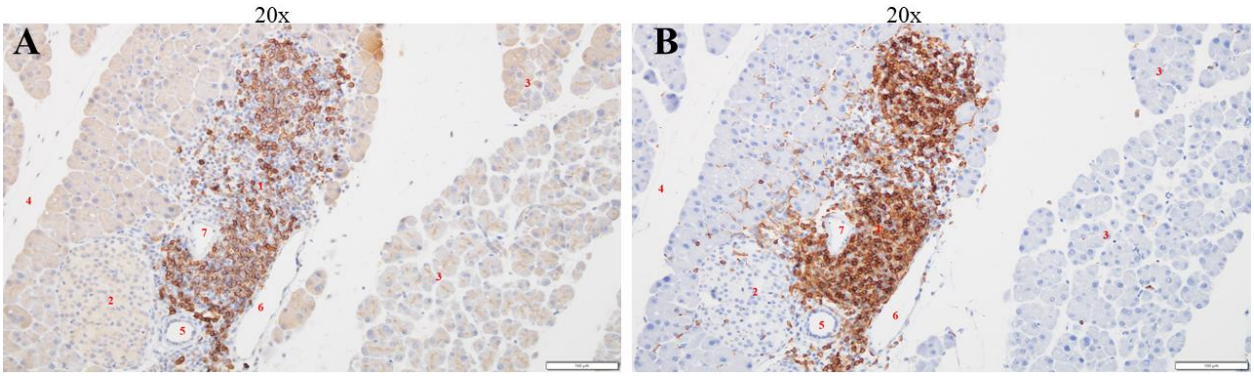

Figure 31: Depict TLS in pancreatic tissue of a 34-week-old, proteinuric and anti-dsDNA positive J 18 NZB/W mouse.*(A)positively stained B220 cells (brown), (B)positively stained CD3 cells(brown). (1) TLS, (2) Islet of Langerhans, (3) Exocrine secretory acini, (4) Interlobular septum, (5) Intracellular duct, (6) Vein, (7) Artery. Tissue morphology: Optimal. Scale bars: 100µm.*

Lung tissue exhibited abundant amount of positively stained cells throughout the tissue compared to all the tissue samples of J18 NZB/W mouse (**Figure 32**). Cells stained with B220 and CD3 were not only concentrated in the zone where TLS aggregate was located, rather these were observed, scattered, throughout the tissue (**Figure 32 A** and **B**, respectively). The overall score for lung tissue stained with B220 was thereby ++++, and the overall score for lung tissue stained with CD3 was therefore ++++ (**Table 10**).

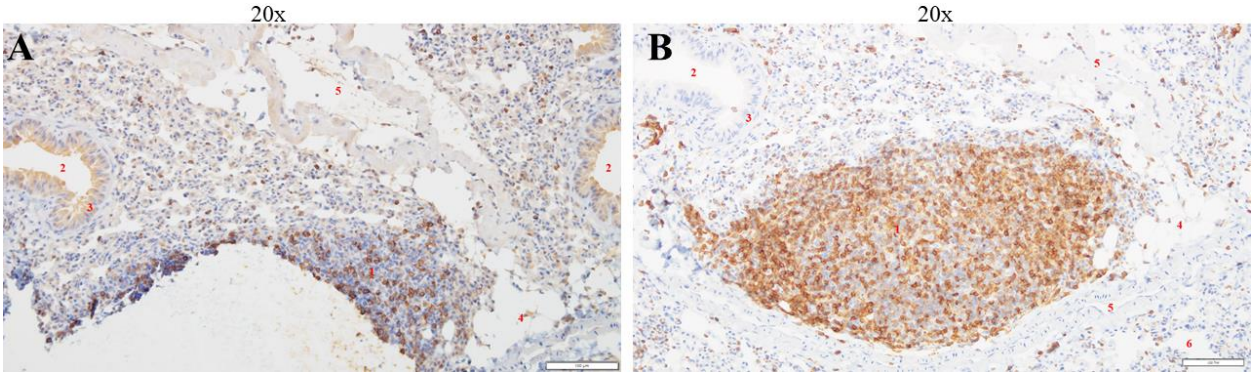

Figure 32: Depict TLS in lung tissue of a 34-week-old, proteinuric and anti-dsDNA positive J18 NZB/W mouse*. (A)positively stained B220 cells (brown), (B)positively stained CD3 cells(brown). (1) TLS, (2) Bronchiole, (3) Epithelium, (4) Alveolar sac, (5) Artery, (6) Vein. Tissue morphology: Optimal. Scale bar: 100µm.*

3.3 RNA expression: qualitative assessment of RNA isolation from pancreas, spleen, and lung tissue of NZB/W lupus prone mice.

To be able to measure the gene expression levels of selected genes total RNA was isolated and the quality assessed. For this experiment, 18 different mice categorized by age were utilized. Various tissue sample, preserved in RNAlater, such as spleen, lung, and pancreatic tissue from these 18 mice were used in the study. **Table 13** catalogues the different mice, organs, the amount of tissues used and the RNA concentration isolated. RNA integrity was maintained by utilizing RNA later for storage of tissue and TRIzol during tissue homogenization. It was observed, from nanodrop readings, that pancreatic tissue often yielded higher RNA concentration value than other tissues (**Table 13**). Additionally, Spleen occasionally yielded high RNA concentration while lung, in comparison, yielded the lowest RNA concentration value from the RNA isolated (**Table 13**).

Concentration as well as quality of total extracted RNA was evaluated utilizing Agilent RNA 600 nano kit. Furthermore, qualitative analysis of total RNA isolated from the various tissues gave a ribosomal integrity number (RIN) value. The RIN value determined the RNA quality and degree of RNA degradation of all samples. A RIN value of 10 equates with perfect RNA sample, a sample that is without any degradation, while a RIN value of 1 equates with a completely degraded RNA sample. RIN value between 1-10 signified a continuing degradation condition of RNA sample. The various sample yielded an array of RIN values (**Table 13**). It was observed that most of the RIN values from pancreatic tissues were the lowest, with a RIN value ranging between the 2.40 - 2.60. The RIN value observed in spleen tissue ranged from 2.20- 8.60 (**Table 13**). Only 2 of the 18 mouse, NZB/W-F2 and NZB/W-F13 yielding the lowest values of 2.20 and 2.80, respectively. Some of the highest RIN values were detected in lung samples. The RIN values of lung samples ranged between 4.30-8.70 (**Table 13**).

Table 9: Overview of RNA concentration and RIN value from RNA isolated from lung, pancreas, and spleen of lupus prone NZB/W-F mice.

Sample ID	Strain	Sex	Age (wo)	Organ isolated from	Tissue measured (mg)	RNA-concentration (ng/µL)	RIN Value
F1	NZB/W	Female	5	Pancreas Spleen Lung	20.2 8.6 23.1	513.9 369.4 216.9	2.50 6.60 4.30
F2	NZB/W	Female	5	Pancreas Spleen Lung	7.9 8.9 26.7	435.3 353.2 147.5	2.60 2.20 7.70
F3	NZB/W	Female	5	Pancreas Spleen Lung	12.7 9.8 18.9	74.5 357.8 98.0	2.50 6.80 6.70
F7	NZB/W	Female	12	Pancreas Spleen Lung	14.5 7.4 18.9	151.1 51.4 18.8	2.40 7.20 5.90
F8	NZB/W	Female	12	Pancreas Spleen Lung	19.4 33.3 16.2	166.4 26.8 24.43	2.40 N/A 5.20
F9	NZB/W	Female	12	Pancreas Spleen Lung	19.6 13.1 31.9	305.1 30.5 40.46	2.50 N/A 5.30
F13	NZB/W	Female	17	Pancreas Spleen Lung	16.1 10.9 23.6	533.0 24.7 26.36	2.60 2.80 5.20
F14	NZB/W	Female	17	Spleen Lung	10.7 30.6	27.6 12.95	N/A 4.70
F15	NZB/W	Female	17	Spleen Lung	9.2 13.5	17.0 16.75	6.50 4.60
F19	NZB/W	Female	5	Spleen Lung	10.9 16	27.9 10.38	6.80 4.40
F20	NZB/W	Female	5	Spleen Lung	10.8 18.5	33.1 17.1	8 6.70
F21	NZB/W	Female	5	Spleen Lung	11.1 18.5	24.0 17.0	8.20 5.20
F25	NZB/W	Female	12	Spleen Lung	6.5 15.1	6.4 2.6	N/A N/A
F26	NZB/W	Female	12	Spleen Lung	11.7 23.4	20.0 4.0	7.30 N/A
F27	NZB/W	Female	12	Spleen Lung	9.7 17.1	14.9 2.2	8.60 N/A

F31	NZB/W	Female	18	Spleen Lung	12.5 21.1	65.1 564.7	7.90 8.50
F32	NZB/W	Female	18	Spleen Lung	12.7 26.2	488.2 165.8	8.20 8.30
F33	NZB/W	Female	18	Spleen Lung	12.7 23.4	556.8 102.3	6.40 8.70

The quality of the isolated RNA was verified using the Agilent 2100 Bioanalyzer. **Figure 37** shows representative graphs of the results obtained from control analysis of RNA isolated from lung, pancreas, and spleen from NZB/W-F mice. RIN values varied among the different tissues, some with inadequate RIN value and other with high adequate RIN value. Pancreas presented with the lowest quality of RNA isolate and low RIN value (**Figure 37C**). When assessing the integrity of some tissue RIN values was not able to be calculated, consequently yielding RIN as N/A (Figure **37D**).

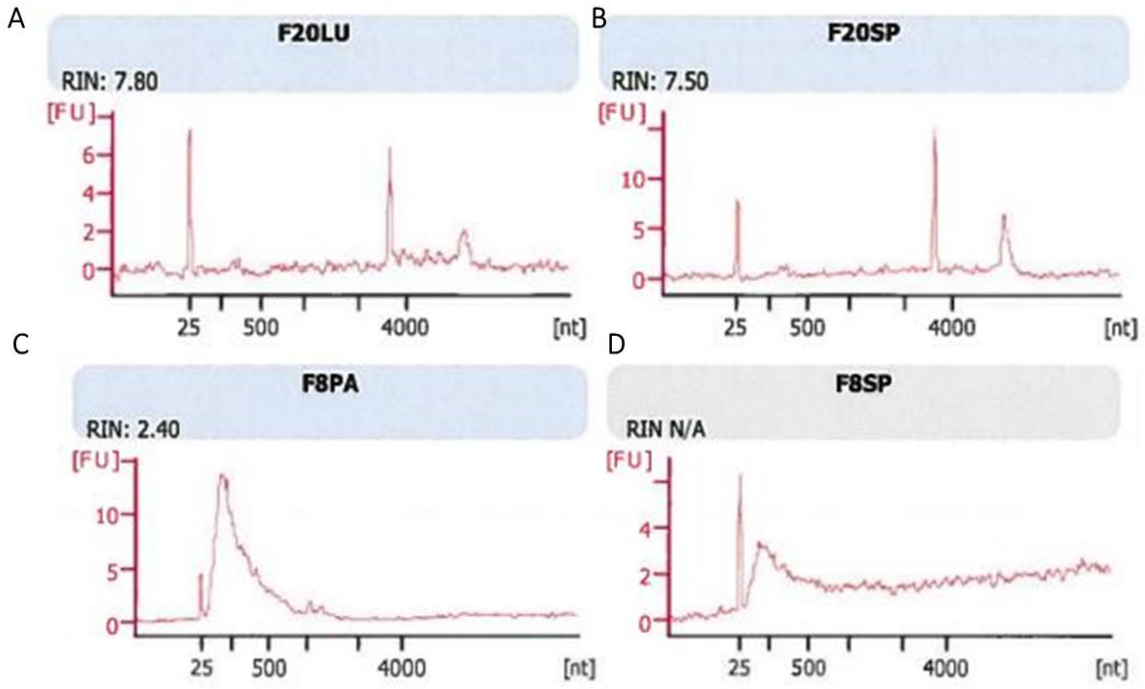

Figure 33: RIN value generated from Agilent 2100 Bioanalyzer software (Santa Vlara, CA, USA). *RNA integrity measurements from RNA isolated from lung, spleen, and pancreatic tissue of NZB/W lupus prone mice. Illustration of four representative RIN values of varying stages of RNA integrality. Adequate quality RIN plots are observed in RNA isolate of lung and spleen of NZB/W-F20 mouse. Almost not much signal in the inter-region and the fast region. Inadequate and low-quality RIN plots are observed in RNA isolate of pancreas and spleen of NZB/W-F8 mouse. LU: Lung, PA: Pancreas, SP: Spleen.*

3.4 Real time PCR: assessment of mRNA expression of lung, spleen, and kidney with various genes

To be able to study and quantify gene expression levels of selected genes, cDNA was synthesized to amplify total RNA previously isolated. The total RNA was converted to cDNA by reverse transcription. From the abovementioned 18 NZB/W mice (excluding NZB/W-F27 spleen and NZB/W-F2 lung), therefore 38 sample of cDNA was prepared, the samples were categorized in a chronologically order number and further divided in their tissue type, where all lungs were placed in one category, all spleen in another and pancreas in a category of their own. The cDNAs were then used in real time PCR and analyzed for the expression of *IL-1B, IL-18, TnFα, Pigr, Gpr132, Emr4*, *CD62L(Sell)*, *Gdf3 and Relt* (**Table 14).** The gene expression levels of these genes were normalized against TBP, a housekeeping gene. Fold change of the various gene were utilized in statistic calculations, where results for 12-week old and 17- 18 week old NZB/W-F mice were compared to the younger, 5- week old NZB/W-F mice (**Figure 34**).

Results were grouped by age, the young mice, 5-week old NZBW had and those slightly older, 12-week-old NZB/W mice, had no anti-dsDNA. The older mice, 17-18-week old, of these only one mouse had anti-dsDNA production, and one had titer positive for anti-dsDNA. Non-parametric statistic test with a 5% (0.05) statistical significant level was ran and the variance between the three different groups were compared utilizing Kruskal Wallis test, the 12, 17 and 18-week-old NZB/W mice were compared to the 5-week-old NZB/W mice. Dunn's multiple comparison test posttest was used with the following hypothesis:

H_o: There is no difference, in the mRNA expression levels of the selected gene, between the groups. The mRNA expression levels of 12, 17+18- week old NZB/W mice is similar to the mRNA expression levels 5-week old NZB/mice

H_1: There is a difference, in the mRNA expression levels of the selected gene, between the groups. The mRNA expression levels of 12, 17+18- week old NZB/W mice is different to the mRNA expression level of 5- week old NZB/W mice. Different results, with different genes, were observed within the tree groups, as illustrated in **Figure 34A-I.** GraphPad prims software version 8.4.3 and 5.0 (GraphPad Software, inc, San Diego, CA) was utilized for statistical comparison analysis. The robustness of the statistical test results was portrayed with the following symbols: ns (no significance) $p > 0.05$, * $p \leq 0.05$, ** $p \leq 0.01$, *** $p \leq 0.001$ and **** $p \leq 0.0001$. Additionally,

cDNA from previously isolated mRNA from kidney of NZB/W mice were analyzed for the expression of the same genes: *IL-1B, IL-18, TnFα, Pigr, Gpr132, Emr4, CD62L(Sell), Gdf3 and Relt* **(Figure 34 A-I).**

Table 10: Statistic results of the fold change values

Gene analyzed	Statistical test	Overall results: Lung	Overall results: Spleen
IL-1B	KRUSKAL-WALLIS TEST p-value:	ns >0.9999	12 wo: * 17+18 wo: ns 0.0261 0.3761
IL-18	KRUSKAL-WALLIS TEST p-value:	ns 0.3522	ns 0.9606
TnFa	KRUSKAL-WALLIS TEST p-value:	12 wo: ns 17 +18 wo: ns >0.2027 0.9999	12 wo: ns 17 +18 wo: ns >0.2325 0.9999
Pigr	KRUSKAL-WALLIS TEST p-value:	* 0.0455	* 0.0139
Gpr132	KRUSKAL-WALLIS TEST p-value:	ns 0.671	ns 0.976
EMRP	KRUSKAL-WALLIS TEST p-value:	12 wo: ns 17wo: ns >0.9999 0.7003	ns 0.6749
CD62L (Sell)	KRUSKAL-WALLIS TEST p-value:	ns 0.2761	* 0.011
Gdf3	KRUSKAL-WALLIS TEST p-value:	* 0.0347	ns 0.1006
Relt	KRUSKAL-WALLIS TEST p-value:	ns 0.3077	ns 0.097

*Ns: no significance. Wo: Week old. *, equals a p-value of <0.05*

There was an overall variation in mRNA expression of *IL-1B* in lungs with an overall p value of >0.9999 when compared with the p values of spleen from 12-wo mice and 17- 18- wo mice as indicated by the results from Dunn's multiple comparison in the Kruskal-Wallis test. The overall mRNA gene expression in lungs of 12-wo NZB/W mice was slightly higher than the overall mRNA expressed in 5-wo NZB/W mice. There was a significant difference observed in spleen, the 12-wo NZB/W mice expresses a higher mRNA expression compared to 17-18-wo NZB/W mice as well as compare to the 5-wo NZB/W mice. There was a statistical difference in mRNA expression of *IL*-1B in spleen between the 5-wo and the 12-wo NZB/W mice group, p-value of

≤0.05. The 17-18-wo NZB/W mice yielded a higher Fold change than the 5-week-old NZB/W mice (**Figure 34 A**). There was a statistical difference amidst the spleen from 12-wo NZB/W mice which has a p value of 0.0261 and the 17+18-wo NZB/W mice which yielded a p value of 0.3761.

IL-18 gene expression in lung of 12-wo NZB/W nice yielded a higher fold change value than 5- and 17-18-wo NZB/W mice. Additionally, the 17-18-wo NZB/W group displayed higher fold change than 5-wo NZB/W group. Furthermore, the fold change of mRNA expression of *IL-18* in spleen of 5-wo and 17-18 wo NZB/W mice yielded a slightly higher fold change than the 12-wo NZB/W group (**Figure 34 B**). The Dunn's multiple comparison test yielded an overall p-value of 0.3522 for lung, and an overall p value of 0.9606 for spleen.

TNFa gene expression in lungs of 17-18 -wo NZB/W mice was higher compared to both groups as expressed by the fold higher fold change. The 5-wo NZB/W mice yielded a higher fold change compared to the 12-wo NZB/W mice. The Dunn's multiple comparison test yielded a p value of > 0.2027 for the 12 -wo NZB/W mice, and a p value of >0.9999 for 17-18-wo NZB/W mice. *TNFa* gene expression in spleen of 5-wo NZB/W mice gave a higher fold change value than in the two other groups, while the 17-18-wo NZB/W mice yielded a higher fold change than the 12-wo NZB/W mice (**Figure 34 C**). The Dunn's multiple comparison test yielded a p value of > 0.2325 for the 12-wo NZB/W mice, and a p value of >0.9999 for 17-18-wo NZB/W mice.

The fold changes of mRNA expression of *Pigr* in lungs revealed that the 17-18 -wo NZB/W mice gave an exceedingly higher fold change value than 12 and 5- week-old NZB/W mice, and the 12 -wo NZB/W mice gave a higher fold change of mRNA expression of *Pigr* compared to the 5 -wo NZB/W mice. The fold changes of mRNA expression of *Pigr* in spleen revealed that the 17-18 -wo NZB/W mice gave a higher fold change value than 12 and 5- wo NZB/W mice, and the 12 -wo NZB/W mice gave a higher fold change of mRNA expression of *Pigr* compared to the 5 -wo NZB/W mice. In lung as well as in the spleen there were statistical differences in mRNA expression of *Pigr between* the 5-wo group and the 17-18-wo NAB/W mice group, p-value of ≤0.05. (**Figure 34 D**). The Kruskal-Wallies test showed an overall difference in expression of the two tissues, lungs expressed an overall p value of 0.0563 while spleen had an overall p value of 0.0139.

Fold change of *Gpr132* in 17-18 -wo NZB/W mice fold lung as well as in spleen was higher than the two other groups combined. The 12-wo NZB/W mice gave a higher fold change in mRNA

expression of *Gpr132* in lungs as well as in spleen than the 5-wo NZB/W mice (**Figure 34 E**). The Kruskal-Wallies test showed an overall difference in expression of the two tissues, lungs expressed an overall p value of 0.6710 while spleen had an overall p value of 0.9760.

Gene expression of *Emrp4* in lung of 12-week-old NZB/W mice yielded a lower fold change value compared to 5-wo NZB/W mice, while 17-18-wo NZB/W mice yielded a higher fold change compared to both groups (**Figure 34 F**). The Dunn's multiple comparison test shows that there are statistical differences between the two groups: 12-wo NZB/W mice with a p value of >0.9999 and the 17-18-wo NZB/W mice with a p value of 0.7007. Gene expression of *Emr4* in spleen; the 12-wo NZB/W mice resulted with higher fold change compared to 5- and 17-18 -wo NZB/W mice, whereas the 17-18-wo NZB/W mice expressed a lower fold change contrary to the two groups. The Kruskal-Wallis test produced a p value of 0.6749.

The fold changes of mRNA expression of *CD62L(Sell)* in lungs revealed that the 17-18 -wo NZB/W mice gave a higher fold change value than 12 and 5- wo NZB/W mice, and the 12 -wo NZB/W mice gave a lower change value than the 5 -wo NZB/W mice. In spleen the 12-wo NZB/W mice yielded a lower fold change in mRNA expression of *CD62L(Sell),* the 17+18-wo NZB/W mice gave a higher fold change in mRNA expression of *CD62L(Sell)* compared to the 12 wo NZB/W mice. The 5-wo NZB/W yielded a higher fold change in mRNA expression of *CD62(sell)* compared to both groups. In spleen, there were statistical differences in mRNA expression of *CD62L(Sell) between* the 5-wo and the 12-wo NZB/W mice group, p-value of ≤0.05, and 5-wo and 17-18 wo NZB/W mice group, p value ≤0.05 (**Figure 34 G**). The Kruskal-Wallies test showed an overall difference in expression in of the two tissues; lungs expressed an overall p value of 0.296 while spleen had an overall p value of 0.0110.

The fold changes of mRNA expression of *Gdf3* in lungs revealed that the 17-18 -wo NZB/W mice gave an exceedingly higher fold change value than 12 and 5- week-old NZB/W mice, and the 12 -wo NZB/W mice gave a higher fold change value than the 5 -week-old NZB/W mice. In spleen the 17+18 -wo NZB/W mice yielded a higher fold change in mRNA expression of *Gdf3* compared to the two other groups. The mRNA expression of *Gdf3* of the 12-wo NZB/W mice gave a lower fold change than in the mRNA expression of *Gdf3* in the 5-wo NZB/W mice. There was a statistical difference in mRNA expression of *Gdf3 between* the 5-wo and the 17-18-wo NZB/W mice group,

p-value of ≤0.05 (**Figure 34 H**). The Kruskal-Wallies test showed an overall difference in expression in the lungs with an overall p value of 0.0347.

Fold change of mRNA expression of *Relt* in lung of 17-18-wo NZB/W mice was significantly higher than the two other groups. The fold change of mRNA expression in 5 -wo NZBW mice was however higher than that of the 12 -wo NZB/W mice. Fold change of mRNA expression of *Relt* in spleen of 5 -wo NZB/W mice was higher than the two other groups while the 17-18 -wo NZB/W mice fold change of mRNA expression of *Relt* was higher than the mRNA expression of *Relt* in the 12-wo NZB/W mice (**Figure 34 I**). For lungs, the Kruskal-Wallis test yielded an overall p value of 0.3077, while for spleen the p value was only 0.0970.

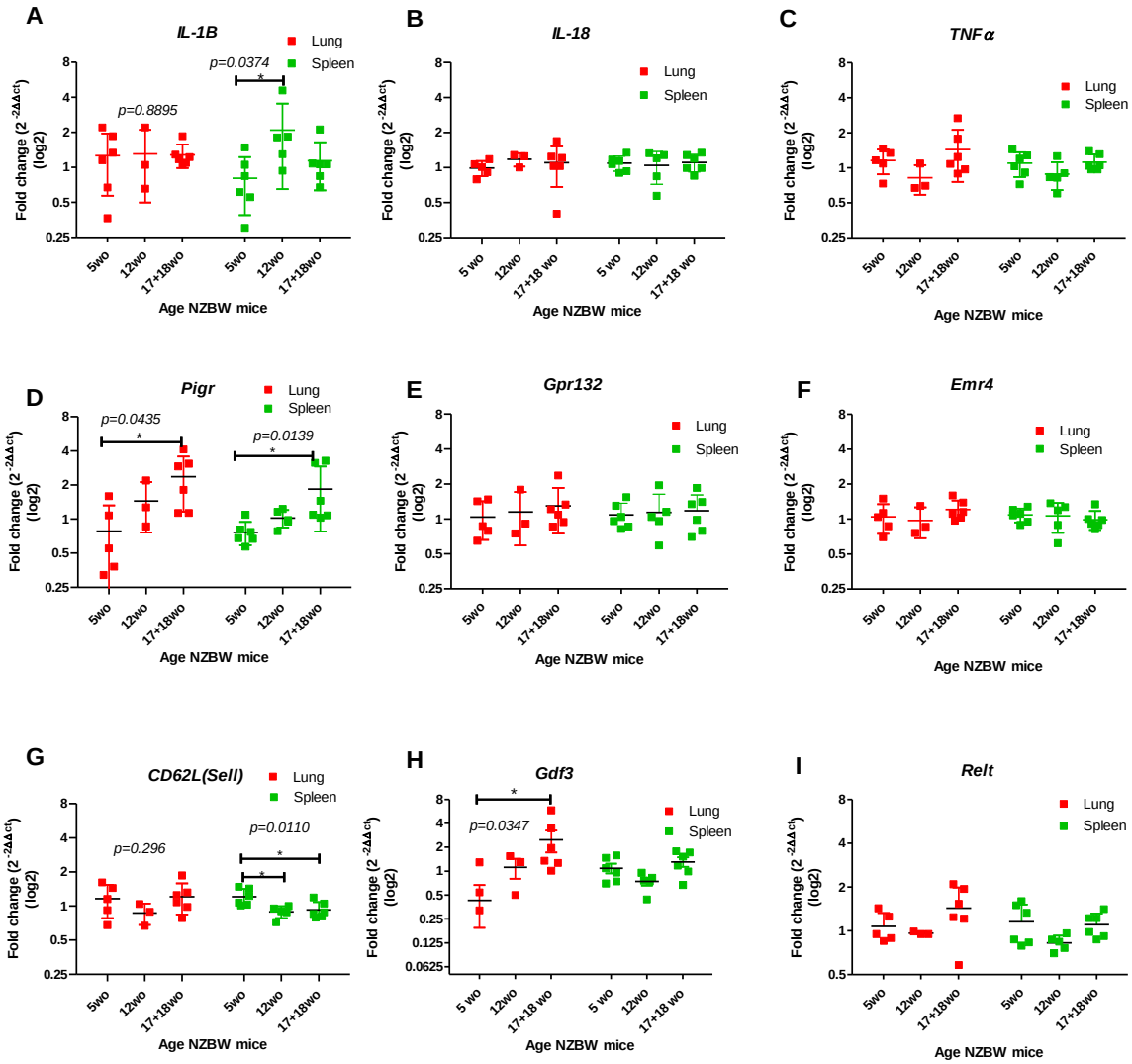

Figure 34: A thorough overview of the statistical resultsof the various differences in mRNA gene expression between the tree groups. (A) *Statistic results of mRNA expression of Il-1β in lung tissue showed no difference in fold change between the groups. The 12-wo NZB/W mice showed a slightly higher mRNA expression IL-1β. The spleen showed an overall difference with a p value of 0.0374. 12-wo NZB/W mice had higher expression of IL-1β with a p value of 0.0261.* ***(B)*** *There were no statistical differences in mRNA expression of IL-18 in lungs or spleen in all groups.* ***(C)*** *Statistic results in mRNA expression of TnFα: mRNA gene expression in lungs of 17-18 -wo NZB/W mice was higher compared to both groups. TNFa gene expression in spleen of 5-wo NZB/W mice had a higher fold change value than in the two other groups.* ***(D)*** *Statistical results in mRNA expression of Pigr, fold change of mRNA expression of Pigr in lung and spleen of the 17-18 -week-old NZB/W mice was higher than the two other groups. While the fold change of mRNA expression of Pigr in lung and spleen of the 12-wo NZB/W mice were higher than the 5-wo NZB/W mice.****(E)*** *Statistic results in mRNA expression of Gpr132, fold change of Gpr132 in 17-18 -wo NZB/W mice lung as well as in spleen, was higher than the two other groups. The 12-week-old NZB/W mice gave a higher fold change in lungs as well as in spleen than the 5-wo NZB/W mice.* ***(F)*** *Statistic results in mRNA expression of Emr4 in lung, the 12-wo NZB/W mice gave a lower fold change value compared to 5-wo NZB/W mice, while 17-18-wo NZB/W mice gave a higher fold change compared to both groups. The mRNA expression of Emr4 in the spleen, the 12-wo NZB/W mice had a higher fold change compared to two other groups.* ***(G)*** *Statistic results in mRNA expression of CD62(Sell), in lungs the 17-18 -wo NZB/W mice gave a higher fold change value than the two other groups. In spleen the 5-wo NZB/W mice gave higher fold change in mRNA expression of CD62(sell) compared to both groups,* ***(H)*** *Statistic results in mRNA expression of Gdf3, in the lung the 17-18 -wo NZB/W mice gave a*

higher fold change value than 12 and 5- wo NZB/W mice. In spleen the 17-18 -wo NZB/W mice had a higher fold change in mRNA expression of Gdf3 compared to the two other groups. ***(I)*** *Statistic results in mRNA expression of Relt, in lung of 17-18-wo NZB/W mice, the fold change was higher than the two other groups. Fold change in mRNA expression of Relt was higher in spleen of the 5-wo NZB/W mice group than the other two groups.*

The expression of the same genes analyzed on mRNA isolated from lungs and spleen from 5, 12 and 17-18-wo NZB/W mice were analyzed on mRNA from kidney of NZB/W mice at different ages and disease stages **(Appendix Table 3A and 4A).**

The mRNA expression of *IL-1B* demonstrated that there were statistical differences between some of the groups compared to the Young NZB/W Ab- (4 WO) (**Figure 35A**). The Kruskal-Wallis test illustrated an overall p-value of 0.0016. The Dunn's multiple comparison test yielded a statistical difference between the Young NZB/W Ab- (4 wo) and prot +(22-34 WO) with a p-value ≤0.01. There was also a statistical difference between prot +(22-34 WO) compared with BALB/c (22-39 WO), the p-value was ≤0.05 (**Figure 35 A**). The fold change values varied between all groups. *Prot* +(22-34 WO) had the highest fold change for the mRNA expression of *IL-1B.*

There was no significant p-value difference in mRNA expression of *IL-18*. The Kruskal-Wallis test gave an overall p-value of 0.1152 for the mRNA expression of *IL-18* (**Figure 35 B**). The Dunn's multiple comparison test shows there is no significant differences between the groups. Fold chance in prot + (22-34 WO) was slightly higher than all the other groups.

There were statistically differences in mRNA expression of *TNFα* amongst the groups. The Kruskal-Wallis test displayed an overall difference between the groups, with an overall p-value of <0.001 (**Figure 35C)**. The Dunn's multiple comparison test showed two clear difference between the various groups. There was a statistical difference in mRNA expression of *TNFα* between Young NZB/W Ab- (4 wo) and the Ab+ (21-27 WO) group, p-value of ≤0.01 and Ab+ (21-27 WO) and BALB/c (22-39 WO) group with a p-value of <0.01.

The mRNA expression of *Pigr* showed a statistical difference between the groups. The Kruskal-Wallis test revealed that there was an overall difference between the groups with a p-value of 0.0018 (**Figure 35 D**). The Dunn's comparison test demonstrated a difference between the Young NZB/W Ab- (4 wo) and the Ab+ (21-37 WO) group, p-value <0.01, and between the Ab+(21-37 WO) and the BALB/c (22-39 WO) with a p-value of <0.05.

There were statistically differences in *Gpr132* mRNA expression amongst the groups. The Kruskal-Wallis test displayed an overall difference between the groups, with an overall p-value of 0.0010. The Dunn's comparison test showed three clear difference between the various groups (**Figure 35 E**). There was a statistical difference in mRNA expression of *Gpr132* between Young NZB/W Ab- (4 wo) and Prot +(22-34 WO), p-value of <0.05. The second statistical difference was observed between the Ab+ (21-27 WO) and BALB/c (22-39 WO) group, p value <0.05. The final statistical difference in mRNA expression of *Gpr132* was between Prot +(22-34 WO) and BALB/c (22-39 WO) group with a p-value of <0.05.

There were statistically differences mRNA expression of *Emr4* amongst the groups. The Kruskal-Wallis test displayed an overall difference between the groups, with an overall p-value of 0.0037 (**Figure 35 F**). The Dunn's multiple comparison test showed three clear difference between the various groups. There was a statistical difference in mRNA expression of *Emr4* between Young NZB/W Ab- (4 wo) and Prot +(22-34 WO), p-value of <0.05. The second statistical difference was observed between the NZB/W Ab- (22-32 WO) and Prot +(22-34 WO) group, p value <0.05. The last statistical difference in mRNA expression of *Emr4* was between Prot +(22-34 WO) and BALB/c (22-39 WO) group with a p-value of <0.05.

There was a statistical difference in mRNA expression of *CD62L(Sell).* The overall p-value of the samples was 0.0459 as demonstrated by the Kruskal-Wallis test (**Figure 35G**). The Dunn's multiple comparison test displayed a statistical difference in mRNA expression of *CD62L(Sell)* between NZB/W Ab- (22-32WO) and the BALB/c (22-39 WO) group with a p-value of <0.05. There were no other statistical significances between any other group.

The Kruskal Wallis test showed that there were overall differences in the mRNA expression of *Gdf3*, the overall p value was 0.0020 (**Figure 35 H**). The Dunn's multiple comparison test demonstrated a clear statistical difference between the groups. There were statistical dissimilarities between the Young NZB/W Ab- (4 wo) and Prot +(22-34 WO), p-value <0.05. Additional statistical differences in the mRNA expression of *Gdf3* in the NZB/W Ab- (22-32WO) and the Prot +(22-34 WO), p-value <0.01.

There were statistically differences in mRNA expression of *Relt* amongst the groups. The Kruskal-Wallis test displayed an overall difference between the groups, with an overall p-value of <0.0001 (**Figure 35 I**). The Dunn's multiple comparison test showed four clear difference between the

various groups. There was a statistical difference in mRNA expression of *Relt* between Young NZB/W Ab- (4 wo) and the Ab+ (21-27 WO) group, p-value of <0.05. The second statistical difference in mRNA expression of *Relt* was observed between the Young NZB/W Ab- (4 wo) and the Prot +(22-34 WO) group, p value <0.01. The third statistical difference in mRNA expression of *Relt* was between Ab+ (21-27 WO) and BALB/c (22-39 WO) group with a p-value of <0.01 The last statistical difference in mRNA expression of *Relt* was observed in Prot +(22-34 WO) and the BALB/c (22-39 WO) group, p-value <0.001.

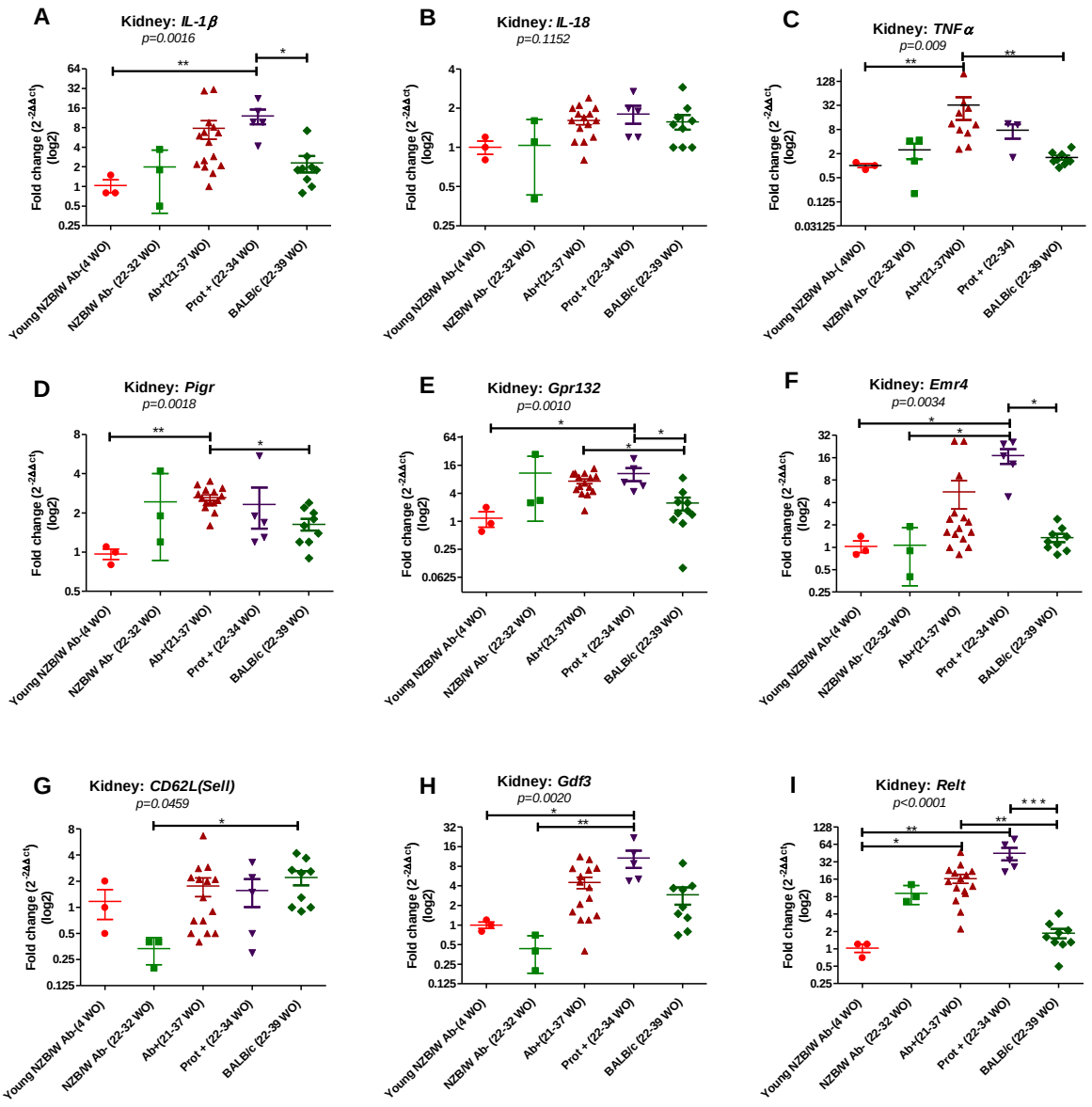

Figure 35: Detailed overview of the statistical results and differences mRNA gene expression of selected genes. (A) *Display fold change values of the various for mRNA expression of IL-1B within the various groups. Statistical result in mRNA expression of IL**,** the Kruskal-Wallis test illustrated an overall p-value of 0.0016.* ***(B)*** *Fold change values of mRNA expression of IL-18, the Kruskal-Wallis statistic test shows an overall p-value of 0.1152 in mRNA expression of IL-18, the Dunn's multiple comparison test showed no significant differences amongst the groups.* ***(C)*** *Fold change values of mRNA expression of TNFα statistically varied between the groups. Kruskal-Wallis test gave an overall p-value of <0.001.****(D)*** *The mRNA expression of Pigr showed an overall statistical difference, as revealed by Kruskal-Wallis test, overall p-value of 0.0018* ***(E)*** *Fold change and Statistical result in mRNA expression of Gpr132 expression.: Kruskal Wallis test gave an overall difference between the groups with p-value of 0.0010.* ***(F)*** *Fold change and Statistical result of expression of Emr4, Kruskal Wallis test gave an overall difference between the groups with p-value of 0.0037.****(G)*** *Fold change and Statistical result of expression of CD62L(Sell), Kruskal-Wallis test showed an overall difference between the groups, p-value of 0.0459.* ***(H)*** *Gdf3 expression is statistically dissimilar between the groups, with an overall p-value of 0.0020* ***(I)*** *The mRNA expression of Relt statistically varied between the groups, Kruskal-Wallis test gave an overall p-value of <0.0001.*

4 Discussion

TLS are produced during the course of chronic inflammation, the formation of TLSs are linked with tissue damage and are believed to be inductive sites for self-reactive T-and B-lymphocytes, including plasma that can produce autoantibodies thereby promote and contribute to the state of disease. This present study evaluates TLS in different tissue types, pancreas, lung, spleen, and salivary gland in a lupus prone mouse model at various stages of disease advancement. In addition, TLS was characterized and evaluated utilizing antibody markers for T-and B-lymphocytes, thus accentuating the distinct T- and B-lymphocyte zones. Additionally, mRNA gene expression of *IL-1β, IL-18, TNFα, Pigr, Gpr132, Emr4, CD62L(Sell), Gdf3* and *Relt*, possibly involved in TLS or immune cell expression, were studied in the aforementioned tissues, including kidney tissue.

The antigen CD3 appears in the cytoplasm of thymocytes prior to its detection on the cell surface, and more than 95% bears surface and/or cytoplasmic CD3 (140). CD3 is s specific cell surface marker that appears in resting and activated T-lymphocytes (140). When thymocytes differentiate into medullary thymocytes, the cytoplasmic CD3 expression is lost (140). Positive stained cells are thymocytes, peripheral T-cells and NK cells (140). Anti-CD3 is the most specific T-cell antibody, and it is a useful marker as it only exists in T-lymphocytes, thus distinguishes it from B-lymphocyte (140). CD45 which is leukocyte specific are expressed on all hematopoietic cells excluding red blood cells (141). B220 is an isoform of CD45 and is specific and expressed predominantly on B-lymphocytes (141). B220 is expressed in pre-B-, immature B- and mature B-lymphocytes and is downregulated at the late plasma cell stage (142).

CD3 and B220 markers can, therefore, be utilized for labeling T-lymphocyte and B-lymphocytes in association with TLS, as TLSs are characterized as lymphoid organs with a B-lymphocytes region and a T-lymphocytes region. Nevertheless, the CD3 marker utilized in this study can also stain NK cells in the cytoplasm, even though the CD3 marker is a specific marker for T-lymphocytes. this CD3 marker is thus not entirely optimal in that only T-lymphocytes are labelled. The IHC results of anti-CD3 and anti-B220 showed that there were CD3 positive and B220 positive cells, each in their distinct regions, in various analyzed tissues of lupus prone NZB/W mice. Hypercellularity was frequently observed in anti-dsDNA antibody positive NZB/W mice, often yielding high IHC score. Additionally, of all sections assessed for TLS, 12 NZB/W mice

exhibited TLS within various tissues, and 11 out of the 12 NZB/W mice exhibiting TLS were proteinuric as well as anti-dsDNA antibody positive. Nevertheless, the age of these mice varies between 25-35-week-old. Moreover, the Spearman correlation measuring the degree of association of clinical parameters demonstrated there were no significant statistical associations between TLS and age, nor were there any correlations between proteinuria and TLS. The one significant statistical correlation in association to TLS was Ab+. One could argue that these results highlight anti-dsDNA antibodies implication in disease progression and pathogenesis of SLE. This is supported by a previous study carried out by Yung and colleagues where it was suggested that anti-dsDNA antibodies are specific to SLE and can be detected in the circulation of patients' years prior to clinical (143). In addition, they showed that anti-dsDNA antibodies are present in over 80% of SLE patients and that there is a correlation between the levels of anti-dsDNA antibodies and disease activity (143). Studies have promulgated that more than 100 distinct autoantibodies have been depicted and presented with SLE where the prevailing and frequent in correlation with SLE is anti-DNA and anti-chromatin, in addition to anti-nucleosomes in lupus nephritis (77). Furthermore, it has been reported that the autoantibodies when coupled with their analogous antigen form immune complexes, which activates complement and phagocytes, can play a consequential role in the severity of disease (77). Additionally, the formation of anti-dsDNA suggests there is a pathological disturbance in the mechanisms that should hinder B-and T-lymphocyte reactivity of self-antigens (101).

The IHC results on TLS assessment further solidifies anti-dsDNA antibody correlation and implication in SLE. The production of anti-dsDNA is one of characteristic hallmark of SLE, and the rising titers of these antibodies (Abs) correspond with exacerbation of the malady (144). Levels of anti-dsDNA antibodies is therefore closely associated with disease progression. Moreover, TLS and assessment of immune cell infiltration in various tissues disclosed a pattern of immune cell aggregation. The pattern revealed accumulation or aggregate of lymphocytes (TLS) occurred predominantly around or adjacent to large and small arteries and veins, including ducts**.** This is supported by an earlier study showing that TLS occurred close to the pelvic wall, large arteries, and large veins within the kidney of lupus-prone mice (145). In the pancreatic tissues, however, TLS were either observed in the Islets of Langerhans or next to the Islets of Langerhans. Moreover. Moreover, it was observed that TLS was not present elsewhere in the pancreatic tissues. The development of T1DM, an autoimmune disease distinguished by self-reactive lymphocytes

mediated destruction of insulin producing pancreatic β cells, has been associated with the formation of islet autoantibodies (146, 147). Additionally, evidence advocate the presence of autoantibodies to be one of the best prognosticators of T1DM progression (147). Individuals with high-affinity anti-insulin antibodies or even a single antibody to more than one islet antigen are more susceptible to, and will almost indubitably develop T1DM during their lifespan (147). A study by Kendal *et al* affirmed lymphocytic infiltration in the islets of prediabetic NOD mice formed TLS, demonstrating that B and T-lymphocytes attacking islets in pancreas of NOD mice were organized into lymphoid structures with germinal centers (148). Furthermore, the TLS structures were consistently present in heavily infiltrated islets, they were additionally also found in the majority of those islets that were 25-50% infiltrated (148). Increasing evidence indicates that these ectopic lymphoid structures, start to generate at the early stage of peri-insulitis (149). There is continuous development of TLSs in the pancreas during diabetes advancement in NOD mice (48). Moreover, these TLSs that develop in the pancreas provide a milieu for the proliferation of autoreactive T cells, thereby supporting the supposition that autoantigen is locally presented (52). NOD mice spontaneously develop T1DM as a result of destruction of insulin secreting pancreatic islet cells by autoreactive T-lymphocytes (52). In a recent study carried out by Smeets *et al*, lymphoid structures were observed in the islets of Langerhans of a 66-year-old patient with long-standing T1DM (150). In the study, the lymphoid structures were observed in three insulin-containing islets and were characterized by distinct T- and B-lymphocyte zones (150). Additionally, no TLS-like structures were detected outside the pancreatic islets or in other gland regions (150). Collectively, these data support the above claim by the fact that most TLS were located in or next to Islets of Langerhans.

The Spearman correlation disclosed, as previously stated, a correlation between Ab+ and TLS. It. It further discloses that this correlation occurred in pancreas, and particularly in the kidney. TLS in lung and SG did not exhibit any considerable statistical correlations. There were no correlations between TLS in lung and SG with either age, proteinuria, or Ab+. Nevertheless, a statistical correlation was observed with T and B-lymphocytes infiltration in lung tissues. Further, another statistical correlation was detected between Ab+ and T-lymphocyte infiltration in SG. Additionally, a statistical correlation was also seen between age and B-lymphocyte infiltration in tissues of SG.

How then did TLS in lung not correlate with any of the other TLSs? This could be indicative of the fact that lungs possess its own circulation, the pulmonary circulation. Additionally, lungs also has bronchial circulation, even though it is quite small, it is still considered as secondary circulation of the lungs (19). The bronchial circulation plays a vital role in many lung and airway diseases through its ability to increase in size. It. It is also capable of providing lung parenchymal perfusion when pulmonary circulation is compromised (151). The IHC results, including the assessment of tissues displaying TLS, demonstrated that when TLS was observed in kidney, it was also observed in SG. Additionally, if a mouse displayed TLS in SG it frequently also displayed TLS in pancreas, and if a mouse displayed TLS in two or all the three mentioned tissues then the probability was high for TLS detection in lung. Excluding TLS detected in kidneys, one NZB/W mice exhibited TLS solely in lung (**Table 11**). The other tissues did not display TLS. This could be due to not cutting deep into the location of the tissue embedded in paraffin, or that or that there simply were nothing of significant to be extricated, or it could also have been a coincidence. However, all the other tissues have something in which they have in common, the systemic circulatory system, while lung possesses its own circulation. This could explain why TLS in the lungs was only detected in three mice and why lung TLSs did not correlate with the other or Ab+.

However, if TLS is presumed to originate in the kidneys, how would it come to manifest in SG? It is comprehensible with pancreas and spleen as these organs are located in the abdomen area. One has to take into consideration that SLE is a systemic malady, a multiorgan autoimmune disorder that is regarded as a quintessence of immune complexes mediated disease. Additionally, it is a disorder abundant in a vast range of circulating autoantibodies,, and when the autoantibodies then comes into contact with antigens, they ultimately produce immune complexes which are deposited in different organs of the body (82). Immune complex aggregation institute a procession of unfortunate events that contribute to renal inflammation and kidney injury (152). Moreover, the functional unit of the kidney, the nephron, which is composed of the glomerulus and cortical and medullary tubular system, filtrate blood and concentrate metabolic waste into urine (8, 153). All the circulating blood in the body passes through the kidneys (33). It therefore seems like, due to filtration of blood in kidneys, that immune complexes would deposit first in the kidney where more TLSs are frequently observed than other organs. Immune. Immune complex deposition in other organs and TLSs development could then originate due to systemic inflammation. Some SLE patients can present with SS, clinical coexistence of SLE and SS is recognized, but prevalence of

SS among patients with SLE varies (154). SS is a chronic autoimmune malady of the exocrine glands affiliated with lymphocytic infiltration of the affected glands (154). Primary Sjøgren'ssyndrome (pSS) is a multifactorial rheumatic disorder that mainly targets salivary and lacrimal glands, TLS is found in pSS salivary glands of pSS patients (155). Autoantibody production as well as infiltration of the exocrine glands, especially salivary glands,, represent pathognomonic features of pSS (156). TLSs correlate with the presence of immune complexes, meaning that locally generated autoantibodies can activate complement thus causing tissue inflammation and damage. Similarly, B-lymphocytes responses are associated with TLS in other autoimmune diseases, including salivary gland in SS (51).

IgA is the most ubiquitous antibody isotype in the body (157), it is the main immunoglobulin that is present in secretions, such as nasal, bronchial, intestinal, and prostatic, as well as in tears, saliva, and vaginal fluid (33). IgA is found in secretions as a dimer of trimer called secretory IgA (SIgA) (33). Additionally, IgA is the predominant antibody in the secretions that immerses mucosal surfaces like the gastrointestinal, respiratory, and genitourinary tracts (158). IgA that is directed towards the mucosal secretions is produced locally by organized mucosal-associated lymphoid tissues. IgA is carried across the epithelium into the mucosal lumen by binding to the polymeric immunoglobulin receptor (*pIgR*))) (158). IgA is a heterogenous structure and exists in various forms, such as monomeric, polymeric, in secretory form (158). These variants of IgA are thus distributed into two sections, the systemic circulation and mucosal secretions (158). IgA producing cells have been localized in all lymphoid tissues including bone marrow, spleen, lymph nodes, exocrine glands, lamina propria of the gastrointestinal and respiratory tract, and in salivary glands (158). IgA is mostly recognized as noninflammatory, as it plays a vital role in host defense at mucosal sites, hindering invasion of pathogens by neutralization (159). Moreover, IgA antibodies can form immune complexes with antigens without inducing inflammatory reactions that can cause damage to the host tissue (158). It has, however, become evident that IgA can also mediate other immunological processes, as IgA can mediate potent response in cells that have receptors for it (158, 159). Furthermore, a study by Hansen et al revealed that immune complex formation of serum IgA plays a vital role in orchestration of inflammation in response to pathogens at various non-mucosal sites by eliciting proinflammatory cytokines (159). Seeing as IgA is secreted from these various locations/organs, one could thus postulate that perhaps this too could be a reason

why TLS is observed in the various tissues, nevertheless the reason could also be immune complex deposition in these tissues as seen in kidneys.

The quality of immunohistochemical staining is greatly dependent on various factors, including fixation, washing and incubation condition (160). The staining quality also depends on the appropriate mounting of tissue specimens into the slides (160). Fixations tend to change the chemical properties of tissues substances and alter three-dimensional protein conformation by cross-linking. This has a big impact on antibody affinity as well as selectivity of antibody (161). The tethering of primary antibody to its corresponding antigen is a pivotal step responsible for good quality of immunohistochemical staining (162). Antibody with high specificity and high affinity binds only a certain part of the antigen, it does not bind to other protein with similar features as its corresponding antigen (163). An antibody with high specificity binds therefore exclusively to their target antigen epitope (163). Antibodies with low specificity and affinity tend to cross-react with proteins/antigens with resembling feature to the specific target (163). Secondary antibody was used in control slides with the absence of primary antibody. If anything would have been detected, it could suggest that the secondary antibody had tethered somewhere. The secondary antibody should only bind the primary antibody, which it did from observing negative controls. Furthermore, if secondary antibody has tethered to something other than primary antibody, this would have, additionally, suggested that the blocking step did not work as it should have. However, in some of the slides some background staining was observed, meaning it is not the detection system that causes this background staining, rather it is the primary antibody. As previously mentioned, antibody with low affinity and specificity have a higher probability of cross-reacting and binding other protein/antigen epitopes that resembles the epitope of interest. Another possibility could be that other cells can have the same/similar epitopes with low expression.

Cytokines play a significant role in regulating the innate and adaptive immune system through different receptors and signaling pathways (164). As such, cytokines are in essence also implicated in the development of disorders and maladies (164). *TNFα* is a puissant promoter inflammation as well as many normal physiological functions in homeostasis, health, and antimicrobial immunity (164). *IL-1β* and *TNFα* are cytokines that play a role in inflammation, especially in the early pro-inflammatory phase, thus notably elevated levels of these cytokines are often observed in generalized inflammatory states(165). Increased levels of *IL-18* can be observed in biological

fluid and organs of individuals affected by several autoimmune pathologies, and it can also be detected in autoimmune animal models (166). Moreover, not only are increased levels of *IL-18* frequently correlated with severity of autoimmune pathologies in animal models, but also in clinical situations (166). Additionally, *IL-18* can stimulate production of inflammatory cytokines such as TNFα and IL-1β in mature Th1 cells, monocytes/macrophages, and NK cells, upregulate chemokine production increase expression of adhesion and costimulatory molecules enhance perforin- and FasL-mediated cytotoxicity by NK and T- lymphocytes and prompt the release of matric metalloproteases. All of which are fundamental and central to the inflammatory reaction and ensuing tissue damage (166). Blocking of IL-18 has shown to display advantageous effect in several models of autoimmune/inflammatory maladies such as rheumatoid, autoimmune thyroiditis, SLE,, suggesting *IL-18* has pathological role in these maladies (166). Furthermore, production of *IL-18* is suggested to occur early during the defensive innate immune reaction, it is further implicated in the activation of Th1 and Th17 inflammatory immune responses, which can be the ground for the autoimmune pathology (166).

Our results showed that, mRNA expression of *IL-1β* in the lung tissue, did not display any statistical significance between the groups, neither were there any difference in fold change between the groups. However, statistical significance in mRNA expression of *IL-1β* was observed in spleen. Expression of *1β* mRNA was significantly upregulated in spleen tissue of 12-wo NZB/W mice, slightly higher the expression of *IL-1β* was observed in tissue of 17-18-wo NZB/w contrarily to the normalized 5-wo NZB/W group. In kidney, the mRNA expression of *IL-1β* showed a statistical difference between the groups compared to the Young NZB/W Ab- (4-wo). The mRNA expression of *IL-1β* was upregulated in all groups compare with Young NZB/W Ab- (4 wo) groups. The significant increase expression of *IL-1β* mRNA in splenic tissue compare to kidney could be correlated to the fact that spleen is a site where activated lymphocytes are produces. Additionally, the spleen is a lymphoid tissue, the only lymphatic organ interposed into the systemic vasculature (33). It is a lymphopoietic organ that pays a pivotal role in antibody formation and T-and B-lymphocyte proliferation (73). Moreover, in mice, the spleen is the site of hematopoiesis that can provide a hematopoietic response to different stimuli which includes different diseases and infectious agents (31).

There were no statistical differences in mRNA expression of *IL-18* in lung or spleen in all groups. Moreover, no significant statistical differences in expression of *IL-18* mRNA was observed, additionally, in kidney tissues no significance differences between the groups was observed. Nevertheless, when comparing the fold change expression of *IL-18* mRNA in kidney tissue of all groups to that of Young NZB/W Ab- (4wo) group, one can conclude that the expression of *IL-18* mRNA was upregulated the different groups. Upregulation of several cytokines are observed in human lupus nephritis kidneys, along with monocyte chemoattractant protein-1 (MCP-1) and macrophage inflammatory protein-1-alpha (MIP-1α), *IL-6,IL-10,IL-12,IL-17*, *IL-18*, *IFN*-gamma, *TNFα* and Eta-1/osteospontin(167) . Production of *IL-18* is observed early during protective innate immune response and is connected to the activation of Th1 and Th17 inflammatory immune response, thereby testifying to *IL-18* implication and pathological role *i*n autoimmune diseases (166).

Expression of mRNA in *TNFα* in splenic tissue showed no difference in fold change between the groups. A clear difference in expression of *TNFα* mRNA in lung tissue was detected between the groups. Fold change in expression of *TNFα* mRNA in lung tissue of the 12-wo NZB/W mice were lower compare to the 5-wo NZB/W group, decline in expression of *TNFα* mRNA implies the genes expression of *TNFα* mRNA was downregulated. On the other hand, fold change in expression of *TNFα* mRNA in lung tissue of the 17-18-wo NZB/W mice was highly elevated compared to the normalized 5-wo NZB/W mice. Increase in expression of *TNFα* mRNA suggest upregulation the gene in the lung tissue of this group. Statistical differences in expression of *TNFα* was detected amongst the groups. There was a significant statistical difference in expression of *TNFα* between Young NZB/W Ab- (4 wo) and the Ab+ (21-27 WO) group, p-value of ≤0.01 and Ab+ (21-27 WO) and BALB/c (22-39 WO) group with a p-value of ≤0.01. Cytokines have been proven to play a role in early pro-inflammatory phase and that elevated levels are often detected in inflammatory states. Therefore, in tissues of mice where no elevation or where decline in expression of IL-1β,and TNFα mRNA was observed, compared to the normalized "healthy" mice, suggest that these mice had yet to or had not displayed any inflammation. While tissues exhibiting with elevated inflammatory cytokines suggest inflammation in these lupus prone mice. SLE is after characterized by heterogenous symptoms such as inflammation, fever and various serious symptoms(147).Persistent inflammation is considered the herald of tissue damage which damage, which ultimately prefigure organ damage. This is particularly seen in SLE, as SLE can result in

serious multi-system organ damage (76), the occurrence of organ damage in SLE due to disease activity, treatment, and/or comorbidities is another grisly outcome of SLE (75). Early detection is therefore critical considering that it can have significant implications for morbidity and management of the malady (76).

Expression of *pIgR* is believed to be restricted to mucosal and glandular epithelial cells(158).. Upregulation of *pIgR* expression would increase the capacity for epithelial transcytosis of IgA (158). Only one molecule of *pIgR* is synthesized for every molecule of IgA transported, as *pIgR* is cleaved and released at the apical surface after transporting IgA (158). It is therefore very important to be able to control the cellular level of *pIgR* for IgA-mediated mucosal defense (158). Various host and microbial factors have been demonstrated in the regulation of *pIgR* expression trough intricate and interconnected mechanism (158). For instance, the proinflammatory cytokines interferon (*IFN)-γ*, tumor necrosis factor *(TNFα)* and *IL-1* which are engendered in response to different bacterial and viral infections, play an important role in the upregulation of *pIgR* gene transcription (158). Glucocorticoids is believed to upregulate *pIgR* in human breast and colon cancer cell-lines, and rat liver and intestine (158). Double stranded RNA upregulates *pIgR* in human intestinal epithelial cell line (158). Multiple mechanism exists for accommodating high levels of *pIgR* expression during inflammatory responses (158). A study by Reséndiz-Ablor *et al* demonstrated that the expression of *pIgR* was more elevated in the proximal than the distal segment of the small intestine in normal BALB/c mice (168). TheThe study further suggest the high expression of *pIgR* discovered in the proximal segment could have been related to the effect on epithelial cells of the high production of *TNFα, IFN-γ* and *TGF-β,* as well as the high expression of glucocorticoid receptors (168).

The mRNA expression of *pIgR* in kidney tissue showed a statistical difference between the groups, there was a gradual increase in expression of *pIgR* mRNA in all groups when compared to the normalized Young NZB/W Ab- (4wo) group. In spleen and lung tissue, the fold change expression of *pIgR* mRNA were increasing in the two groups compared to the standardized 5-wo NZB/W group. Expression of *pIgR* mRNA in the various tissue were upregulated. Moreover, the upregulation of *pIgR* could be related to presence of proinflammatory cytokines such as TNFα, as these cytokines play a role in the upregulation of *pIgR*. Our results are commensurate with previous studies wherein high expression of *Pigr* were demonstrated.

G protein-coupled receptor 132 (*Gpr132*) is a stress-inducible transmembrane receptor that actively regulates several cellular biological activities, namely cell cycle, proliferation, and immunity (169). *Gpr132* is significantly expressed in macrophages (169). Significant statistical differences in kidney tissues were observed in the expression *Gpr132* mRNA among the groups. All groups yielded higher fold change in expression of *Gpr132* mRNA compared to that of the normalized Young NZB/W Ab- (4wo) group, thus the expression of *Gpr132* mRNA were upregulated in these groups. Fold change in expression of *Gpr132* mRNA in lung and spleen tissue were marginally increased compared to the fold change in expression of *Gpr132* mRNA of the normalized 5-wo NZB/W group, thus the expression of *Gpr132* mRNA slightly upregulated in spleen and lung tissue. Under normal homeostatic circumstances, macrophages activation and release of inflammatory mediators are strictly regulated (170). During pathological conditions, however, these regulatory control mechanisms can be compromised thereby leading to influx of macrophages in tissues thus intensifying their activity (170). Increased macrophage activity leads to excessive release of cytotoxic, proinflammatory and fibrogenic products, all of which stimulate and promote tissue damage and chronic disease pathogenesis (170). High levels of proinflammatory products in tissue of patients with SLE is connected with inflammation and tissue damage(95). Thus, the increase in *Gpr132* expression may reflect increased influx of macrophages in the tissues.

Emr4, an epidermal growth factor said to be upregulated subsequent macrophage activation (171). *Emr4* is over-expressed in macrophages treated with *TNFα*, the expression of *EMR4* is drastically reduced or downregulated by IL-4 and IL-10 (171). *Emr4* is expressed in monocytes, and in certain tissues macrophages (172). A study carried out by Shiffer *et al* revealed the involvement of macrophages in the development of lupus nephritis. In the study they reported that renal macrophages were amongst the first immune cells to be activated and also increase in the occurrence of lupus nephritis(173).In kidney tissue, expression of *Emr4* mRNA displayed a statistical difference among the groups. Fold change in expression of *Emr4* mRNA was significantly elevated in Ab+(21-37 wo) and prot + (22-34 wo) NZB/W group, and slightly elevated in NZB/W Ab- (22-32 wo) and BALB/c (22-29 wo) group compared to the normalized Young NZB/W Ab- (4wo) group. From the results, it is clear the expression of *Emr4* mRNA in kidney tissues were upregulated. In lung tissue, the fold change in expression of *Emr4* mRNA was marginally increased in 17-18-wo NZB/W group, and marginally decreased in 12-wo NZB/W

group compared to the 5-wo NZB/W control group. Expression of *Emr4* mRNA was upregulated in the older mice and downregulated in the younger mice (12-wo NZB/W group) indicating an increases influx of monocyte or activation of tissue specific macrophages in NZB/W mice.

L-selectin (*CD62L*) is fundamental for homing of naïve lymphocytes to all SLO with HEV (174). It is known as a lymph node homing receptor, and it is important to the control of lymphocyte recirculation (175). *CD62L* function as a primary adhesion receptor for many naïve lymphocytes and a proportion of memory cells, *CD62L* mediates the binding and rolling of lymphocytes along the apical aspects of HEV (174). Additionally, *CD62L* is widely apportioned on most leukocyte in the blood and it is involved in many instances of inflammatory leukocyte trafficking (174). A study by Lange-Sperandio *et al* demonstrated that selectins are important mediators of macrophage infiltration in unilateral ureteral obstruction (UUO) , leading to tubular apoptosis, tubular atrophy, and intestinal fibrosis(176).. Statistical difference in expression of CD*62L (Sell)* mRNA were observed. Expression of *CD62L (Sell*) mRNA in Ab+(21-37 wo), prot + (22-34 wo) NZB/W and BALB/c (22-29 wo) group was elevated compared to the normalized Young NZB/W Ab- (4wo) group. From these results it is clear that the expression of *CD62L (Sell)* mRNA was upregulated in these groups. AA decrease in expression of *CD62L (Sell)* mRNA was displayed in the NZB/W Ab- (22-32 wo) compared to the control Young NZB/W Ab- (4wo) group. Result here provided evidence that expression of *CD62L (Sell)* mRNA downregulation. Expression of*CD62L (Sell)* mRNA in lung marginally increased in 17-18-wo NZB/W group, while it was decreased in 12-wo NZB/W group comparison to the control 5-wo NZB/W group. In spleen however, expression of *CD62L (Sell)* mRNA was decreased in both groups compared to the normalized 5-wo NZB/W group. The increase of *CD64L (Sell)* in the kidney and the reduced expression in spleen may indicate splenocytes accumulation in the kidneys during disease progression.

Growth differentiation factor 3 (*Gdf-3*) is a member of transforming growth factor-β (TGF-β) superfamily, its effect is affiliated with a vast range of differentiation processes during embryonic development (177). *Gdf-3* is presumed to have cytokine activities in cell regulation and in vivo biological processes, nonetheless, its exact function has yet to be elucidated (178). In humans, *Gdf-3* expression levels are really low and undetectable in tissue by Northern blot analysis (178). A previous study by McPherron and colleague, demonstrated that *Gdf-3* mRNA was detected in several adult animal tissues, including thymus, spleen, bone marrow and adipose tissue (177). In

this study, they found that *Gdf-3* was expressed at high level in adipose tissue, thymus, spleen and bone marrow, lower levels were observed in the uterus and ovary (177). The study further further revealed based on the expression model of *Gdf-3*, that *Gdff-3* plays various regulatory roles in adult animals (177). In kidney tissue, there were overall differences in expression of *Gdf3* mRNA, the overall p value was 0.0020. Fold change in expression of *Gdf3* mRNA were all highly elevated in all groups compared with Young NZB/W Ab- (4wo) group, while decline in *Gdf3* mRNA expression was seen in NZB/W Ab- (22-32 wo). In lung, the fold change in expression of *Gdf3* mRNA was significantly increased in 12-wo and 17-18 wo NZB/W groups compared to the normalized 5-wo NZB/W group. Fold change in expression of *Gdf3* mRNA in splenic tissue was increased in 17-18-wo NZB/W group, while decline in *Gdf3* mRNA expression was detected in 12-wo NZB/W. Since *Gdf3* expression normally is higher in lymphoid tissue, expression in kidneys and other organs may reflect TLS formation.

Tumor necrosis factor receptor (TNFR) superfamily members are immensely vital for diverse processes which include inflammation, apoptosis, and development (179). Currently, about 29 TNFRs are identified in humans (179). Receptor. Receptor expressed in lymphoid tissues (*Relt*) was recently identified as TNFR, and is mostly transcribed in lymphoid tissues (179). The corresponding TNF ligand of RELT has yet to be discovered (179). *Relt* has been observed to be expressed in apoptotic cells in an acute pancreatitis model (179). Sica *et al* revealed in their study that *Relte* expression was limited primarily to hematological significant tissues and immune cell-derived lines (180). *Relt* mRNA was observed to be abundant in peripheral blood leukocytes, lymph node, spleen, and bone marrow (180). Additionally, the study identified that *Relt* mRNA was expressed in most of hematopoietic cell lines that were tested, include T-lymphocytes, B-lymphocytes, and myeloid cell lines. However, *Relt* mRNA was also found to be expressed in cell lines that were not hematopoietic (180). At such, *Relt* mRNA expression proved to not only be exclusive to a particular hematologic cell subset, rather the distribution pattern was widespread among all hematological subsets (180). The study further identified that tissues which are known to have high levels of aforementioned cell types also exhibited high level of *Relt* mRNA (180). Another study, conducted by Moua *et al*, reported similar results, although elevated *Relt* protein expression was only observed in the spleen and lymph node but not in the bone marrow (179). These results were congruent with expression of *Relt* mRNA observed in lymphoid tissues from previous study(179). *Relt* was, additionally, identified as a TNFR capable of inducing

programmed cell death (179). Cusick *et al*, reported in their study, that overexpression of RELT in HEK 293 epithelial cells with morphological features consistent with the activation of apoptotic pathway (181).

Statistically differences were identified in *Relt* mRNA expression in the kidney tissue. Significant high expression of *Relt* mRNA in kidney tissue were detected in NZB/W Ab- (22-32 wo), Ab+(21-37 wo) and prot + (22-34 wo) NZB/W groups. Expression of *Relt* mRNA was also slightly elevated in BALB/c (22-39 wo) compared to the normalized Young NZB/W Ab- (4wo) group. In lung tissue, expression of *Relt* mRNA was increased in 17-18-wo NZB/W, while declined *Relt* mRNA expression was observed in 12-wo NZB/W group. Decreased expression of *Relt* mRNA in spleen tissue was observed in all groups of NZB/W mice. When comparing our findings to those of older studies, it must point out that there was no congruency. Even though we did not obtain or replicate the previously reported elevation in *Relt* mRNA expression, our results suggest that expression of *Relt* mRNA in splenic tissue of NZB/W mice were receded, thus the *Relt* was downregulated and not upregulated.

A potential source of error can arise when tissue sections dry out. If tissue sections are dried out during the analysis, then false signals can be observed, particularly false-negative immune staining of tissue and intense background staining. Unfortunately, this is an issue that is often not discovered until the section is analyzed under the microscope. In some cases, false-negative immunostaining can only occur due to background staining, in other cases, it is a combination of multiple factors. Over fixation of tissue can also lead to negative results, as over fixation can mask antigen epitopes, nevertheless, this is rarely an issue. Under fixation of tissue or delay in fixation are more serious issues. Additionally, complete removal of paraffin is vital considering paraffin residues in the tissue are the critical and major source of error in immunohistochemistry. The probability for masking of antigen is high if paraffin residues is not completely removed. Limitations of the study included sample size; not enough slides were studied. Only a few slides were cut and analyzed, at such, TLS could have been detected in samples where it was not displayed had more tissue samples been studied. If one had investigated and analyzed half of the tissue or even analyzed the entirety of the tissue by cutting deeper into the tissue beyond the surface, then perhaps more TLS could have been detected in all tissues. In the studied samples, even if TLS was not displayed, it does not necessarily mean nothing was present. One should not

rule out the idea that there might, in fact, have a larger TLS structure hidden further down in the tissue where smaller TLSs were displayed. A lot of factors need to be taken into consideration when performing an immunohistochemical analysis, this also includes the cutting of tissue sample, the direction in which the tissues are cut will ultimately affect how the structure in the tissues are preserved/ how the will look. Additionally, some cells tissues have normally contained a lot of immune cells than others. If different other cells. For instance, if an immune cell markers marker were performed on kidney tissues, one would have seen a lot of macrophages compare to T- and B-lymphocytes. T, this would possibly have been the case for SG as well. Lungs, on the other hand, contain more T-lymphocytes, in this study, we only ran CD3 as a T-lymphocyte marker, it is therefore not clear what type of T-lymphocytes were observed. Another limitation includes the heterogeneity, as organs analyzed for mRNA expression were not from the same mouse. Moreover, RNA isolation of pancreas presented quite a challenge, as it is a ribonuclease-rich tissue.

5 Conclusion

The initial aim of this thesis was to detect TLS formation in various tissue of lupus-prone mice at different stages of disease progression. Additionally, the objective was also to analyze gene expression during TLS formation and investigate the correlation between gene expression and TLS formation in tissues of lupus-prone mice during SLE progression. While acknowledging the limitations of the study, this study is potentially important. This present study demonstrates, based on immunostaining of CD3 and B220, TLS formation in the various tissues of lupus prone NZB/W mice models. Hypercellularity was repeatedly detected in anti-dsDNA antibody positive NZB/W mice and it was observed that these mice frequently yielded high scores. Moreover, assessment of TLS in salivary gland, lung, and pancreatic tissue revealed that TLS was displayed in anti-dsDNA antibody positive NZB/W mice, thereby authenticating or rather solidify anti-dsDNA antibodies pathological role in SLE.TLS aggregates were distinctly organized in T-and B-lymphocyte regions. Furthermore, accumulation of immune cell infiltration in various tissues showcased that TLSs predominantly manifested around or adjacent large and small arteries, veins, including ducts**,** and in case of pancreatic tissue, in islets of Langerhans. An additional associated with TLS was that the formation of these lymphoid aggregated in lung tissues did not correlate with the other TLSs displayed in the pancreas or salivary gland. However, TLS formation in lung correlated with the presence of anti-dsDNA antibody. Anti-dsDNA correlated with T- and B-lymphocyte infiltration in lung tissue of lupus-prone NZB/W mice. Moreover, this study demonstrates that proteinuria and age did not correlate with TLS and that anti-dsDNA antibody and immune complexes correlated with TLS. The gene expression analyses demonstrated upregulation in expression in mRNA of the various genes within the various tissues of lupus prone NZB/W mice, and some. The upregulation of these genes may therefore reflect TLS formation in SLE.

Further research is necessary for determining the signals implicated in TLS development, this will further elucidate whether TLS formation plays an active role in disease exacerbation or if TLS plays a role in ameliorating the disease advancement.

6 References

1. Bradley PJ, Guntinas-Lichius O, Nieuw Amerongen Av. Salivary gland disorders and diseases : diagnosis and management. Stuttgart ;,New York: Thieme; 2011.
2. Scudamore CL. A Practical Guide to the Histology of the Mouse. New York: New York: John Wiley & Sons, Incorporated; 2014.
3. Treuting PM, Dintzis SM, Frevert CW, Liggitt D, Montine KS. Comparative anatomy and histology : a mouse and human atlas. London: Elsevier; 2012.
4. Marieb E, Hoehn K. Human Anatomy & Physiology. 8th edn, 1264. Pearson; 2010.
5. Treuting PM, Valasek MA, Dintzis SM. 11 - Upper Gastrointestinal Tract. In: Treuting PM, Dintzis SM, editors. Comparative Anatomy and Histology. San Diego: Academic Press; 2012. p. 155-75.
6. Parker S, Winston R. The Human Body Book: DK Pub.; 2007.
7. Thiriet, Marc. Anatomy and Physiology of the Circulatory and Ventilatory Systems: Biomathematical and Biomechanical Modeling of the Circulatory and Ventilatory Systems 6. US: US: Springer; 2014.
8. Stevens A, Lowe JS. Human histology. 3rd ed. ed. Philadelphia: Elsevier Mosby; 2005.
9. Stoelting RK, Hillier SC. Handbook of Pharmacology and Physiology in Anesthetic Practice. Philadelphia, UNITED STATES: Wolters Kluwer; 2005.
10. Chambers D, Huang CLH, Matthews G. Basic physiology for anaesthetists. Cambridge: Cambridge University Press; 2019.
11. Gray H, Pick T, Howden R. Anatomy, Descriptive and Surgical. 1974. Philadelphia: Philadelphia, Pa. Running Press.
12. Richard LD, Vogl AW, Adam WMM, Richard T, Paul R, Ansell H. Gray's Anatomy for Students. US: US: Churchill Livingstone; 2015.
13. Chambers D, Huang C, Matthews G. Basic Physiology for Anaesthetists. 2 ed. Cambridge: Cambridge University Press; 2019.
14. Marieb EN, Hoehn K. Human anatomy & physiology: Pearson education; 2007.
15. Kroeker C. Cardiovascular System: Anatomy and Physiology. Cardiovascular Mechanics. 2018:1-17.
16. Lou M, Zhang J, Wang Y, Qu Y, Feng W, Ji X, et al. Cerebral Venous System in Acute and Chronic Brain Injuries. Cham: Cham: Springer; 2019.

17. Hall JE. Guyton and Hall textbook of medical physiology. 13th edition.; International edition. ed. Philadelphia, PA: Elsevier; 2016.
18. Caro CG, Pedley TJ, Schroter RC, Seed WA. The Mechanics of the Circulation. GB: GB: Cambridge University Press; 2011.
19. Caro CG, Pedley TJ, Schroter RC, Seed WA, Parker KH. The Mechanics of the Circulation. Cambridge, UNITED KINGDOM: Cambridge University Press; 2011.
20. Naeije R, Westerhof N. Pulmonary Vascular Function. In: Yuan JXJ, Garcia JGN, West JB, Hales CA, Rich S, Archer SL, editors. Textbook of Pulmonary Vascular Disease. Boston, MA: Springer US; 2011. p. 61-72.
21. Kiefer F, Schulte-Merker S. Developmental Aspects of the Lymphatic Vascular System. Vienna: Springer Vienna : Imprint: Springer; 2014.
22. Murray C. Encyclopedia britannica. Chicago: Encyclopedia Britannica Inc. http://www. britannica. com/EBchecked …; 2013.
23. Santambrogio L. Immunology of the Lymphatic System. New York, NY: Springer New York : Imprint: Springer; 2013.
24. Abbas AK, Lichtman AH, Pillai S. Cellular and molecular immunology. 7th ed. ed. Philadelphia: Elsevier Saunders; 2012.
25. Karunamuni G. The Cardiac Lymphatic System : An Overview. New York, NY: Springer New York : Imprint: Springer; 2013.
26. Yun JW, Granger DN, Granger JP, Alexander JS. The Lymphatic System in Health and Disease. San Rafael, UNITED STATES: Morgan & Claypool Life Science Publishers; 2018.
27. Barone F, Gardner DH, Nayar S, Steinthal N, Buckley CD, Luther SA. Stromal fibroblasts in tertiary lymphoid structures: a novel target in chronic inflammation. Frontiers in Immunology. 2016;7:477.
28. von Andrian UH, Mempel TR. Homing and cellular traffic in lymph nodes. Nature Reviews Immunology. 2003;3(11):867-78.
29. Willard-Mack CL. Normal Structure, Function, and Histology of Lymph Nodes. Toxicologic Pathology. 2006;34(5):409-24.
30. Dunphy C. Neoplastic Hematopathology : An Atlas and Concise Guide. New York, UNITED STATES: Demos Medical Publishing; 2012.

31. Treuting PM, Frevert CW, Liggitt D, Dintzis SM. Comparative Anatomy and Histology: A Most. Louis, Mo, Usae and Human Atlas. San Diego: San Diego: Elsevier Science & Technology; 2011.
32. Scudamore CL, Thompson S, McInnes E. A practical guide to the histology of the mouse. Chichester, England: Wiley-Blackwell; 2014.
33. Junqueira LC, Carneiro J. Basic histology : text & atlas. 11th ed. ed. New York: McGraw-Hill; 2005.
34. Boehm T, Bleul CC. The evolutionary history of lymphoid organs. Nature immunology. 2007;8(2):131-5.
35. Schulz O, Hammerschmidt SI, Moschovakis GL, Förster R. Chemokines and Chemokine Receptors in Lymphoid Tissue Dynamics. Annual Review of Immunology. 2016;34(1):203-42.
36. Pearl ER, Vogler LB, Okos AJ, Crist WM, Lawton AR, Cooper MD. B Lymphocyte Precursors in Human Bone Marrow: An Analysis of Normal Individuals and Patients with Antibody-Deficiency States. The Journal of Immunology. 1978;120(4):1169-75.
37. Ovalle WK, Nahirney PC, Netter FH. Netter's essential histology. Philadelphia: Saunders/Elsevier; 2008.
38. Sandel PC, Monroe JG. Negative Selection of Immature B Cells by Receptor Editing or Deletion Is Determined by Site of Antigen Encounter. Immunity. 1999;10(3):289-99.
39. Schweighoffer E, Vanes L, Nys J, Cantrell D, McCleary S, Smithers N, et al. The BAFF Receptor Transduces Survival Signals by Co-opting the B Cell Receptor Signaling Pathway. Immunity. 2013;38(3):475-88.
40. Ploegh H. Cell Biology of the B Cell Receptor. San Diego, UNITED STATES: Elsevier Science & Technology; 2014.
41. Melchers F, Rolink A, Grawunder U, Winkler TH, Karasuyama H, Ghia P, et al. Positive and negative selection events during B lymphopoiesis. Current Opinion in Immunology. 1995;7(2):214-27.
42. Nemazee D. Mechanisms of central tolerance for B cells. Nature Reviews Immunology. 2017;17(5):281-94.
43. Balogh P. Developmental Biology of Peripheral Lymphoid Organs. Berlin, Heidelberg: Springer Berlin Heidelberg : Imprint: Springer; 2011.

44. Ruddle NH. Lymphatic vessels and tertiary lymphoid organs. The Journal of clinical investigation. 2014;124(3):953-9.
45. Kain MJW, Owens BMJ. Stromal cell regulation of homeostatic and inflammatory lymphoid organogenesis. Immunology. 2013;140(1):12-21.
46. Ruddle NH. High endothelial venules and lymphatic vessels in tertiary lymphoid organs: characteristics, functions, and regulation. Frontiers in immunology. 2016;7:491.
47. Pipi E, Nayar S, Gardner DH, Colafrancesco S, Smith C, Barone F. Tertiary lymphoid structures: autoimmunity goes local. Frontiers in Immunology. 2018;9:1952.
48. Neyt K, Perros F, GeurtsvanKessel CH, Hammad H, Lambrecht BN. Tertiary lymphoid organs in infection and autoimmunity. Trends in Immunology. 2012;33(6):297-305.
49. Buckley CD, Barone F, Nayar S, Benezech C, Caamano J. Stromal cells in chronic inflammation and tertiary lymphoid organ formation. Annual review of immunology. 2015;33:715-45.
50. Sarajo M, Andreas JRH, Changjun Y, Pasquale M. Tertiary Lymphoid Organs (TLOs): Powerhouses of Disease Immunity: Frontiers Media SA; 2017.
51. Shipman WD, Dasoveanu DC, Lu TT. Tertiary lymphoid organs in systemic autoimmune diseases: pathogenic or protective? F1000Research. 2017;6.
52. van de Pavert SA, Mebius RE. New insights into the development of lymphoid tissues. Nature Reviews Immunology. 2010;10(9):664-74.
53. Chang A, Henderson SG, Brandt D, Liu N, Guttikonda R, Hsieh C, et al. In situ B cell-mediated immune responses and tubulointerstitial inflammation in human lupus nephritis. The Journal of Immunology. 2011;186(3):1849-60.
54. Myers EN, Ferris RL. Salivary Gland Disorders. Berlin, Heidelberg: Springer Berlin Heidelberg : Imprint: Springer; 2007.
55. Treuting PM, Dintzis SM. 8 - Salivary Glands. In: Treuting PM, Dintzis SM, editors. Comparative Anatomy and Histology. San Diego: Academic Press; 2012. p. 111-20.
56. Holmberg KV, Hoffman MP. Anatomy, Biogenesis and Regeneration of Salivary Glands. Saliva: Secretion and Functions. 2014;24:1-13.
57. Pancreas: Anatomy and Structural Anomalies. Oxford, UK: Oxford, UK: Wiley-Blackwell; 2009. p. 508-13.

58. Lowe JS, Anderson PG. Chapter 11 - Alimentary Tract. In: Lowe JS, Anderson PG, editors. Stevens & Lowe's Human Histology (Fourth Edition) (Fourth Edition). Philadelphia: Mosby; 2015. p. 186-224.
59. Ash R, Morton DA, Scott SA. The big picture : histology. New York: McGraw-Hill Medical; 2013.
60. Mitchell B, Peel S. Histology : an illustrated colour text. Edinburgh: Churchill Livingstone Elsevier; 2009.
61. Peate I, Nair M. Anatomy and Physiology for Nurses at a Glance : Anatomy and Physiology for Nurses at a Glance. Somerset, UNITED KINGDOM: John Wiley & Sons, Incorporated; 2015.
62. Gartner LP. Textbook of Histology E-Book. Philadelphia, UNITED STATES: Elsevier; 2016.
63. Gunasegaran JP. Textbook of histology and a practical guide. 3rd ed. ed. New Delhi: Reed Elsevier India; 2016.
64. Netter FH. Atlas of Human Anatomy E-Book : Digital EBook. Philadelphia, UNITED STATES: Elsevier; 2018.
65. Suarez CJ, Dintzis SM, Frevert CW. 9 - Respiratory. In: Treuting PM, Dintzis SM, editors. Comparative Anatomy and Histology. San Diego: Academic Press; 2012. p. 121-34.
66. Standring S, Gray H, Borley NR. Gray's anatomy : the anatomical basis of clinical practice. 40th ed. ed. Edinburgh: Churchill Livingstone Elsevier; 2008.
67. Drake RL, Mitchell AWM, Vogl W, Gray H. Gray's anatomy for students. Philadelphia: Elsevier/Churchill Livingstone; 2005.
68. Moore KL, Agur AMR, Dalley AF. Essential clinical anatomy. 5th ed. ed. Philadelphia: Wolters Kluwer/Lippincott Williams & Wilkins; 2015.
69. VanPutte C. Seeley's anatomy & physiology. 10th ed. ed. New York: McGraw-Hill; 2014.
70. Ellis H, Mahadevan V. Clinical anatomy : applied anatomy for students and junior doctors. 13th ed. ed. Chichester: Wiley-Blackwell; 2013.
71. Petroianu A. Spleen: Bentham Science Publishers; 2011.
72. Cesta MF. Normal structure, function, and histology of the spleen. Toxicol Pathol. 2006;34(5):455-65.

73. Zhang L, Shao H, Alkan S. Diagnostic Pathology of Hematopoietic Disorders of Spleen and Liver. Cham: Cham: Springer International Publishing AG; 2020.
74. Hiatt JR, Phillips EH, Morgenstern L. Surgical Diseases of the Spleen: Springer Berlin Heidelberg; 2012.
75. Gordon C, Isenberg D. Systemic Lupus Erythematosus. Oxford, UNITED KINGDOM: Oxford University Press, Incorporated; 2016.
76. Al Daabil M, Massarotti EM, Fine A, Tsao H, Ho P, Schur PH, et al. Development of SLE among "potential SLE" patients seen in consultation: long-term follow-up. International Journal of Clinical Practice. 2014;68(12):1508-13.
77. Tsokos G. Systemic Lupus Erythematosus : Basic, Applied and Clinical Aspects. San Diego, UNITED STATES: Elsevier Science & Technology; 2016.
78. Lech M, Anders H-J. The pathogenesis of lupus nephritis. Journal of the American Society of Nephrology. 2013;24(9):1357-66.
79. Systemic Lupus Erythematosus: InTech.
80. Arnaud L, van Vollenhoven R. Advanced Handbook of Systemic Lupus Erythematosus. Cham: Cham: Springer International Publishing AG; 2017.
81. Tan EM, Cohen AS, Fries JF, Masi AT, Mcshane DJ, Rothfield NF, et al. The 1982 revised criteria for the classification of systemic lupus erythematosus. Arthritis & Rheumatism. 1982;25(11):1271-7.
82. Daca A, Czuszyńska Z, Smoleńska Ż, Zdrojewski Z, Witkowski JM, Bryl E. Two systemic lupus erythematosus (SLE) global disease activity indexes—the SLE Disease Activity Index and the Systemic Lupus Activity Measure—demonstrate different correlations with activation of peripheral blood CD4+ T cells. Human Immunology. 2011;72(12):1160-7.
83. Liang MH, Fortin PR, Isenberg DA, Snaith L. Quantitative clinical assessment of disease activity in systemic lupus erythematosus: progress report and research agenda. Rheumatology International. 1991;11(3):133-6.
84. Romero-Diaz J, Isenberg D, Ramsey-Goldman R. Measures of adult systemic lupus erythematosus: updated version of British Isles lupus assessment group (BILAG 2004), European consensus lupus activity measurements (ECLAM), systemic lupus activity measure, revised (SLAM-R), systemic lupus activity questionnaire for population studies (SLAQ), systemic lupus erythematosus disease activity index 2000 (SLEDAI-2K), and systemic lupus

international collaborating Clinics/American College of Rheumatology damage index (SDI). Arthritis care & research. 2011;63(0 11).
85. HAY EM, BACON PA, GORDON C, ISENBERG DA, MADDISON P, SNAITH ML, et al. The BILAG index: a reliable and valid instrument for measuring clinical disease activity in systemic lupus erythematosus. QJM: An International Journal of Medicine. 1993;86(7):447-58.
86. Mikdashi J, Nived O. Measuring disease activity in adults with systemic lupus erythematosus: the challenges of administrative burden and responsiveness to patient concerns in clinical research. Arthritis Res Ther. 2015;17(1):183-.
87. Yee C-S, Farewell V, Isenberg DA, Rahman A, Teh L-S, Griffiths B, et al. British isles lupus assessment group 2004 index is valid for assessment of disease activity in systemic lupus erythematosus. Arthritis & Rheumatism. 2007;56(12):4113-9.
88. Griffiths B, Mosca M, Gordon C. Assessment of patients with systemic lupus erythematosus and the use of lupus disease activity indices. Best Practice & Research Clinical Rheumatology. 2005;19(5):685-708.
89. Schur PH, Massarotti EM. Lupus Erythematosus: Clinical Evaluation and Treatment. 1. Aufl.,2012 ed. New York, NY: New York, NY: Springer-Verlag; 2012.
90. Carter EE, Barr SG, Clarke AE. The global burden of SLE: prevalence, health disparities and socioeconomic impact. Nat Rev Rheumatol. 2016;12(10):605-20.
91. Muñoz LE, Janko C, Schulze C, Schorn C, Sarter K, Schett G, et al. Autoimmunity and chronic inflammation — Two clearance-related steps in the etiopathogenesis of SLE. Autoimmunity Reviews. 2010;10(1):38-42.
92. Sebastiani GD, Galeazzi M. Infection—genetics relationship in systemic lupus erythematosus. Lupus. 2009;18(13):1169-75.
93. Graham RR, Ortmann W, Rodine P, Espe K, Langefeld C, Lange E, et al. Specific combinations of HLA-DR2 and DR3 class II haplotypes contribute graded risk for disease susceptibility and autoantibodies in human SLE. European Journal of Human Genetics. 2007;15(8):823-30.
94. Ka S, Lee S, Hong J, Cho Y, Sung J, Kim H-N, et al. HLAscan: genotyping of the HLA region using next-generation sequencing data. BMC Bioinformatics. 2017;18(1):258.
95. Postal M, Appenzeller S. The role of Tumor Necrosis Factor-alpha (TNF-α) in the pathogenesis of systemic lupus erythematosus. Cytokine. 2011;56(3):537-43.

96. Yap DYH, Lai KN. Cytokines and their roles in the pathogenesis of systemic lupus erythematosus: from basics to recent advances. BioMed Research International. 2010;2010.
97. López P, Gutiérrez C, Suárez A. IL-10 and TNFα genotypes in SLE. BioMed Research International. 2010;2010.
98. Sabry A, sheashaa H, El-husseini A, Mahmoud K, Eldahshan KF, George SK, et al. Proinflammatory cytokines (TNF-α and IL-6) in Egyptian patients with SLE: Its correlation with disease activity. Cytokine. 2006;35(3):148-53.
99. Zuniga J, Vargas-Alarcón G, Hernández-Pacheco G, Portal-Celhay C, Yamamoto-Furusho J, Granados J. Tumor necrosis factor-α promoter polymorphisms in Mexican patients with systemic lupus erythematosus (SLE). Genes & Immunity. 2001;2(7):363-6.
100. Cano PO, Jerry LM, Sladowski JP, Osterland CK. Circulating immune complexes in systemic lupus erythematosus. Clin Exp Immunol. 1977;29(2):197-204.
101. Pisetsky DS, Lipsky PE. New insights into the role of antinuclear antibodies in systemic lupus erythematosus. Nature Reviews Rheumatology. 2020.
102. Mahajan A, Herrmann M, Muñoz LE. Clearance deficiency and cell death pathways: a model for the pathogenesis of SLE. Frontiers in immunology. 2016;7:35.
103. Mevorach D, Mascarenhas JO, Gershov D, Elkon KB. Complement-dependent Clearance of Apoptotic Cells by Human Macrophages. Journal of Experimental Medicine. 1998;188(12):2313-20.
104. Botto M, Dell'Agnola C, Bygrave AE, Thompson EM, Cook HT, Petry F, et al. Homozygous C1q deficiency causes glomerulonephritis associated with multiple apoptotic bodies. Nature genetics. 1998;19(1):56-9.
105. Elkon KB. Review: Cell Death, Nucleic Acids, and Immunity. Arthritis & Rheumatology. 2018;70(6):805-16.
106. Mandache E, Penescu M. Renal subcapsular tertiary lymphoid aggregates in chronic kidney diseases. Romanian journal of morphology and embryology = Revue roumaine de morphologie et embryologie. 2011;52(4):1219-25.
107. Steinmetz OM, Velden J, Kneissler U, Marx M, Klein A, Helmchen U, et al. Analysis and classification of B-cell infiltrates in lupus and ANCA-associated nephritis. Kidney International. 2008;74(4):448-57.

108. Dorraji SE, Kanapathippillai P, Hovd A-MK, Stenersrød MR, Horvei KD, Ursvik A, et al. Kidney Tertiary Lymphoid Structures in Lupus Nephritis Develop into Large Interconnected Networks and Resemble Lymph Nodes in Gene Signature. The American Journal of Pathology. 2020;190(11):2203-25.
109. Peters LL, Robledo RF, Bult CJ, Churchill GA, Paigen BJ, Svenson KL. The mouse as a model for human biology: a resource guide for complex trait analysis. Nature Reviews Genetics. 2007;8(1):58-69.
110. Paul WE. Fundamental Immunology. Philadelphia, UNITED STATES: Wolters Kluwer; 2012.
111. Dabbs DJ. Diagnostic immunohistochemistry e-book: Elsevier Health Sciences; 2013.
112. Key M. ▪ Immunohistochemistry Staining Methods. Education Guide Immunohistochemical Staining Methods Fourth Edition. 2006:47.
113. Buchwalow IB, Böcker W. Immunohistochemistry. Basics and Methods. 2010;1:1-149.
114. Buchwalow IB, Böcker W. Immunohistochemistry: Basics and Methods. Berlin, Heidelberg: Springer Berlin Heidelberg : Imprint: Springer; 2010.
115. Ramos-Vara J, Miller M. When tissue antigens and antibodies get along: revisiting the technical aspects of immunohistochemistry—the red, brown, and blue technique. Veterinary pathology. 2014;51(1):42-87.
116. Akkoyunlu G, Tepekoy F. Immunohistochemistry of Paraffin Sections from Mouse Ovaries. Methods in molecular biology (Clifton, NJ). 2016;1457:269.
117. Buchwalow IB, Böcker W. Working with antibodies. Immunohistochemistry: Basics and Methods: Springer; 2010. p. 31-9.
118. Gu-Trantien C, Garaud S, Migliori E, Solinas C, Lodewyckx J-N, Willard-Gallo K. Quantifying tertiary lymphoid structure-associated genes in formalin-fixed paraffin-embedded breast cancer tissues. Tertiary Lymphoid Structures: Springer; 2018. p. 139-57.
119. Fedchenko N, Reifenrath J. Different approaches for interpretation and reporting of immunohistochemistry analysis results in the bone tissue - a review. Diagn Pathol. 2014;9:221-.
120. Kramer C. Isolation of total RNA from Neurospora mycelium. Circadian Rhythms: Springer; 2007. p. 291-303.
121. Peirson SN, Butler JN. RNA extraction from mammalian tissues. Circadian Rhythms: Springer; 2007. p. 315-27.

122. Farrell RE. Chapter 3 - The Truth about Tissues. In: Farrell RE, editor. RNA Methodologies (Fourth Edition). San Diego: Academic Press; 2010. p. 81-103.
123. Farrell RE. Chapter 2 - RNA Isolation Strategies. In: Farrell RE, editor. RNA Methodologies (Fourth Edition). San Diego: Academic Press; 2010. p. 45-80.
124. Stangegaard M, Dufva IH, Dufva M. Reverse transcription using random pentadecamer primers increases yield and quality of resulting cDNA. BioTechniques. 2006;40(5):649-57.
125. Precision Molecular Pathology of Neoplastic Pediatric Diseases. Cham: Springer International Publishing, Cham; 2018.
126. Sharon A. Molecular and cell biology methods for fungi / edited by Amir Sharon. New York, NY: New York, NY, Humana Press; 2010.
127. Corthell JT. Basic Molecular Protocols in Neuroscience : Tips, Tricks, and Pitfalls. San Diego, UNITED STATES: Elsevier Science & Technology; 2014.
128. Singleton P, Sainsbury D, Credo R. Dictionary of microbiology and molecular biology. Chichester, West Sussex Eng. ;,Hoboken, N.J.: Wiley; 2006.
129. Ortutay C, Ortutay Z. Molecular data analysis using R2016.
130. Constantinides A, Moghe PV, Dunn S. Numerical Methods in Biomedical Engineering. Burlington, UNITED STATES: Elsevier Science & Technology; 2005.
131. Yilmaz A, Onen HI, Alp E, Menevse S. Real-time PCR for gene expression analysis. Polymerase Chain Reaction. 2012:229-54.
132. Quantitative Real-Time PCR: Methods and Protocols. New York, NY: Springer New York, New York, NY; 2014.
133. Löfström C, Josefsen MH, Hansen T, Søndergaard MSR, Hoorfar J. 9 - Fluorescence-based real-time quantitative polymerase chain reaction (qPCR) technologies for high throughput screening of pathogens. In: Bhunia AK, Kim MS, Taitt CR, editors. High Throughput Screening for Food Safety Assessment: Woodhead Publishing; 2015. p. 219-48.
134. Walker JM, O'connell J. RT-PCR Protocols. Totowa, NJ: Totowa, NJ: Humana Press; 2002.
135. Boisseau P, Lahmani M. Nanoscience : Nanobiotechnology and Nanobiology. Berlin, Heidelberg: Springer Berlin Heidelberg : Imprint: Springer; 2009.
136. McChlery SM, Clarke SC. The use of hydrolysis and hairpin probes in real-time PCR. Molecular Biotechnology. 2003;25(3):267-73.

137. Gupta GS. Animal Lectins: Form, Function and Clinical Applications. Vienna: Springer Vienna : Imprint: Springer; 2012.
138. Barclay AN, Brown MH, Law SKA, McKnight AJ, Tomlinson MG, van der Merwe PA, et al. The Leucocyte Antigen Factsbook. Oxford, UNITED KINGDOM: Elsevier Science & Technology; 1997.
139. Gangisetty O, Reddy DS. The optimization of TaqMan real-time RT-PCR assay for transcriptional profiling of GABA-A receptor subunit plasticity. J Neurosci Methods. 2009;181(1):58-66.
140. Chetty R, Cooper K, Gown A. Leong's Manual of Diagnostic Antibodies for Immunohistology. West Nyack: West Nyack: Cambridge University Press; 2016.
141. Johnson P, Samarakoon A, Saunders AE, Harder KW. CD45 (PTPRC). In: Choi S, editor. Encyclopedia of Signaling Molecules. Cham: Springer International Publishing; 2018. p. 912-9.
142. Nikolic T, Dingjan GM, Leenen PJM, Hendriks RW. A subfraction of B220+ cells in murine bone marrow and spleen does not belong to the B cell lineage but has dendritic cell characteristics. European Journal of Immunology. 2002;32(3):686-92.
143. Yung S, Chan TM. Anti-dsDNA antibodies and resident renal cells — Their putative roles in pathogenesis of renal lesions in lupus nephritis. Clinical Immunology. 2017;185:40-50.
144. Mandik-Nayak L, Bui A, Noorchashm H, Eaton A, Erikson J. Regulation of Anti–double-stranded DNA B Cells in Nonautoimmune Mice: Localization to the T–B Interface of the Splenic Follicle. Journal of Experimental Medicine. 1997;186(8):1257-67.
145. Dorraji SE, Kanapathippillai P, Hovd A-MK, Stenersrød MR, Horvei KD, Ursvik A, et al. Kidney Tertiary Lymphoid Structures in Lupus Nephritis Develop into Large Interconnected Networks and Resemble Lymph Nodes in Gene Signature. The American Journal of Pathology. 2020;190(11):2203-25.
146. Sheashaa HA, Abbas TM, Moustafa FE. Lupus Nephritis: Frontiers and Challenges. Hauppauge: Hauppauge: Nova Science Publishers, Incorporated; 2010.
147. Smith MJ, Simmons KM, Cambier JC. B cells in type 1 diabetes mellitus and diabetic kidney disease. Nature Reviews Nephrology. 2017;13(11):712.

148. Kendall PL, Yu G, Woodward EJ, Thomas JW. Tertiary Lymphoid Structures in the Pancreas Promote Selection of B Lymphocytes in Autoimmune Diabetes. The Journal of Immunology. 2007;178(9):5643.
149. Yang M, Rui K, Wang S, Lu L. Regulatory B cells in autoimmune diseases. Cellular & molecular immunology. 2013;10(2):122-32.
150. Smeets S, Staels W, Stangé G, Gillard P, De Leu N, in't Veld P. Insulitis and lymphoid structures in the islets of Langerhans of a 66-year-old patient with long-standing type 1 diabetes. Virchows Archiv. 2020.
151. McCullagh A, Rosenthal M, Wanner A, Hurtado A, Padley S, Bush A. The bronchial circulation—worth a closer look: a review of the relationship between the bronchial vasculature and airway inflammation. Pediatric pulmonology. 2010;45(1):1-13.
152. Kimmel PL, Rosenberg ME. Chronic renal disease. San Diego, California,London, England: Academic Press; 2015.
153. Scott RP, Quaggin SE. The cell biology of renal filtration. The Journal of cell biology. 2015;209(2):199-210.
154. Manoussakis MN, Georgopoulou C, Zintzaras E, Spyropoulou M, Stavropoulou A, Skopouli FN, et al. Sjögren's syndrome associated with systemic lupus erythematosus: Clinical and laboratory profiles and comparison with primary Sjögren's syndrome. Arthritis & Rheumatism. 2004;50(3):882-91.
155. Rizzo C, Grasso G, Destro Castaniti GM, Ciccia F, Guggino G. Primary Sjogren Syndrome: Focus on Innate Immune Cells and Inflammation. Vaccines. 2020;8(2):272.
156. Barone F, Colafrancesco S. Sjogren's syndrome: from pathogenesis to novel therapeutic targets. Clin Exp Rheumatol. 2016;34(4 Suppl 98):58-62.
157. Fagarasan S, Cerutti A, Alt FW. Advances in Immunology. San Diego, UNITED STATES: Elsevier Science & Technology; 2010.
158. Kaetzel CS. Mucosal Immune Defense: Immunoglobulin A. New York, NY: Springer US : Imprint: Springer; 2007.
159. Hansen IS, Hoepel W, Zaat SA, Baeten DL, den Dunnen J. Serum IgA Immune Complexes Promote Proinflammatory Cytokine Production by Human Macrophages, Monocytes, and Kupffer Cells through FcαRI–TLR Cross-Talk. The Journal of Immunology. 2017;199(12):4124-31.

160. Buchwalow IB, Böcker W. Immunohistochemistry. Berlin, Heidelberg: Berlin, Heidelberg: Springer Berlin / Heidelberg; 2010.
161. Fritschy JM. Is my antibody-staining specific? How to deal with pitfalls of immunohistochemistry. European Journal of Neuroscience. 2008;28(12):2365-70.
162. Buchwalow IB, Böcker W. Immunohistochemistry: Basics and Methods. Berlin, Heidelberg: Berlin, Heidelberg: Springer Berlin Heidelberg; 2009.
163. Kalyuzhny AE. Immunohistochemistry: Essential Elements and Beyond. 1st ed. 2016 ed. Cham: Cham: Springer International Publishing AG; 2016.
164. Cytokines: IntechOpen.
165. Suzuki T, Chow C-W, Downey GP. Role of innate immune cells and their products in lung immunopathology. The International Journal of Biochemistry & Cell Biology. 2008;40(6):1348-61.
166. Favilli F, Anzilotti C, Martinelli L, Quattroni P, De Martino S, Pratesi F, et al. IL-18 activity in systemic lupus erythematosus. Annals of the New York Academy of Sciences. 2009;1173(1):301.
167. Rovin B, Bomback A, Radhakrishnan J. Chapter 41 - Lupus Nephritis. In: Kimmel PL, Rosenberg ME, editors. Chronic Renal Disease. San Diego: Academic Press; 2015. p. 501-12.
168. Reséndiz-Albor AA, Reina-Garfias H, Rojas-Hernández S, Jarillo-Luna A, Rivera-Aguilar V, Miliar-García A, et al. Regionalization of pIgR expression in the mucosa of mouse small intestine. Immunology Letters. 2010;128(1):59-67.
169. Chen P, Zuo H, Xiong H, Kolar MJ, Chu Q, Saghatelian A, et al. Gpr132 sensing of lactate mediates tumor–macrophage interplay to promote breast cancer metastasis. Proc Natl Acad Sci U S A. 2017;114(3):580-5.
170. Laskin DL, Sunil VR, Gardner CR, Laskin JD. Macrophages and tissue injury: agents of defense or destruction? Annu Rev Pharmacol Toxicol. 2011;51:267-88.
171. Stacey M, Chang G-W, Sanos SL, Chittenden LR, Stubbs L, Gordon S, et al. EMR4, a novel epidermal growth factor (EGF)-TM7 molecule up-regulated in activated mouse macrophages, binds to a putative cellular ligand on B lymphoma cell line A20. Journal of Biological Chemistry. 2002;277(32):29283-93.
172. Gordon S, Hamann J, Lin HH, Stacey M. F4/80 and the related adhesion-GPCRs. European journal of immunology. 2011;41(9):2472-6.

173. Schiffer L, Bethunaickan R, Ramanujam M, Huang W, Schiffer M, Tao H, et al. Activated renal macrophages are markers of disease onset and disease remission in lupus nephritis. The Journal of Immunology. 2008;180(3):1938-47.
174. Rosen SD. Ligands for L-Selectin: Homing, Inflammation, and Beyond. Annual Review of Immunology. 2004;22(1):129-56.
175. Chao C-C, Jensen R, Dailey MO. Mechanisms of L-selectin regulation by activated T cells. The Journal of Immunology. 1997;159(4):1686-94.
176. Lange-Sperandio B, Cachat F, Thornhill BA, Chevalier RL. Selectins mediate macrophage infiltration in obstructive nephropathy in newborn mice. Kidney international. 2002;61(2):516-24.
177. McPherron AC, Lee S-J. GDF-3 and GDF-9: two new members of the transforming growth factor-beta superfamily containing a novel pattern of cysteines. Journal of Biological Chemistry. 1993;268(5):3444-9.
178. Wang W, Yang Y, Meng Y, Shi Y. GDF-3 is an adipogenic cytokine under high fat dietary condition. Biochemical and Biophysical Research Communications. 2004;321(4):1024-31.
179. Moua P, Checketts M, Xu L-G, Shu H-B, Reyland ME, Cusick JK. RELT family members activate p38 and induce apoptosis by a mechanism distinct from TNFR1. Biochemical and Biophysical Research Communications. 2017;491(1):25-32.
180. Sica GL, Zhu G, Tamada K, Liu D, Ni J, Chen L. RELT, a new member of the tumor necrosis factor receptor superfamily, is selectively expressed in hematopoietic tissues and activates transcription factor NF-κB. Blood, The Journal of the American Society of Hematology. 2001;97(9):2702-7.
181. Cusick JK, Mustian A, Goldberg K, Reyland ME. RELT induces cellular death in HEK 293 epithelial cells. Cellular Immunology. 2010;261(1):1-8.

7 Appendix

Table A1. Overview of materials used in this thesis.

Material	Product name	Product ID	Manufacturer	Purpose
Microtome	Microtome HM 355S Microtome cool-cut		Thermo scientific	Used to make thin slices of tissue
Various paraffin embedded tissues				Sectioned 4µm tissue for IHC
Microscope slides	Superfrost®Plus	J1800AMNZ	Thermo scientific	Mounting of tissue, hold tissue for examination. Ensures adhesion of tissue section.
Incubator	Lab drying oven	TS 8024	Termarks AS	Remove paraffin and dry slides
Cover slips/Cover glass				Cover tissue
Moist chamber				
Antigen retrieval	PT-link	PT10126	DAKO	Heat induced epitope retrieval
Hydrophobic pen	Super PAP pen	00-8899	Invitrogen	
Gassbind	Nonwoven Swabs	Mesoft ®	Mölnlycke Health Care	Used to wipe around tissue senction
Magnetic stirring and heater	Heidolph MR 3001	HEIDMR3001		Magnetic stirring of solutions
pH meter	Mettler toledo seven easy pH meter	SevenEasy™pH meter S20	Mettler Toledo	pH meter calibrator
Histokitt	Hencht Assistant Histokitt 500ml	1025/500	Glaswarenfabrik Karl Hecht GnbH & co KG	Slide mounting medium
Eppendorf tubes	DNA loBind Eppendorf tubes 1.5 mL		Eppendorf	Used for dilution and mixing
Various size sterile pipet tips			Fisher Scientific by Thermo	Measuring and transporting of measured solutions
Microscope	Olympus BX51TF	BX51TF	Olympus Europa SE & CO.KG	Visual antigen-antibody binding

Scapel				
Beads tubes	Magma lyser green beads tubes 2mL	3358941001	Roche by Life science	For homogenizing tissue samples
Homogenizer	Precelys 24			
IIICG Columns	Zymo-spin™ IIICG Column	C1006-50-G	Zymoresearch	Bind RNA, silica matrix allows for RNA purification
Collecting Tube			Zymoresearch	Collects the flow-through
Centrifuge	Eppendorf Centrifuge 5424	5424FL170164	Eppendorf AG	
Nanodrop®	Nanodrop® DN-1000 spectophotometer		Saveen Werner	Measurement of RNA concentration
Vortex mixer	Vibrofix VF1 Electronic		IKA®-Werke CmbH & CO. KG	
Agielent bioanalyzer	Agilent 2100 Bioanalyzer with 2100 expert software	DE72903005	Agilent technologies	Measure RNA purity
RNA nano chips	RNA Nano chips One-chip electrophoresis	UJ21BK20	Agilent technologies	
RNA chip priming station				Utilized to load gel matrix into chip with a syringe
"dry bath"	GeneAmp® PCR system 9700		Applied biosystems by life technologies	Amplification of nucelic acids
Vortex Mixer	IKA-model MS3			
96 well plate	Multiwell plate 96		Lightcycler®	
Optical adhesive cover	Lightcyler®480 sealing foil		Lightcycler®	
Alluminum foil				Shield fluoroscence sensitive samples and reagents from light
Centriguge	Tabletop centriguge Model 4200	K20142-1400	KUBOTA	Centrifuge pCR product
Eppendorf	Ependorf Master cylcer Gradient		Eppendorf AG	

Real time PCR machine	Lightcyler®96 Real time PCR	5815916001	Roche	
GraphPad	GraphPad®Prism 8		GraphPad®	Statistic analyzer

Table A2. Overview of experiments and reagents used

Experiments	Reagents	Manufacture	Purpose
Immuno histochemistry			
	Xylene	Sigma Aldrich	Deparaffinization and dehydration of slides
	Absolut Ethanol	Sigma Aldrich	Deparaffinization and dehydration of slides
	Ethanol 96%	Sigma Aldrich	Deparaffinization and dehydration of slides
	3% H_2O_2		Blocking for endogenous peroxidase
	10% Normal goat serum		Used to block nonspecific antibody in tissues
	Primary antibody		Bind directly to the antigen of interest
	Secondary antibody		Detect primary antibody,and bind to the primary antibody
	Chromogen	DAKO	Used for detection of secondary HRP-conjugated antibody. Used to microscopically vizualize the antigen of interest
	MilliQWater		Dilution purposes
	Hematoxylin		Stain that allows localization of nuclei and extracellular matrix. Counter stain
	Scott's solution		Blueing reagent, enables bluingof the hematoxylin stain
	Tri-sodiumcitrate dihydrate		Buffer for antigen retrieval, unmask epitopes and antigens in paraffin embedded tissues

	PBS powder without Ca2+, Mg2+		Used to make PBS buffer, utilized as a wash and dillution buffer
	Hydrochloric acid		Used in buffer, to calibrate buffers pH
	Tween 20		Added to buffers
	Rnase free H_2O		Used in dilutions and washing
RNA Isolation			
	Tri reagent®	Zymoresearch	For isolation of total RNA, inhibits Rnase activity, used to homogenize tissue
	Ethanol (95-100%)		Used in purification and extraction of RNA
	Dnase I	Zymoresearch	Digest double and ssDNA into oligo and mono nucleotides Digest DNA, eliminating DNA from RNA extraction
	DNA digestion buffer	Zymoresearch	Dilutes and mixed with Dnase I
	RNA wash buffer	Zymoresearch	Washing buffer, RNA purification
	Direct-zol™ RNA preWash	Zymoresearch	RNA purification
	Dnase/Rnase-free water	Zymoresearch	Used to elute RNA
Agilent			
	Electrode cleanser	Agilent Technologies	Cleaning of electrodes
	RNA 6000 NanoLadder	Agilent Technologies	For quantification of RNA sample
	RNA Nano Dye concentrate	Agilent Technologies	For quantification of RNA sample
	RNA Nano Gel Matrix	Agilent Technologies	For quantification of RNA sample
	RnaseZAP	Agilent Technologies	Electrode decomtanimation and routine electrode cleaning
Reverse transcription			
	10x reverse transcription buffer		Used in reverse transcription reaction to synthesize cDNA
	25x dNTPs		cDNA synthesis, extend DNA strand.
	10x random primers		Prime mRNAs for cDNA synthesis
	MultiSribe™ Reverse Transcriptase (50U/µL)		Recombinant RNA-dependent DNA polymerase, used to synthesize cDNA
Real time PCR			
	TaqMan ™ Universal master mix	Thermo Fisher Scientific	Aplification complentary DNA (cDNA)

	primer/probe mix		Primer: hybdridize with the cDNA, provide the region of to synthesize new DNA to be amplified. Probe; fluorescently labelled, that emites a signal during PCR reaction.
	dH_2O		solvent

Table A3. Overview of mice used in this thesis

Mouse ID	STRAIN	AGE (w.o)	AGE + Weeks with AB	Weeks with Ab+	PROTEINURI	TLS
PET03	NZB/W	29	29 wo 9w Ab+	9		?
PET04	NZB/W	21	21 wo 5w Ab+	5		(+)
PET05	NZB/W	25	21 wo 6w Ab+	6	3/+4	++
PET08	NZB/W	28	28 wo 6w Ab+	6	4	?
PET09	NZB/W	22	neg	0		+
PET10	NZB/W	34	34 wo 8w Ab+	8		+++
PET13	NZB/W	34	34 wo 6w Ab+	6	4	neg!
PET15	NZB/W	29	29 wo 7w Ab+	7		++
PET16	NZB/W	29	29 wo 5w Ab+	5		+++
PET17	NZB/W	30	30 wo 6w Ab+	6		+++
PET22	BALB/c	29	neg	0		
PET24	BALB/c	24	neg	0		
PET27	BALB/c	32	neg	0		
PET29	BALB/c	22	neg	0		
PET30	BALB/c	27	neg	0		
PET31	BALB/c	29	neg	0		
PET36	BALB/c	35	neg	0		
PET37	BALB/c	32	neg	0		
PET38	BALB/c	37	neg	0		
PET39	BALB/c	39	neg	0		
PET41	NZB/W	27	27 wo 8w Ab+	8	4	++
PET42	NZB/W	31	(OD+)	0		++
PET44	NZB/W	29	29 wo 9w Ab+	9		+++
PET45	NZB/W	21	21 wo 7w AB+	7		
PET46	NZB/W	23	23 wo (OD +)	0	4	?
PET47	NZB/W	25	neg	0		
PET49	NZB/W	34	(OD+)	0		++
PET54	NZB/W	30	33 wo 7w Ab+	7		++
PET55	NZB/W	24	24 wo 8w Ab+	8		?
PET56	NZB/W	30	30 wo 8w Ab+	8		+++
PET57	NZB/W	29	29 wo 9w Ab+	9		++++
PET59	NZB/W	37	36 wo 4w Ab+	4		++++
PET60	NZB/W	27	27 wo 3w Ab+	3		++
L4	NZB/W	4				
L5	NZB/W	4				
L6	NZB/W	4				

Table A4. Overview of mice used in this thesis

Mouse ID	STRAIN	AGE (w.o)	AGE + Weeks with AB	Weeks with Ab+	PROTEINURI	TLS
F1	NZB/W	5	neg		+/-	
F2	NZB/W	5	neg		+/-	
F3	NZB/W	5	neg		+/-	
F7	NZB/W	12	(OD>0.2)		+/-	
F8	NZB/W	12	(OD>0.2)		+/-	
F9	NZB/W	12	neg		+/-	
F13	NZB/W	17	neg		+/-	
F14	NZB/W	17	neg		+/-	
F15	NZB/W	17	neg		+/-	
F19	NZB/W	5	neg		+1	
F20	NZB/W	5	neg		+1	
F21	NZB/W	5	neg		+1	
F25	NZB/W	12	neg		+1	
F26	NZB/W	12	neg		+1	
F27	NZB/W	12	neg		+1	
F31	NZB/W	18	1.677 (titer pos)		+1	
F32	NZB/W	18	neg		+1	
F33	NZB/W	18	neg		+/-	

Table A5. Overview of different kits used

Experiment	Kit Name	Product ID	Kit content	Manufacturer
Immunohisto-chemistry	Envision+ system-HRP	K4003	Peroxidase block, Labbeled Polymer HRP Anti-Rabbit, Substrate buffer, DAB+ Chromogen	DAKO
	Liquid DAB+ substrate Chromogen system	K3467	DAB+ Chromogen DAB+ substrate Buffer	DAKO
	Polink-2 plus HRP Detection Kit for Rabbit Primary Antibody(with DAB chromogen	D39-18		GBI Labs
RNA Isolation	Direct-zol™ RNA MiniPrep	R2073	Tri Reagent®, Direct-zol™ RNA prewash, RNA Wash Buffer, Zymo-Spin™ IIICG columns, Collecting tubes, Dnase/Rnase-free Water, Dnase I, DNA digestion buffer	Zymoresearch
Reverse transcription	High-capacity cDNA reverse transcription Kit		10x reverse transcription buffer 25x dNTPs, 10x random primers, MultiScribe reverse transciptase (50U/µl)	Applied biosystems® by Life Technologies
Agilent	Agilent RNA 6000 Nano Kit		Electrode cleanser, RNA Nano-Ladder, RNA Nano Dye concentrate, RNaseZAP, RNA marker	Agilent Technologies

Table A6. Overview of buffers used in IHC.

Name	Composititon	Purpose
10x citrate buffer	2.94 g Tri-sodium citrate (dehydrate) 1000mL MilliQ water 1N HCl	Diluted and used for antigen retrival
1x Citrate buffer	100 mL 10X sodium citrate buffer 900 mL MilliQ water	Antigen retrival
PBS	9.55 g/L PBS Dulbecco w/o Ca^{2+} w/o Mg^{2+} 5000 mL MilliQ water	Washing/Rinsing

Table A7. Equipment and software used in this thesis.

Experiment ID	Software name	software version	Manufacturer
Immuno-Histochemistry			
RNA isolation	Nanodrop® DN-1000 software	V3.8.1	Saveen Werner
Agilent 2100 Bioanalyzer	2100 Expert software		
Real Time PCR	LightCycler ® 96		Roche
Statitstic tool	Graphpad® Prism8 Graphpad® Prism 5		GraphPad®

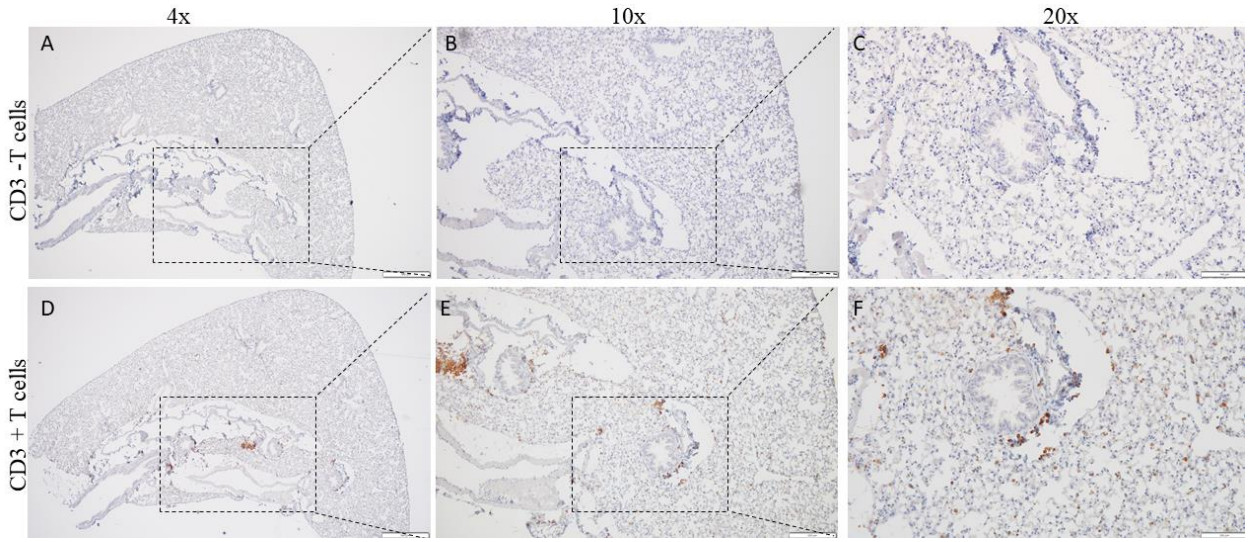

***Figure A1**: **Representative picture of T cells in lung tissue of proteinuric NZB/W mice.** (A-C) negative control in lung tissue of a 22-week-old proteinuric J1 NZB/W mouse. (D-F) CD3 positive cells (brown) detected within lung tissue of a 32-week-old proteinuric, J1 NZB/W mouse, with an overall score of ++. Tissue morphology was optimal in both tissues. Scale bars: (A and D) 500µm, (B and E) 200µm, (C and F) 100µm.*

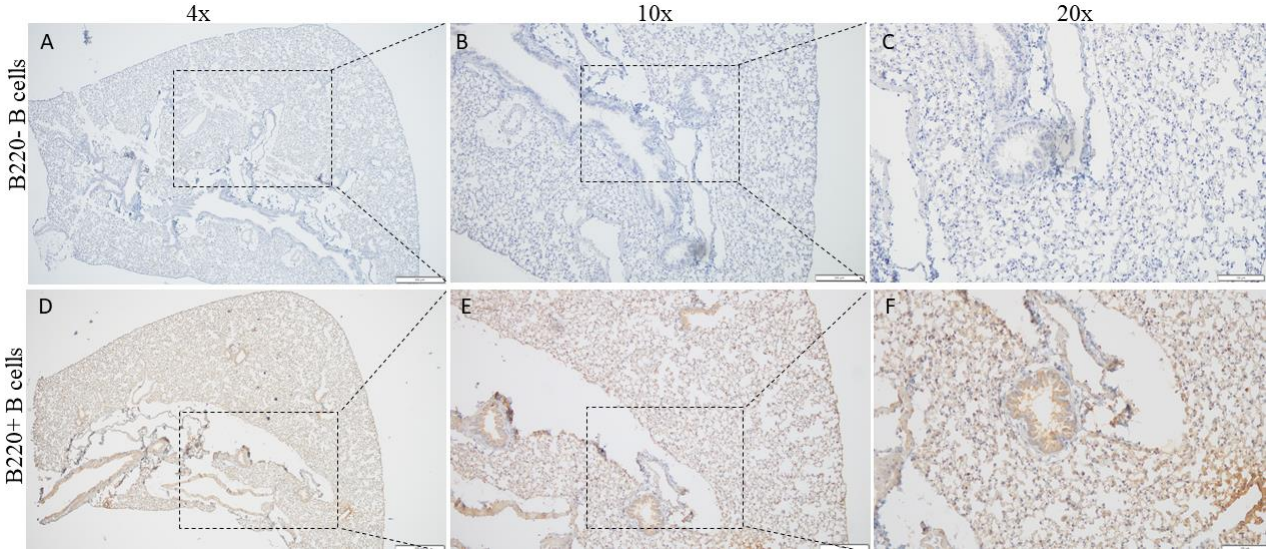

***Figure A1**: **Representative picture of B cells in lung tissue of proteinuric NZB/W mice.** (A-C) negative control in lung tissue of a 22-week-old proteinuric J1 NZB/W mouse. (D-F) B220 positive cells (brown) detected within lung tissue of a 32-week-old proteinuric, J1 NZB/W mouse, with an overall score of +. Tissue morphology was optimal in both tissues. Scale bars: (A and D) 500µm, (B and E) 200µm, (C and F) 100µm.*